UNIVERSITÀ DEGLI STUDI DI SALERNO

UNIVERSITÀ DEGLI STUDI DI SALERNO

Dipartimento di Farmacia

PhD Program

in **Drug Discovery and Development**

XXXIII Cycle   —   Academic Year 2020/2021

PhD Thesis in

Design and production of personalised medicines via innovative 3D printing technologies

Candidate   Supervisor

Marilena Saviano   Prof. *Paola Russo*

PhD Program Coordinator: Prof. Dr. *Gianluca Sbardella*

Table of content

3

4

6

Abbreviations

3DP	3D printing
ABS	Acrylonitrile butadiene styrene
AM	Additive Manufacturing
AMF	Additive Manufacturing File Format
API	Active pharmaceutical ingredient
ASCII	American Standard Code for Information Interchange
AUC	Area Under Curve
CAD	Computer-Aided Design
CAM	Computer-Aided Manufacturing
CDER	Center for Drug Evaluation and Research
CDRH	FDA's Center for Devices and Radiological Health
CGMP	Current Good Manufacturing Practice
CIPHCL	Ciprofloxacin Hydrochloride
DDS	Drug Delivery System
DSC	Differential Scanning Calorimetry
EMA	European Medicines Agency
FDA	U.S. Food and Drug Administration
FDM™	Fused Deposition Modeling
FFF	Fused Filament Fabrication
FT-IR	Fourier Transform Infrared Spectroscopy
HME	Hot Melt Extrusion
HPLC	High-Performance Liquid Chromatography
ICMRA	International Coalition of Medicines Regulatory Authorities
IIG	Inactive Ingredient Guideline

IPA	2-propanol
IT	Information technology
IT	Information Technology
NIH	National Institutes of Health
NIH 3DPX	NIH 3D Print Exchange
NME	New molecular entities
PAM	Pressure-assisted Micro-syringe Printing
PC	Polycarbonates
PEG	Poly(ethylene glycol)
PLA	Polylactic acid
PMC	Personalized Medicine Coalition
PPE	Personal protective equipment
PVA	Poly(vinyl alcohol)
PVAc	Polyvinyl acetate
SEM	Scanning Electron Microscopy
SFF	Solid Freeform Fabrication
SLA	Stereolithograpy
SSE	Semi-Solid Extrusion
TA	Thermal Analysis
TPO	Diphenyl(2,4,6-trimethylbenzoyl)phosphine oxide
TPU	Thermoplastic polyurethane
UV	Ultraviolet–visible spectrophotometry
VA	Department of Veterans Affairs
DC	Drug Content
DLE	Drug loading efficiency
HEC	Hydroxyethyl cellulose

PRPHCL	Propranolol Hydrochloride
SA	Sodium alginate
TW	Tween® 85

Outline of the PhD project

The perspective of personalized therapies in recent years is projecting the community towards a rampant hankering for individualization of healthcare.

Paramount is the necessity of re-organizing the healthcare services and the production scales to meet the expectations of patients for targeted medicine. Thus, worldwide organizations are fostering the re-centering of the development and the design of medicines on the single patient, supporting the individual-oriented research, the flexibility of manufacturing processes, and the decentralization of medicine production.

All these changes in the healthcare system could improve the effectiveness of pharmaceutical treatments, leading to a reduction of the associated costs for care and enhancing patient compliance to therapeutic plans.

Particularly three-dimensional printing (3DP, also known as additive manufacturing, AM) is a disruptive technology, encompassing a wide range of techniques, which is revolutionizing the perspective of pharmaceutical production, especially in the personalized medicine frame.

The approval of the marketing authorization for the first 3D printed drug, SPRITAM® (Aprecia Pharmaceuticals, Langhorne, PA, USA) in 2015 has been a landmark for the application of 3DP technologies in pharmaceutical compounding. This approval reflected the interest of the pharmaceutical companies in these novel manufacturing processes and spurred the research in finding new solutions also for clinical practice.

3DP could allow targeted use of well-known drugs for subcategories of patients and can become a daily approach in pharmaceutical prescriptions.

In fact, in the context of individual healthcare, 3DP is a functional tool with countless benefits: accurate dosing of drugs, flexibility in dose adjustments, tailored release profiles, combination of multiple active principles in one dosage form,

personalization of the delivery system in shape, geometry, needs, and rapid on-demand decentralized production.

This technology applied in the pharmaceutical compounding could increase the therapeutic efficacy of both new and old active principles, raising the possibility of success of therapeutic plans, and thus the safety of treatments and the patient's adherence.

Thanks to the personalization of healthcare connected to 3D printing techniques, the selection of the adequate formulation will become more straightforward, and the setup of the manufacturing of individualized medicines will be accelerated and addressed to the specific patients' need.

In this context of novel approaches to the development of personalized drug delivery systems, this PhD project aims to investigate the potential of 3D printing technologies (i.e. FDM, SSE, and SLA) for the development of innovative manufacturing processes and the design of customized drug delivery systems.

All the overmentioned 3DP technologies are herein deeply studied in order to improve properties of printed vehicles, investigate novel methodologies for producing 3D printed products, and set up the optimized production conditions for different formulations.

Particularly, the first section of the project was aimed to produce an optimized protocol for the manufacture of high homogeneous drug-loaded printouts customizable in dosage, using filaments obtained *via* Hot Melt Extrusion (HME) as feeds for Fused Deposition Modelling 3DP (FDM).

Different particle size ranges of poly(vinyl alcohol) (PVA) were systematically screened for their effect during the mixing-extrusion-printing steps of the thermoplastic polymer and the drug (Ciprofloxacin hydrochloride added in different ratios). All to identify the optimal polymer particle size able to improve the process efficiency and to maximize the versatility of the 3DP, essential for personalized therapies. Operative specifics, formulation variables, and extrusion-

printing parameters were adjusted and refined for an optimal print of drug-loaded filaments into cylindrical dosage forms. The prints were fully characterized in terms of homogeneity, process efficiency, chemical-physical properties, drug content, and release kinetics. Hence, information about the impact of fundamental process variables on the final product and on drug release patterns was collected. Thus, a standardized method for the loading of a thermostable API into the polymeric carrier for 3DP was proposed, demonstrating the possibility of producing low and high dosage oral drug delivery systems exploiting HME and FDM 3DP with similar release kinetics.

Starting from the acquired know-how about potentialities and limits of the FDM technology coupled with HME as pre-loading technique, in the second section, PVA was printed as a blank model by FDM 3DP and, in this case, was post-loaded using oversaturated drug solutions and processed *via* a microwave-assisted impregnation.

Mainly, Stereolithography (SLA) 3DP technology was exploited for the rapid prototyping of a modular floating system (capsules in capsule) thanks to its rapidity and highest resolution of production. Hence, the optimized models were produced as blank PVA scaffolds *via* FDM 3DP, and a morphological analysis on the FDM printed models was conducted to set out an easy re-tune of the desired model with respect to the patients' needs.

The printed gastro-retentive systems were then subjected to microwave irradiation for drug loading, and the research was focused on the impact of the radiations on the chemical and physical properties of the polymer and the drug (Anhydrous Caffeine). Therefore, the drug-loading efficiency, thermal and chemical characteristics of components, the morphology and the stability of the drug and the processed printouts were disclosed. Parameters of this unexplored microwave-assisted post-loading technique were optimized, and the process

resulted in the preservation of the polymeric matrix and enhancement of drug adhesion.

Hence, the microwave impregnation confirmed its potentialities in supersede the traditional post-loading methods, such as the soaking technique, being faster and more efficient.

In the third section, a different creative manufacturing process was projected taking advantages of the ionotropic gelation property of sodium alginate; indeed a co-axial Semi-Solid Extrusion (SSE) 3DP process was designed for *in situ* gelations of alginate gels.

Primarily, the FDM technology was used as a tool for the production of a co-axial extruder system, the latter exploited for the SSE 3DP of an alginate gel and a cross-linking gel (with Ca^{2+}). The feeds were simultaneously dispensed through micrometric co-axial nozzles to obtain (after drying) floating dosage forms characterized by hollow filaments. The process was improved to gain an adequate resolution of the printouts, indeed the feeds were characterized for viscosity, shape retention after deposition, and their extrudability. Furthermore, the obtained dosage forms were analysed in medium uptake capacity, buoyancy time, chemical interactions, and thermal properties. The addition of the drug (Propranolol Hydrochloride) in two different concentrations into the SSE formulations was carried out; drug content, drug loading efficiency and release kinetics of different models were evaluated.

The developed formulations were physico-chemically stable, and the unconventional use of a co-axial SSE 3DP process for pharmaceutical compounding led to obtaining innovative floating systems customizable in terms of dosage. The content adjustment can be attained by varying the output deriving from the digital models, resulting in release kinetics strictly similar and independent from the drug amount.

This pioneering use of alginate gelation for the manufacture of floating systems paves the way for the application of co-axial SSE 3DP in the manufacture of novel forms and in the tailoring of dosage for personalized medicine.

In conclusion, the obtained results were:

- the development by HME and FDM-3D printing technologies of a protocol for the production of oral delivery systems easily customizable in dosage, varying the amount of drug loaded into the polymeric filaments;

- the development of an unexplored rapid impregnation process enhanced by the microwave irradiation for the controlled post-loading of FDM printouts;

- the development of innovative gastro-retentive dosage forms with unique technological characteristics *via* a co-axial SSE 3DP process, tailorable in dosage varying the digital model design;

- the underline of the criticalities and potentialities of the 3D-printing processes in producing personalized medications;

- the corroboration of the applicability of various 3D printing technologies as polyhedral tools for drug delivery.

Finally, the scientific research conducted during this PhD path provides a tangible introduction to different 3D printing technologies (Fused Filament Fabrication, Semi-Solid Extrusion, and Stereolithography) in the domain of pharmaceutical compounding. All of them were implemented and optimized for the production of different innovative drug delivery systems and processes. Hence, the possible benefits of these techniques were highlighted, and the potentialities of these novel techniques were discovered.

The results herein described and obtained can help the arise of the awareness and the acknowledgment about the 3D printing capabilities in the scope of pharmaceutical sciences and healthcare. Indeed, 3DP is disruptively re-shaping the world in a wide array of production, and may also play a complementary or alternative role to the manufacture of conventional medicines.

1. INTRODUCTION

1.1 Personalized path in healthcare: precision medicine and 3D printing

> *"It's far more important to know what person the disease has*
>
> *than what disease the person has."*
>
> Hippocrates
> c. 460 - c. 370 B.C.

A holistic health perspective recognizes the whole human features to achieve optimal physical and mental wellness. This outlook intersects not only genes but also lifestyles, environmental, social and cultural factors to understand how people's lives and health are affected by these concomitant aspects.

In this context, stately is the emergence of the precision medicine, often referred as stratified, targeted or personalized medicine. It is considered *"the science of individualized prevention and therapy"* (National Institutes of Health - NIH) and promises to potentially fulfil patient expectations for individual needs and care. Indeed, thanks to the streamline of clinical decisions based on personal upshots, patients who will probably benefit from a given treatment can be distinguished in advance from those who will have the possibility of incurring in side effects.

The highest aim of personalized care, in fact, in addition to prevention, diagnosis, and follow-up, is to produce medicines tailored to suit the single patient profile and requirement (e.g. gender, age, weight, shape, size, formulation type, and dosage). Accordingly, therapeutically plans arise from a patient's genotypical and phenotypical characteristics and clinical outcomes, in opposition to the well-

established industrial approach of *one-size-fits-all* (FDA, 2013; Collins & Varmus, 2015; Merchant et al., 2016).

The growth of genomics, next-generation sequencing technologies, new diagnostic and computer science approaches is providing an understanding of the molecular basis that underlie illness. These advancements lead to identifying patients based on their predictable response, risk of disease, and clinical information (Hamburg & Collins, 2016). Considering anatomical and physiological differences, genetic, variability of the metabolizing enzymes and therapeutic sensitivity, the prescription of precise pharmaceutical formulations and appropriate dosing regimens can be purposely determined (Jeroen et al., 2014).

Thus, the era of technological advancements is deeply modifying the way the healthcare system looks at diagnostics and therapeutics, actualizing a tantalizing perspective for the overcome of the actual limitations of the trial-and-error medicine, instead related to prescriptions devised on statistical averages of broad populations.

Organizations such as U.S. Food and Drug Administration (FDA) and European Medicines Agency (EMA) are encouraging the targeted treatments and individualized plans with annual approvals of personalized new molecular entities (NMEs). Indeed, in the last six years, the personalized medicines covered consecutively at least the 20% of all the FDA's new approvals (PMC Report, 2020*;* Figure 1). Moreover, every year FDA accepts several significant novel personalized indications for molecularly defined subsets of patients in relation to previously existing drugs and medicines.
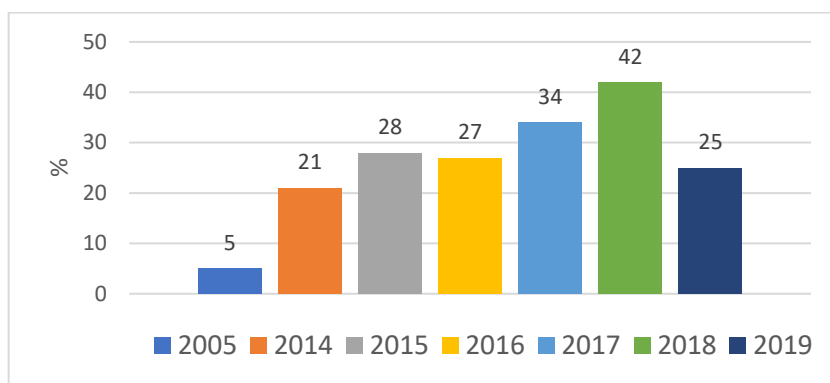
Figure 1. Percentage of approved new molecular entities classified as personalized medicines (PMC Report, 2020)

The path of targeted medicine started from the pharmacogenomic studies on breast cancer which led to the approval in 1998 (Issa, 2007) of the chemotherapeutic trastuzumab (Herceptin®). It is a genetically engineered humanized monoclonal antibody targeting the human epidermal growth factor receptor-2 (HER-2) expressed in the 25-30% of breast cancer patients (Vogel et al., 2002). The ride passed through the more recent FDA's approval in 2018 of Onpattro® (patisiran), the first approved siRNA (small interfering ribonucleic acid) for the treatment of polyneuropathy in patients characterized by the presence of the transthyretin biomarker (EMA/554262/2018). The trail arrived also at the first approval of the diagnostic software named OsiriX CDE Software Module, a test type for brain injury (MDDT Q161252, 2018), qualified by FDA in 2019 as a development tool for digital medical devices and personalized treatments.

Furthermore, it is recognized that Information Technology (IT) approaches and computational power are essential to drive decisions in the field of stratified medicines and customized prescriptions. In fact, recent years witnessed also the recognition in 2018 of the Clinical Genome Resource database (ClinGen, a National

Institutes of Health funded resource) as a high quality public central program to support the agency's precision medicine initiatives and researches, giving access to accurate human variant interpretation data (https://clinicalgenome.org/).

Despite widespread efforts of the drug discovery processes in hunting candidate drugs for precision medicine, the presence of pharmaceutical formulations available for health care infrastructures for the delivery of tailored medicines is still limited.

Finding new solutions for the immediate and customizable manufacturing of medical products, for use in small populations (exhibiting multi-drug necessities, intolerances, or allergies) and for rare diseases, could flexibly assure the management of illness, especially when commercial solutions are not available (Gudeman et al., 2013).

In recent years, novel methodologies and systems have been considered to this aim; particularly three-dimensional printing (3DP) is stating its disruptive and transformative role in medicines manufacture. Pharmaceutical laboratories and industries are indeed exploiting these techniques intending to develop technological processes and products to meet the patient-centered line of personalized medicine with more elasticity than the blockbuster drugs.

From a medical and therapeutic perspective, the additive manufacturing technology 3DP may be a pragmatic tool for the production of personalized devices (Rebong et al., 2018; Goyanes at al., 2016), implants (Jeroen et al., 2014; Hollander et al., 2016) and drug dosage forms, with optimized shapes, sizes, taste (Goyanes et al., 2019) and doses for a specific patient (Awad et al., 2018). Compared to conventional techniques, 3DP has the advantage of a rapid and smart design of pharmaceutical dosage forms with a high degree of precision and nanometer-scale

resolution. More interestingly, adjusting size, dosage and geometries with functionality and different levels of architecture complexity, the rate of delivery of a drug could be controlled (Melocchi et al, 2016) to comply with patients who respond to the same drugs in different ways. This approach could promptly enhance the efficacy of treatment and reduces adverse drug reactions, avoiding wastes of expensive medicines and the cost of the whole healthcare support. Furthermore, with respect to conventional pharmaceutical compounding, 3D-techniques are timesaving, need few instruments for the manufacturing process and occupy less space for storing materials (Aquino et al., 2018).

Continuous advances in 3D printing technology to produce new products and services or to design new processes are expected to induce improvement in medical and health outcomes, until the tangible fruition of 3DP technologies principally in clinical pharmacy practice. The benefit is the possibility to quickly design and produce freeform personalized drug delivery systems, optimizing a patient therapeutic regimen and delivering *"the right drug at the right dose at the right time"* (Hamburg and Collins, 2010:301; Khan et al., 2019).

Besides, unprecedented products may be produced *via* the unique features of 3DP by pharmaceutical companies, introducing pioneering products on the markets and competing with traditional products manufactured using outdated processes (suffice it to say that the direct compaction press is in use for more than 150 years and still employs the same basic principle of compression).

3DP is indeed commonly considered to be the industrial revolution of the 21st century. An explicatory case study of the industrial application of 3DP techniques is Spritam[®], the first 3D printed pharmaceutical product approved by the FDA in 2015, manufactured by Aprecia Pharmaceuticals. This advanced formulation is

based on levetiracetam and is an orodispersible tablet for the treatment of seizures onsets, designed for pediatric or geriatric patients who may struggle to swallow medicine (FDA 207958Orig1s000; https://www.spritam.com). The unique instantaneous disintegration properties (less than 10 seconds), even at high dose loads, have been achieved optimizing an automated platform to orchestrate production for the scale-up of additively manufactured fast-melt tablets with high porosity. The process is known as ZipDose® Technology and brilliantly surpasses the limits of today's techniques (Table 1).

Table 1. A comparison of currently available fast melt technologies and ZipDose®
(https://www.aprecia.com/)

Technology	Dosage Form	Highest Strength	Description	Advantages	Disadvantages
Lyophilization (Freeze-Drying)	ODT	<200mg	Drug physically trapped in a water-soluble matrix, which is then freeze dried	Highly porous product that rapidly dissolves in mouth	Lower dosage capacity as ideal drug candidate has particle size < 50 microns
Soft Compression	ODT	275mg	Direct compression tablet manufacturing that requires the inclusion of special excipients	Simplest and most cost effective manufacturing technique	Slower disintegration time due to significant loss of porosity and inclusion of special excipients
ZipDose	TOS*	1000mg	3D printed porous structure that allows for rapid dispersion and appropriate taste masking technologies	Highly porous product allowing rapid dispersion within seconds with liquid • High dose loading capabilities • Full range of taste masking options	Requires access to small amount of liquid

* TOS = Tablets, for Oral Suspension

Moreover, ZipDose® Technology does not require any molding or tooling for production; it enables flexibility in product development particularly for the tuning of the medicine dimensions and for the degree of binding, and thus porosity. Hence, Aprecia Pharmaceuticals excellently proved the feasibility of transitioning 3D printed techniques in continuous manufacturing, by planting a milestone in this technology's breeding ground.

22

However, the approach of novel manufacture of medicines is also likely to introduce different and new challenges in drug production and pharmaceutical compounding. Researchers are actively contributing to analyse and solve these issues, as evidenced by the increasing number of publications of research articles about 3D printed medicines (https://www.sciencedirect.com/), which highlight the huge scientific interest in 3DP potentialities (Figure 2).
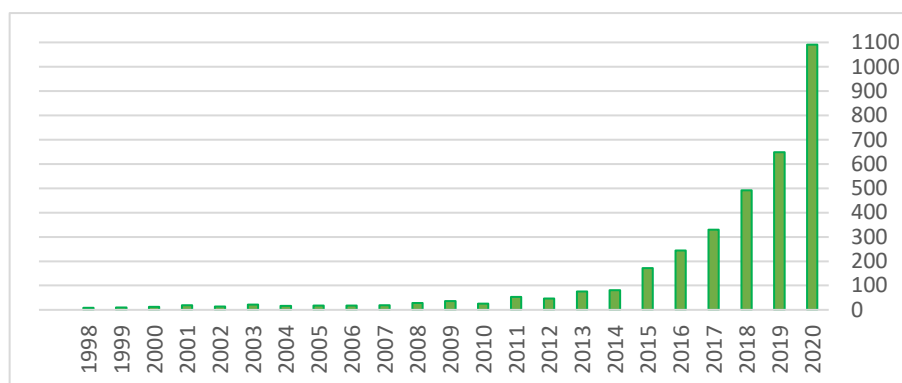
Figure 2. Pictograph of the number of publications (type: research articles) in relation to 3D printing of medicines over the last 23 years (found terms: "3D printing medicine") (ScienceDirect®, accessed on December 2020)

Recently a large number of small biotech companies are emerging in 3D printing reality with the aim of creating personalized delivery systems and medical devices using these novel techniques. For instance, FabRx Ltd. developed in 2020 the world's first pharmaceutical 3D printer for personalized medicines, M3DIMAKER™ (Figure 3), that enables printing using different technologies (i.e. Fused Deposition Modelling and Direct Powder Extrusion). This machine is suitable for research in pharmaceutical compounding, drug development,

preclinical and clinical needs (https://www.fabrx.co.uk/), thanks to its build materials and certifications.
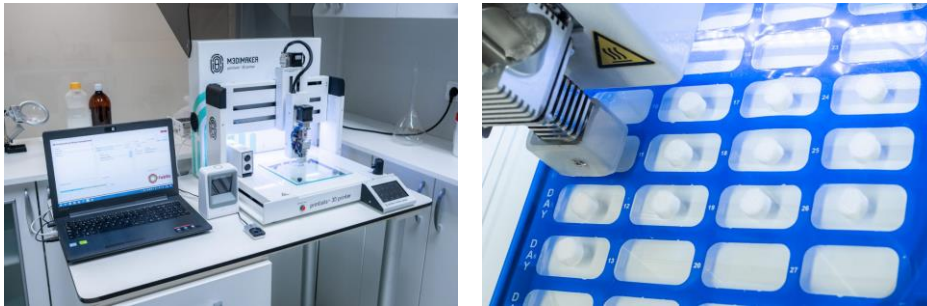
Figure 3. M3DIMAKER™ pharmaceutical 3D printer developed by FabRx Ltd. (https://www.fabrx.co.uk/)

A remarkable aspect of the last few years is that hospitals are already integrating 3D printers (certified for 3DP anatomical models) in their practice (Figure 4). Mostly printing processes are coupled with medical 3D image-based engineering software for the visualization of patient's anatomy. This approach steers individual surgery and is advantageous for the production of personalized implants, prosthetics, (mainly joint replacements - hips, shoulder - cranio-maxillofacial implants and dental restorations), and surgical guides.
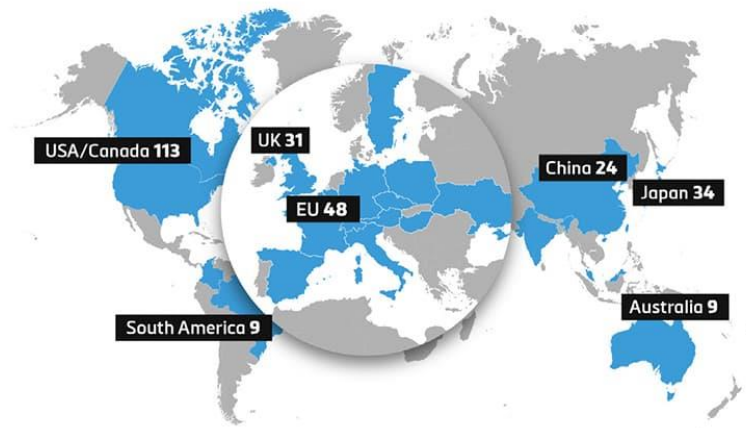
Figure 4. Hospitals worldwide with a 3D printing facility (Materialise Mimics technology; https://www.materialise.com/; June 11, 2019)

In this respect, it is undoubtedly predictable that 3DP can arouse a shift in modern medicines manufacture and in medical care within industrial stetting, clinical trial facilities, hospitals, and dispensing pharmacies, heralding a new era of preventive, proactive, and more effective healthcare.

By improving healthcare ability in scheduling individualized therapeutic plans and in selecting and/or producing the optimal medical and pharmaceutical products (for which benefits outweigh risks in sub-populations of patients), the probability of success will increase, and the costs associated with ineffective treatments will be minimized.

However, economic and social challenges need to be overcome for translating the patients care into personalized therapeutics. In fact, conceivable improved health outcomes and success rates that ascend from precision medicine require policies that actively incentivize the advancement in R&D of the precision field in the industrial and research scale. Moreover, regulatory oversight, health care insurances and reimbursement systems of the countries are not still deeply allied in

promoting the development of targeted prescriptions and treatments. Thus, in this context, it is necessary that policymakers embrace, favour and anticipate the advancement of this progress for shortening product development timelines and make it accessible to users in the foreseeable future.

1.2 Balancing innovation and safety: regulatory state of Additive Manufacturing

So that AM and 3DP assert their enrichment role in healthcare and pharmaceutical compounding, harmonised protocols need to be established address cross-border issues associated with additive manufacturing productions. Relevant datasets and information on process variables, quality, and safety of printed medicines and medical devices need to be coherently defined and agreed.

Stakeholders with interdisciplinary expertise, public-private institutions and governmental professionals from different disciplines are continuously interacting in widespread consultation to depict the frameworks that support the applicability of AM in different domains.

One of the preeminent organizations in AM area is the *ASTM Committee F42 on Additive Manufacturing Technologies*. The board was formed in 2009 with the target of editing a portfolio of approved standards in all segments and aspects of AM techniques, thanks to various technical committees (e.g. subcommittees F42.01 for Test Methods; F42.04 for Design; F42.05 for Materials and Processes; F42.05.02 for Polymers; F42.06 for Environment, Health, and Safety, etc.) (https://www.astm.org/).

More recently in the pharmaceutical field, the *FDA Center for Drug Evaluation and Research's (CDER) Office of Pharmaceutical Quality* laid the

foundation of the *Emerging Technology Program*. The drives of the initiative are filing regulatory documents and interconnecting industries representatives and the agency's members team to discuss and evaluate potential technical and regulatory issues for the applications of advanced emerging technologies. The goal is promoting pharmaceutical innovation and modernization, such as AM and 3DP manufacturing, in industrial and research facilities. This enterprise encloses proposals for optimized control strategies for the manufacturing of technologically advanced products and drugs. Indeed, thanks to this parallel participation of industries and agencies teams, the *FDA's Center for Devices and Radiological Health's (CDRH)* drew up a first guidance, issued on December 5 2017, titled *"Technical Considerations for Additive Manufactured Medical Devices - Guidance for Industry and Food and Drug Administration Staff"*, which clarifies also aspects of 3DP technological processes. Particularly, the guidance is focused on medical devices and it is organized in two main topic areas: *Design and Manufacturing Considerations* and *Device Testing Considerations* (Figure 5).
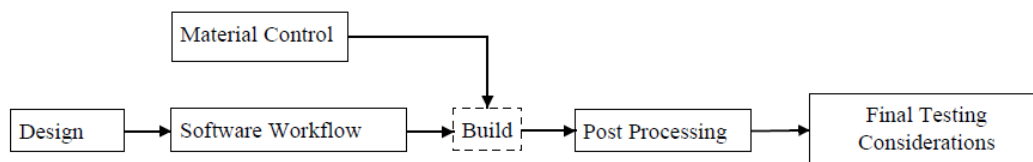
Figure 5. Flow chart of the AM process and sections investigated in the FDA guidance (FDA guidance December 5, 2017)

In the first area, requirements, and technical considerations for the quality of the devices are defined:

   − design models and software configuration options;

- effects and resolution of imaging techniques associated with the draw of digital models (essential for complex design files and patient-matched models);

- storage of the files for printing, archived in a standardized format or rather Additive Manufacturing File Format (AMF) (described in ISO/ASTM 52915 *Standard specification for additive manufacturing file format*);

- manufacturing tolerances of the individual machine and environmental conditions;

- monitoring and control of parameters and output specifications (such as build orientation, build paths, and speeds that are associated with the anisotropic properties of the device, temporary support structures, fill densities, and geometries);

- material controls (particle size and distribution, composition, purity, rheological performances) and material reuse criticalities (changes in chemistry);

- cumulative effects of the processing and post-processing on final devices;

- validation of the process and the final device (quality, features, dimensional specifications, material and mechanical properties, non-destructive evaluation of morphology and microstructure, and destructive mechanical testing, sterilization, biocompatibility).

While in the second section, information for the premarket submissions and approval is set out, related to the intended use, risk profile, and classification/regulation for the device type (information required for approval requests, labelling considerations).

The increase of the availability of novel equipment and the maturation of AM technologies, in recent years, have triggered further explicatory guidance, provided by FDA CDER in 2019 (to date as a draft), titled *"Quality Considerations for Continuous Manufacturing - Guidance for Industry"*. The document provides key quality considerations and recommendations for continuous innovative manufacturing of small molecules and solid oral drug products. Particularly different sections describe:

- process dynamics for mitigation of risks (critical parameters in steady and transient states, process conditions, material traceability, and residence time distribution);
- batch and lot definition with respect to current good manufacturing practice (CGMP);
- control strategy across the whole product's life cycle, to detect and mitigate transient disturbances and deviations (input material attributes, equipment qualification, process monitoring including experimental investigation and software simulation, implementation of active and automated process control for real-time adjustments);
- process validation (following the guidance *Process Validation: General Principles and Practices and ICH Q8, 480 Q9, and Q10*)
- pharmaceutical quality system considerations (elements to consider for design and programs of continuous manufacturing);
- methods for scale-up and scale-out (quality of the finished products, complexity of the changes for approval filing strategy);
- stability (following the guidance *Q1A(R2) Stability Testing of New Drug Substances and Products*);

‒ bridging of existing batch to continuous manufacturing (prior approval supplements with proposed transition and bridging strategy).

These years, FDA thus has been actively committed to maximizing and promoting an agile manufacturing sector and its flexibility in allowing scale-up, scale-down, and scale-out. All these proposals are intended to manage changing supply demands, particularly to help in reducing drug and device shortages preserving quality.

Specifically, these initiatives to encourage a modern and flexible healthcare system have been fundamental in the field of 3DP AM during the COVID-19 pandemic period. This historical phase reached the apex in 2020 and witnessed an acute shortage of essential medical supplies, such as personal protective equipment (PPE as masks and face shields) and device accessories (respirators and medical tools).

During which time, the lack of PPE production and providers has rapidly triggered a range of activities from academic researchers, non-traditional manufacturers, communities of makers, and individuals to fill the gaps in medical supplies, yielding a huge number of PPE produced *via* different 3D printing techniques to public-health facilities. Hence, a *Memorandum of Understanding* between the FDA, the NIH, the Department of Veterans Affairs (VA) and America Makes was compiled in March 2020 (https://www.fda.gov/). These organizations gathered to connect manufacturers and health care entities, with the aim of abridging the distribution of information on 3D printed models uploaded by a variety of users and recognized as clinically appropriate. Indeed, thanks to this collaboration, a community resource named *NIH 3D Print Exchange (NIH 3DPX)* (https://3dprint.nih.gov/) was conceived and executed for the clinical review of

digital models and finished products received from different sources (Figure 6). Specifically, on this website, 3D printable designs and tutorials for the spreading and production of PPE and models related to biosciences are now freely available when safe and certified. This contribution in supporting 3DP manufacturing during the public health emergency of the COVID-19 is a significant effort to enhance the inclusion of the AM adaptive approaches in the healthcare system. Furthermore, operators at all levels have been encouraged to embrace lateral approaches to overcome limits of the traditional manufacturing.
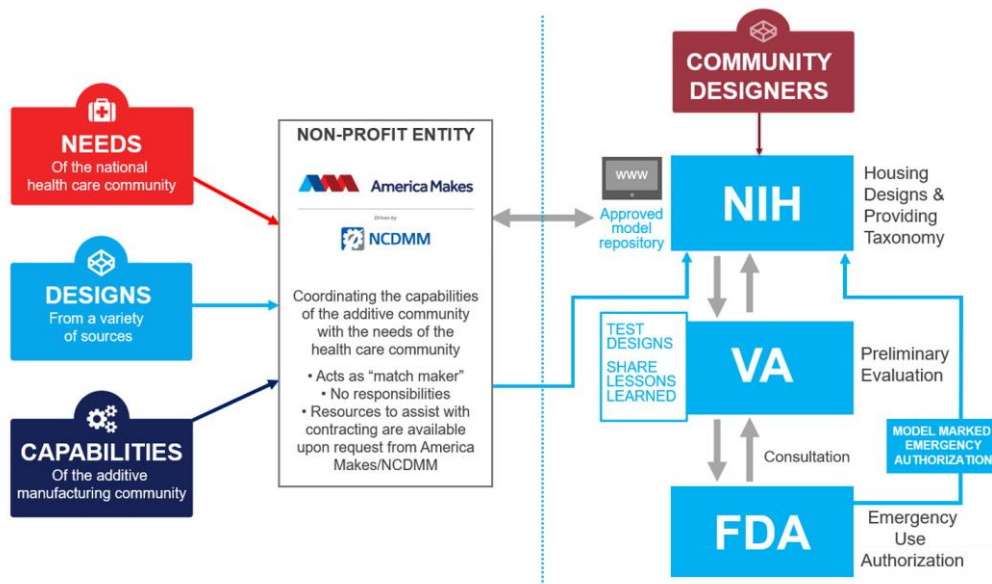
Figure 6. Workflow structured by the Memorandum of Understanding to support the COVID-19 response using 3DP AM (3D Printing in FDA's Rapid Response to COVID-19, 11/13/2020; https://www.fda.gov/)

Given the results, the FDA is also sponsoring a global survey to collect information about *3D Printing in response to COVID-19,* in order to support and improve the practices connected to AM for future applications and/or pandemics.

Moreover, other agencies (such as EMA) are fostering innovation and new development paradigms based on AM 3DP, gene editing, and artificial intelligence.

Mainly in the biologic domain of AM, six regulatory agencies involved in the *International Coalition of Medicines Regulatory Authorities* (ICMRA) published in 2019 a case study about 3D Bio-Printing (*ICMRA Innovation Project 3D Bio-Printing Case Study: Summary of Discussions and Considerations for the New Informal Innovation Network, 2019*). The investigation belongs to their project on emerging technologies launched on 2017, with the aim to draw up a convergent global regulatory framework about novel techniques.

The study is based on a hypothetical 3D bio-printed human knee meniscus, considering the wide scientific literature behind and the recent advancements in tissue engineering and musculoskeletal-vascular engineered therapies. In this case, this model has been chosen to be examined as a standard for regulating the whole life cycle of similar constructs, and to identify regulatory issues for point-of-care production.

Points of discussion highlighted in the document are:
- product classification (advanced therapy medicinal/biological products, hospital exemption or magistral preparation for individual patients);
- safety, efficacy, and quality of process and product (equipment, software, materials as hydrogels and polymers, loaded cells, long-term considerations, clinical trials in respect to member states' jurisdiction, update CGMPs);
- pre-market assessment (certifications, licenses of the process for the final product rather than a market authorization for the product);
- risk-based considerations (high, middle, and low risk classification);

– post-approval oversight (data to provide, traceability of the products and patients, roles and responsibilities among authorities and stakeholders).

Finally, from this summary on regulatory policies of worldwide agencies about different spheres of innovative technologies, it can be concluded that AM manufacturing is gaining huge attention from the healthcare providers. Moreover, legislation is rapidly evolving to facilitate access to pioneering products while protecting patients who aspire to personalized paths of care. In conclusion, future discussions are still planned and required to proactively and cohesively fill out the regulatory aspects of processes and products deriving from disruptive innovative technologies. Certainly, regulatory and modernization in manufacturing are proceeding in a coordinated way for point-of-care production and personalized treatments, awakening the collective consciousness in respect to the necessity of a healthcare revolution.

1.3 Three-dimensional printing: overview and unique facets in pharmaceutics

In the past few decades three-dimensional printing (3DP) has received growing attention as innovative technology used across a wide range of disciplines, due to the inbred characteristic of 3DP of facilitating the iterative and rapid prototyping of more cost-effective and freeform designs (Penny & Hilton, 2020), easily customizable.

In fact, 3DP, generally used as synonym for additive manufacturing (AM), is considered to be part of the fourth industrial revolution for the development of breakthrough engineered systems at the crossing of the digital, the physical and the biological areas.

The AM methodologies are based on joining a broad variety of materials to produce objects starting from 3D model data, usually in a layer-upon-layer manner, as opposed to subtractive manufacturing processes.

The international committee of the American Society for Testing and Materials (ASTM) has proposed a standards terminology for additive manufacturing (ASTM F2792-12a. 2012) in an effort to group the current and future AM technologies and standardize their nomenclature used by all users. The ASTM seven categories of machines based on the additive process involved are summarized in table 2.

Table 2. Classification of 3D printing technologies (Gaisford & Basit, 2018)

ASTM Categories	Technologies	Substrate	Mechanism of layering
Binder jetting	Powder bed inkjet printing S-printing M-printing Theriform™ ZipDose®	Solid particles (plaster, metal, sand, polymer) A liquid binding agent	A liquid binding agent is selectively deposited to join powder materials
Vat polymerisation	Stereolithography (SLA) Digital light projection (DLP) Continuous layer interface production (CLIP)	Liquid (photopolymer)	Liquid photopolymer in a vat is selectively cured by light-activated
Powder bed fusion	Selective laser sintering (SLS) Direct metal laser sintering (DLSM) Selective metal sintering (SLM) Electron beam melting (EBM) Concept laser	Solid particles (metal, plastic, polymer)	Thermal energy selectively fuses regions of a powder bed

Material extrusion	Fused deposition modelling (FDM/FFF) Gel/paste extrusion	Filament (thermoplastic polymers e.g. ABS; PLA; PC, TPU…)	Material is selectively dispensed through a nozzle or an orifice
Material jetting	Ink-jet printing Polyjet Thermojet	Liquid (acrylic-based photopolymers, elastomeric photopolymers, wax-like materials)	Droplets of built material are selectively deposited
Directed energy deposition	Electron beam direct Manufacturing Direct metal tooling (DMT) Be additive manufacturing (BeAM)	Wire (metal)	Focused thermal energy is used to fuse materials by melting as they are being deposited
Sheet lamination	Laminated object manufacturing	Sheets	Sheets of material are bonded to form an object

Thus, 3D-technology, or also Solid Freeform Fabrication (SFF), is an eclectic range of manufacturing processes that can produce complex freeform solid objects directly from freeware design software of digital models (Chia & Wu, 2015).

The general SFF process for all the technologies involves in:

o creating a 3D computer prototype which can be generated from imaging data (such as scans reconstruction or imaging techniques), or by Computer Aided Design (CAD) software;

o conversion of the digital model into a build file (namely STL file format) in binary and ASCII character encodings, with the construction of triangular facets on the CAD model to accurately approximate the shape of the object;

o slicing of the .stl files, processed with Computer Aided Manufacturing (CAM) software, in layers along the x-y plane and stacking the following layers in the z-direction, with the creation of a .gcode file;

o using the surface data of the .gcode to automatically drive machines in the manufacturing of the object by a computer-controlled layer-by-layer 3D printing procedure.

Hence, 3DP is characterized mainly by unprecedented freedom in product designs unachievable with traditional methods, providing endless possibilities in the degrees of customization, without the need of retooling the equipment for the production. Furthermore, options for 3DP materials are extensive, and the recent years are seeing an increasing number of commercial materials available for AM.

Particularly, in the pharmaceutical branch, AM 3DP may supersede the large-scale centralized manufacturing of medicines providing a flexible production of medical products characterized by numerous significant properties:

– meet personalized dosing requirements: fundamental for elderly and paediatric patients, or for medicines formulated in a single discrete strength that usually are split or crushed with the consequence of dose inaccuracy, or dose-dumping (Habib et al., 2014; Richey et al., 2017);

– multi-drug delivery in a single formulation thanks to the accurate spatial distribution of drugs in 3D printed formulations and the unlimited design space: for polypharmacy in ageing population and for complex therapeutic regimes of hospitalized patients, improving therapeutic adherence and compliance (Gioumouxouzis et al., 2017);

– customized release profiles thanks to the variety of materials to be combined (Johnson et al., 2017; Goyanes et al., 2017) and the intricacy of printed geometries with different surface area/volume ratio (Goyanes et al., 2015);

– immediate manufacturing of medical devices with customizable geometries and surface-matching characteristics;

– on-demand manufacturing, particularly for drugs with poor stability or short shelf lives or as adaptive approach to emergencies, pre-clinical studies and clinical trials thanks to the immediate possibility of dose flexibility.

Hence, the potentialities of 3D printing in pharmaceutical compounding are countless; moreover in a multipart community with different necessities, essential is the increase of the complexity of pharmaceutical products inaccessible to the traditional mass production, and in the meanwhile central is the reduction of the complexity of supply chains. In this context, 3DP, nowadays in the fourth decade of its advent in our society, will be one of the major tools for creating bespoke products and services in the next few years.

The following chapters are dedicated to the deepened techniques during this Ph.D. course, introducing the operative concepts and fundaments of three technologies and their application in pharmaceutics:

✓ Stereolithography (SLA)
✓ Fused Deposition Modelling/Fused Filament Fabrication (FDM/FFF)
✓ Gel-paste Extrusion/Semi-solid Extrusion (SSE)

1.4 Stereolithography 3D printing

The first-ever 3D printed object was a tiny black cup for eye wash (Figure 7), produced *via* the new-born 3DP technology named Stereolithography (SLA), invented and patented by Charles W. Hull in 1984 (US Patent 4575330A, 1984).

To commercialize his new build method of solid objects, Hull co-founded 3D Systems in 1986, the forerunner of all AM companies. Then the company specialized in the entire digital manufacturing workflow (digitalization, design, simulation, materials, and on-demand production), paving the way for all the subsequent AM businesses around the globe.

Figure 7. The first-ever 3D printed part: an eye-wash cup
(https://www.3dsystems.com/)

SLA is a liquid-based rapid prototyping technique and is widely used for tooling and prototyping thanks to its superior resolution of small features (1-25 µm for SLA *vs* 100 µm for FFF) (Gardan J., 2016).

The configuration of SLA machines can be: bottom-up (Figure 8) or top-down, depending on the location of the light source, placed on the bottom of the platform and vat for the first set up, while on the top for the latter. The light source (such as UV laser beam or digital projector) is directed by galvo mirrors and traces the pattern for spatial control during the construction of the object; moreover, it

supplies the energy for the photopolymerization of polymeric resins contained in vats, leading to the hardening of sub-sequential layers.

The highest accuracy of this technology is indeed derived from the light source that irradiates photocurable material and induces chemical boding amid monomers/oligomers, creating a high cross-linked hardened polymer (Liravi et al., 2015).
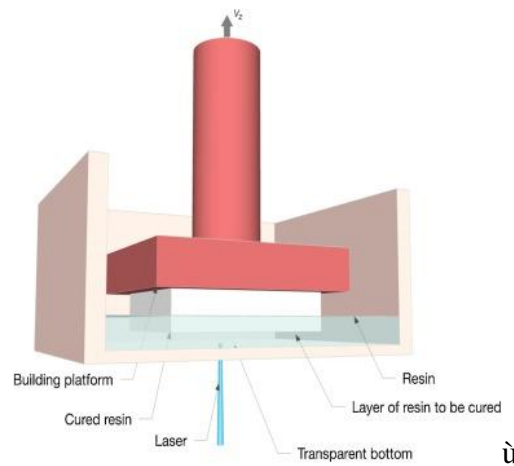
Figure 8. Typical bottom-up configuration of the SLA machines (Zakeri, Minnamari & Levänen, 2020)

This light-based technology, in addition to the superior resolution of printing, offers also the highest layers adhesion, great stiffness and elevated surface smoothness, all due to the chemical linking of subsequentially cured layers, in opposition of the physical fusion of layers for extrusion and melting technologies (i.e. FFF and SSE). Moreover, SLA does not need thermal processing to create solid objects, in fact the construction occurs at room temperature. This is an essential characteristic for the delivery of thermolabile APIs (Vitale & Cabral, 2016; Goyanes et al., 2016), even if usually post-processing may be necessary to ultimate

the hardening of the object, , as removal of the uncured resin and post-curing by UV-exposition (Zakeri, Minnamari & Levänen, 2020). Furthermore, APIs with different solubilities can be incorporated easily into the photocurable materials mixing components prior to printing, with the possibility of curing even solutions and suspensions (Xu et al., 2021), facilitating the delivery of poor water-soluble drugs.

In opposition to these perks, nowadays the main issues to overcome in SLA are: the limited numbers of photopolymerisable biocompatible materials available for pharmaceutical compounding; and the plausible presence in the final printed product of free radicals and reactive monomers/oligomers deriving from resins (inconvenient for oral forms). Whereas a large amount of biocompatible photocurable materials to produce medical prototypes and wearable medical devices are commercialized by numerous companies (such as FormLabs resins for dental and medical applications with class I and IIa of biocompatibility) (https://formlabs.com/).

Indeed, the application of SLA 3DP in diagnosis and surgery process of complex orthopaedic and orthodontic diseases is extremely precise and reliable. Template designs produced *via* SLA can aid preoperative plans, enabling individualised simulations of operation (Figure 9). Finally, the main characteristic of SLA 3DP in medical sector is the fast fabrication and prototyping of models by providing high precision; conversely, the rising of the SLA in the pharmaceutical compounding is still at the dawn of development.
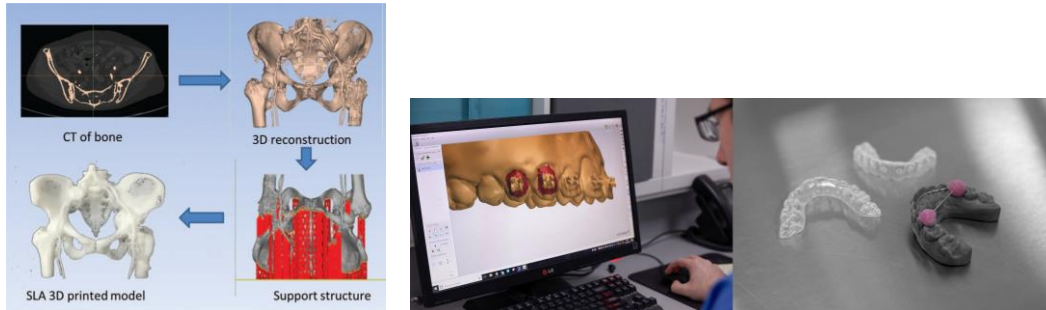
Figure 9. Left) CT data of patient collection, 3D reconstruction and SLA 3D printing of the bone model (Zou et al., 2018); Right) Diverse appliances created by Ashford Orthodontics for supplying orthodontics to clinicians

1.5 Fused-deposition modelling 3D printing

Although conceptualized in 1989 by Scott Crump, the accessibility of FDM/FFF 3D printer to a large audience has been possible only after the expiration of Stratasys patent in 2009 (US5121329A, 1989) (Figure 10).
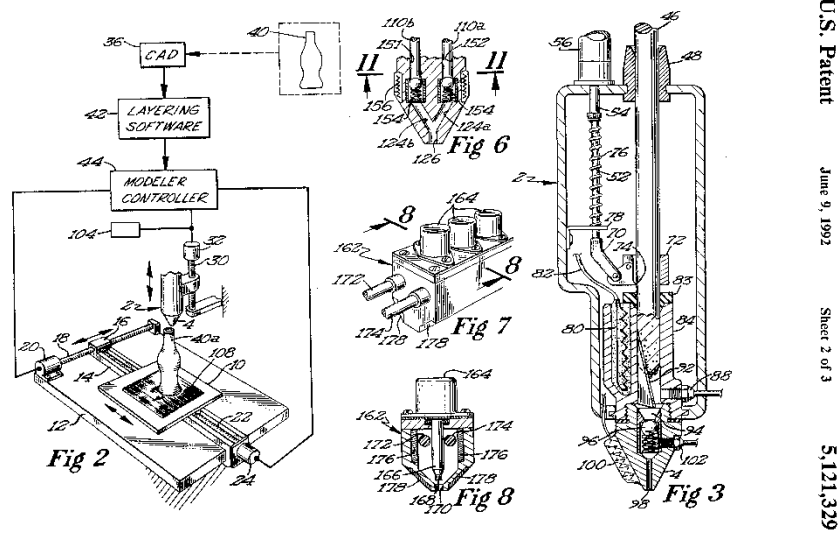
Figure 10: draw of the first 3DP FDM apparatus from Crump's patent, showing the digital set up, the printing process and the extruder-nozzle system

Hence, FDM 3D printing became one of the most investigated AM processes in various realms of production. The main characteristics of this technology that attracted a large audience are: the lowest cost of production, among all the 3DP techniques, the higher accessibility of instruments, and the great reproducibility of printing. Furthermore, FDM is a rapid manufacturing process, with few or absent

post-printing processes. In fact, usually post-processing is merely mechanical, as the removal of supports for printing, and not chemical-based as for other 3DP technologies (i.e. SLA and SSE).

Particularly, FFF belongs to the material extrusion family and consists in the subsequentially deposition of molten thermoplastic materials by heated extrusion heads through small orifices/nozzles (from 0.2 to 1.0 mm). While continuously fed into a heated extrusion chamber (or printcore), materials are deposited as highly viscous fluid in a specific laydown pattern onto the build platform (Mazzanti et al., 2019) (Figure 12). Then object is built in layer-by-layer repeated steps on the workspace and the layers are physically fused together during solidification (Korpela et al., 2013).

The feeds of the FFF printers are synthetic and natural biopolymers in forms of filaments (for instance poly(lactic acid) PLA, poly(lactide-co-glycolide) PLGA, polycaprolactone PCL, polyvinyl alcohol PVA, cellulose ethers and esters).

Hence, the main advantage of this technique in all domains of construction is the possibility of using a wide range of thermoplastic materials in producing custom parts and prototypes with different properties (e.g. flexibility, stiffness, thermal and electrical conductivity).

In pharmaceutical drug delivery and pharmaceutical compounding, FDM may allow to formulate drug materials into complex forms creating patient-tailored dosage forms and devices tailored to unique patient's situations. It has been recently explored to produce medical devices (Muwaffak et al., 2017), implantable systems (Hollander et al., 2016; Le Bras, 2018; Londono et al., 2018; Popov et al., 2018) and dosage formulations, as multi-layer devices (Goyanes et al., 2015b; Haring et al., 2018; Pereira et al., 2019), capsular devices (Maroni et al., 2017; Melocchi et

43

al., 2018; Eleftheriadis et al., 2020) and innovative tablets (Arafat et al., 2018; Sadia et al., 2018), either with immediate or controlled drug release properties (Genina et al., 2017; Đuranović et al., 2021).

These applications of FDM proved during recent years the extreme potential of this 3DP technique in different fields of pharmaceutics.

Particularly, FDM allows endless opportunities to create suitable geometries with diverse levels of complexity (shape and size) and coupling several materials with peculiar functionality in the same print, in order to control the release properties of one or multiple drug substances.

When parameters, inputs (feed materials, drug percentage…) and outputs (model geometries, print speed…) are optimized, huge is the versatility in dosage form production to satisfy patient needs in individualized prescriptions (Figure 11).
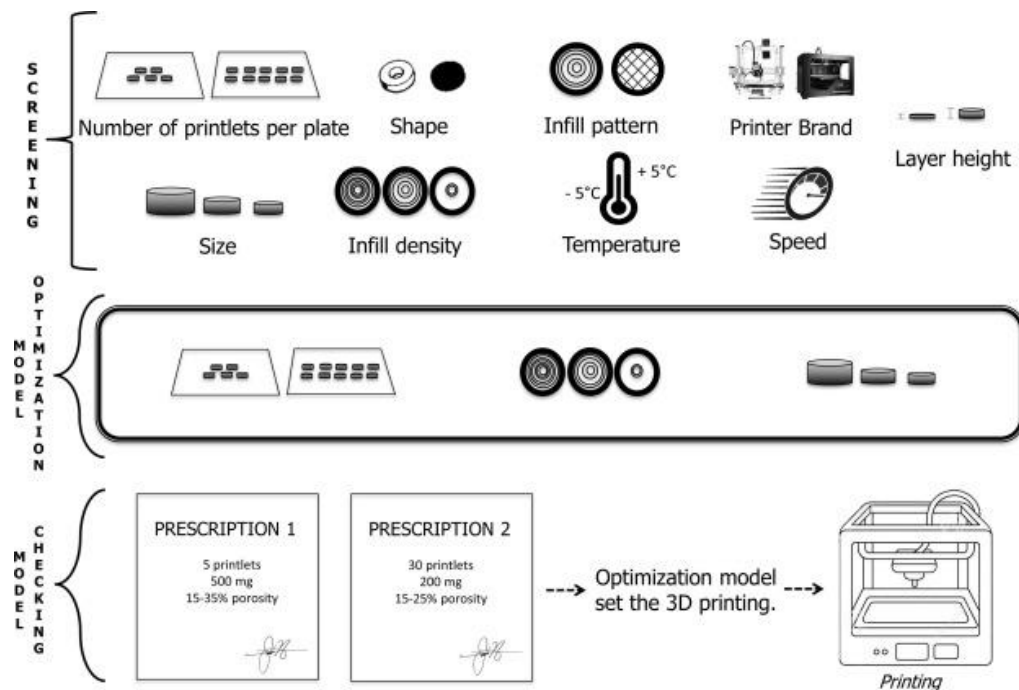
Figure 11. Planning steps of the whole 3D printing setup for personalized prescriptions (Pires et al., 2020)

In fact, once screened the impact of the printed polymeric matrix (such as polymers for immediate or controlled releases) and model shape on a predetermined formulation, the possibility of incorporate variable drug concentrations in the printouts is flexibly attainable using the same optimized key variables (Sandler & Prais, 2016).

However formulating medicines by FDM is a challenge due to the impact of 3D technology on physicochemical properties of drugs and excipients, drug-excipient interaction, polymorphic changes and stability in the dosage form which must be studied on a case by case basis. Moreover, FDM confines the active principles into thermoplastic polymers subjected to elevated temperatures and could produce thermal degradation or undesirable reactions of components. Besides, another relevant criterion to consider is the rheology of melted polymers that can influence the extrudability and printability in terms of deposition behaviour of the used materials.

Therefore, one of the main critical points is the shortage of biocompatible pharmaceutical grade polymers coming in a thermoplastic filament form (blank or drug loaded), with adequate rheological properties and with thermostable active principles (Tan, Maniruzzaman & Nokhodchi, 2018). Indeed, FDM 3DP usually requires the in-house production of loaded filaments, and the most attractive and popular technique for the production of tensile and compressive resistant filaments is the Hot Melt Extrusion (HME). By integrating these two technologies, the range of processable filaments in form of printed formulations is nowadays rapidly in

expansion (Melocchi et al. 2016; Kushwaha, 2018; Ponsar, Wiedey & Quodbach, 2020).

HME is a common industrial method where polymers are thermally processed, melted and mixed in heated chambers. The molten material is then physically extruded through a circular orifice forming a continuous filament, that can be used as feed for FFF 3D printers (Patil, Tiwari & Repka, 2016). (Figure 12).
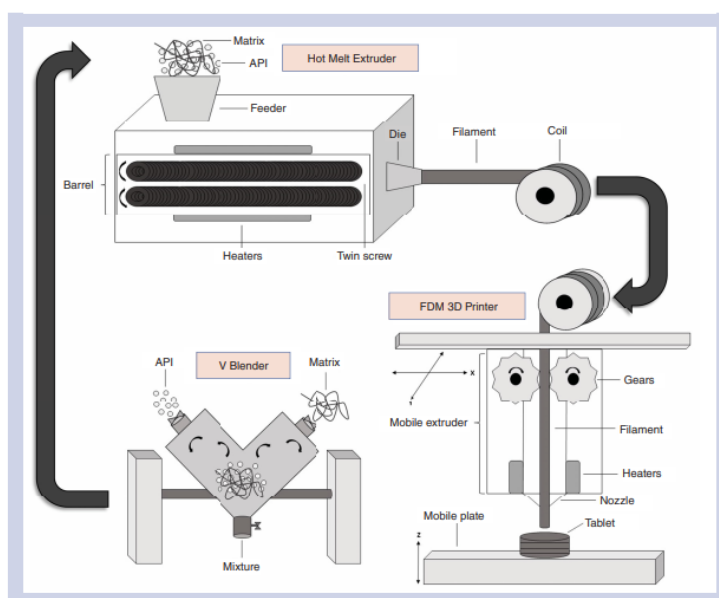
Figure 12. Schematic configuration of the FDM process using hot melt extruded filaments as feeds for pharmaceutical compounding (Cunha-Filho et al., 2017)

The starting materials for the HME are blends of raw powders, in which high amounts of thermostable APIs can be added without affecting the extrusion process.

Frequently, the polymer fraction typically used for the production of printable filaments can be in the range of 35% to 95% w/w of the solid mixture, and the

remaining amount is composed by the drug, or drugs, and the processing adjuvants (such as plasticizers, lubricant and fillers).

The addition of adjuvants (e.g. dibutyl sebacate, Sorbitol, Mannitol, Triethyl citrate, low molecular weight PEG or Triacetin) into the blend for the filament extrusion usually lower the processing temperature of the polymeric matrices allowing gentler melting conditions, decreasing the viscosity but increasing the ductility of filaments (Pereira et al., 2020).

HME is used to produce solid dispersion, usually applied to enhance the solubility of slightly soluble drugs; when coupled with 3DP, it allows the incorporation of higher percentages of drugs into the polymeric matrices compared to other techniques used for drug loading of FFF feeds (i.e. soaking or casting) (Verstraete et al., 2018). Moreover, HME ensures for high dose flexibility, incorporation of different drugs using identical matrices/excipients, and rapidity of filaments production (Sadia et al., 2016).

With the adequate selection of pharmaceutical-grade polymers (PVA, PVP, cellulose-derived polymers or acrylates), thermostable APIs and opportune excipients (such as inert fillers, plasticizers and extrusion enhancers), HME followed by FDM 3DP can guarantee the production of high-quality novel dosage systems.

1.5.1 Polyvinyl alcohol: a milestone for FDM

One of the most used polymeric raw material for FDM 3DP (usually preceded by HME) in the pharmaceutical branch is PVA.

PVA is a versatile artificial polymer with a semi-crystalline nature; it is widely used in the pharmaceutical sector, cosmetics, paper, textiles and food

industries. In fact, it is considered a safe pharmaceutical excipient from both United States and European Pharmacopoeias (USP and Ph.Eur.). Its plenty of applications is due to the biodegradability, biocompatibility, atoxicity, noncarcinogenic and bio-adhesive characteristics. Moreover, PVA is an excellent film forming, coating agent, taste/odour masking, stabilizer and binder; furthermore, it facilitates ingestion and swallowing or acts as a lubricant (Nagarkar & Patel, 2019).

PVA is synthesized from the hydrolysis of polyvinyl acetate (PVAc) (Figure 13) by alkaline catalyst, such as sodium hydroxide. The degree of hydrolysis of its acetate groups influences its melting range, with a peak at about 180°C for partially hydrolysed PVA and at 230°C for fully hydrolysed PVA (Konta et al., 2017; Aslam, Kalyar & Raza, 2018).
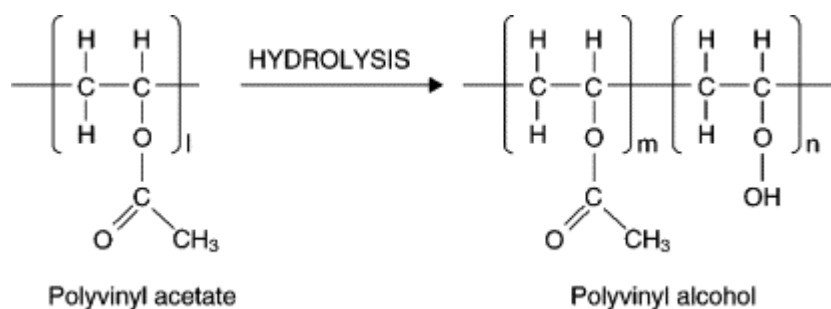
Figure 13. Synthesis of PVA hydrolysing polyvinyl acetate (PVAc)

The highly hydrolysed PVA is the most appropriate for coatings and barrier forming for pharmaceuticals and food packaging of consumer goods (protecting products from oxygen, moisture, and other environmental components). However, the high content of hydroxyl groups makes it particularly akin to water molecules and, thus, sensitive to the surrounding ambient conditions, as the relative humidity (Solaro, Corti & Chiellini, 2000). The main properties involved in the extensive

usefulness of PVA in advanced medical fields are the bio-inertness and the compatibility, which allow its use in drug delivery systems and medical devices, as for drug carrier and tissue engineering approaches.

Considering the domain of 3DP sciences, the thermoplastic properties of this polymer have been the engine for its use in extrusion-based technologies (i.e. FDM and SSE) (Sadia et al., 2016). Particularly for the sector of FDM prototyping, PVA is exploited as a water-soluble support material for layer-by-layer construction of models with complex geometries and features, adhering to other polymeric materials where overhang angles are present. Then, the PVA support is removed from the final object manually or often by solubilizing it into hot aqueous solutions.

Considering its avails in FDM 3DP of pharmaceuticals, the flexibility in printing PVA has been recently studied for the manufacture of various PVA-based drug delivery systems, loaded both using the soaking method (resulting in a very low amount of drug loaded, less than 6% w/w) or by the production of drug-containing filaments by HME (reaching up to 40% w/w of drug amount in the final forms) (Figure 14) (Tagami et al., 2017; Tagami et al., 2018; Palekar et al., 2019; Wei et al., 2020).

Figure 14. Filaments obtained via HME with 80% of PVA and 20% of APIs (left: Carvedilod, right: Haloperidol) (developed by Wei et al., 2020)

Mainly, PVA has been printed *via* FDM 3DP, combined with HME, to produce devices for multi-dose administration of a single active. This aim has been reached by arranging the distribution of API concentration in the device system and by printing gradients of active or chambers containing different contents of the drug (Qijun et al., 2017). Moreover, the possibility of multiple-drug solid dosage forms whose release is governed by different internal printing configurations (a multilayer device or two-compartment device) was investigated and evidenced (Figure 15) (Goyanes et al., 2015; Pereira et al., 2019). Thus, these studies explored the potential of HME and FDM to fabricate polypills with one or more actives controlling the release profiles by designing specialized patterns unattainable with conventional manufacturing methods. This characteristic is essential for the customization of products for elderly patients who undergo multi-drug therapies or for patients who take cocktails of drugs for chronic illness.
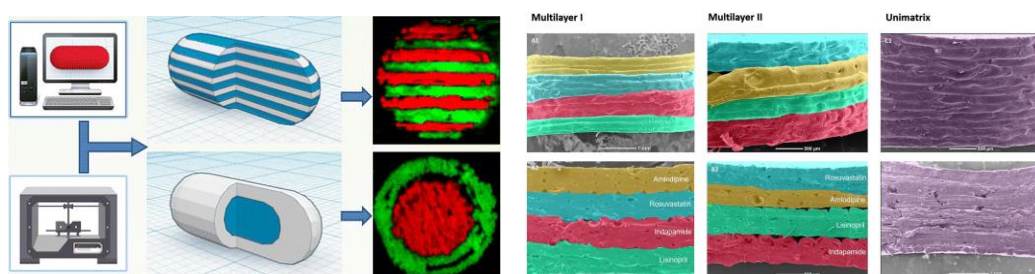
Figure 15. Left) The multilayer device and the two-compartment device carrying two different APIs (developed by Goyanes et al., 2015); Right) The polypill architecture with four different APIs (developed by Pereira et al., 2019)

Furthermore, immediate or modified releases have been realized also by modifying printing parameters, such as infill percentages and patterns (Figure 16),

or by using PVA added with thermostable excipients for the production of filaments and printouts.
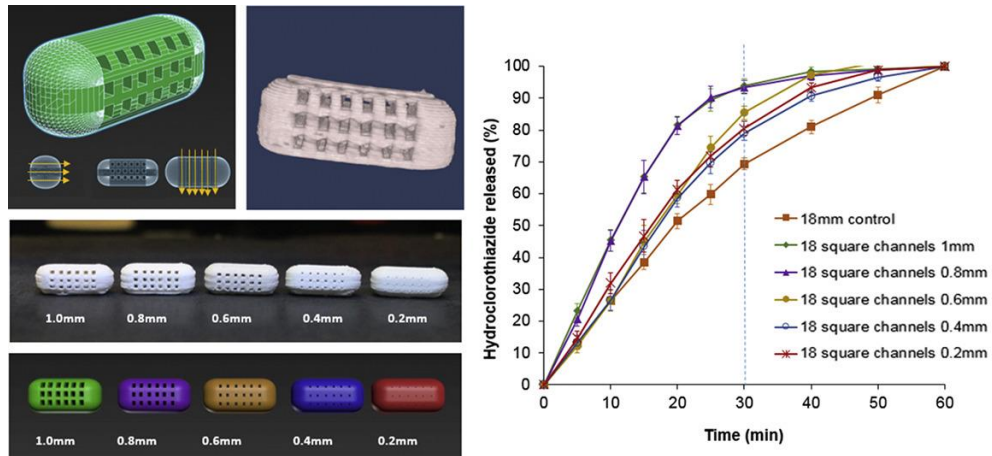
Figure 16. Left) Images of channelled designs of PVA printouts for oral drug delivery; Right) Release profiles modulated by the structures design (developed by Sadia et al., 2018)

In fact, devices with immediate release, sustained and controlled release devices have been successfully produced by numerous researchers as tablets, compartmentalized capsules, gastro-retentive floating systems or orodispersible films (Figure 17) (Jamróz et al., 2017; Ehtezazi et al., 2018; Sadia et al., 2018; Matijaši´c et al., 2019; Wei et. Al, 2020; Charoenying et al., 2020). Most of these works have underlined the feasibility of tailoring not only the shape, the appearance and the drug content of the formulations, but also the release profiles according to therapeutical needs. Moreover, the necessity of just few excipients to develop these formulations is a dominant benefit for pediatrics and geriatrics, to whom forms developed with precise doses and the required release profiles by resorting to

minimal excipients are a fundamental prerequisite to reduce therapeutic complications for these categories of patients.
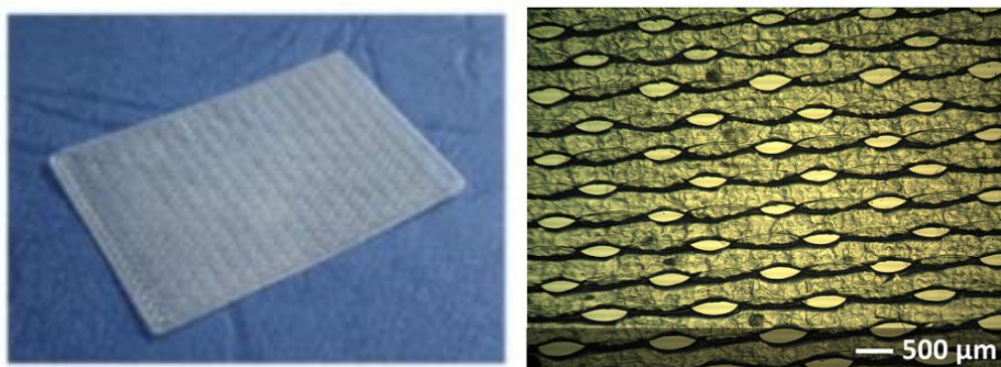
Figure 17. Microphotographs with visible light images of PVA 3D printed orodispersible film (developed by Jamróz et al., 2017)

All these explanatory examples highlight the immense possibility of exploiting the thermoplastic features of PVA for the manufacture of innovative drug delivery systems, especially for oral administration, when FDM 3DP is coupled with HME. PVA is then one of the most versatile polymers that can allow innumerable possibilities of use also in 3DP field and precision medicine.

1.6 Semi-Solid Extrusion 3D printing

Semi-solid extrusion (SSE), sometimes called pressure-assisted micro-syringe (PAM) printing, is an AM technique, part of the deposition systems based on the extrusion through nozzles, together with FDM (Azad et al., 2020) (Table 3).

The distinctive aspect of the SSE technology is the extrusion process starting from semi-solid materials (gels or pastes) which, after the syringe-extrusion, undergo post-processing phases, including drying or cooling of the printed gels, often achieved by mild or fast evaporation of the solvent (Cui et al., 2019). Among the numerous printing technologies currently available, the extrusion of semisolids is one of the latest investigated 3DP technique, particularly for bioprinting and tissue engineering. However, SSE application in pharmaceutical compounding is nowadays rapidly growing for the possibility of using traditional pharmaceutical excipients (Li et al., 2018), offering an acceleration about the material exploitability, characterization and processability also in the medicines field.

Table 3. Comparison between advantages and limitations of FDM and PAM 3D printing technologies (Azad et al., 2020)

Technology	FDM 3D Printing	PAM 3D Printing
Advantages	• Low-cost printing technology. • No post-processing is required. • Better drug uniformity.	○ Works at room temperature. ○ High drug loading is achieved. ○ Suitable for multi-drug pill (polypill) printing.
Limitations	• High-temperature processing is required which is not suitable for thermally labile drugs. • Pre-processing steps of filament making are required. • Lack of suitable biocompatible/biodegradable thermoplastic polymers. • Active pharmaceutical ingredient (API) degradation may occur due to the high processing temperature.	○ Post-processing, drying, is required. ○ Polymer rheological properties impact on structure formation and printing process. ○ Printing resolution is depended on nozzle size. ○ Toxicity and drug instability may occur due to the usage of organic solvents.

The rheological properties, as viscosity, shear rate and stress, and chemical properties of the starting materials, as miscibility of components, can significantly affect the extrusion/printing process. Indeed, usually, the extrusion is governed through pneumatic or mechanical pumping (Figure 18) considering the viscoelasticity and the resilience of the used feeds when stresses are applied to the system.
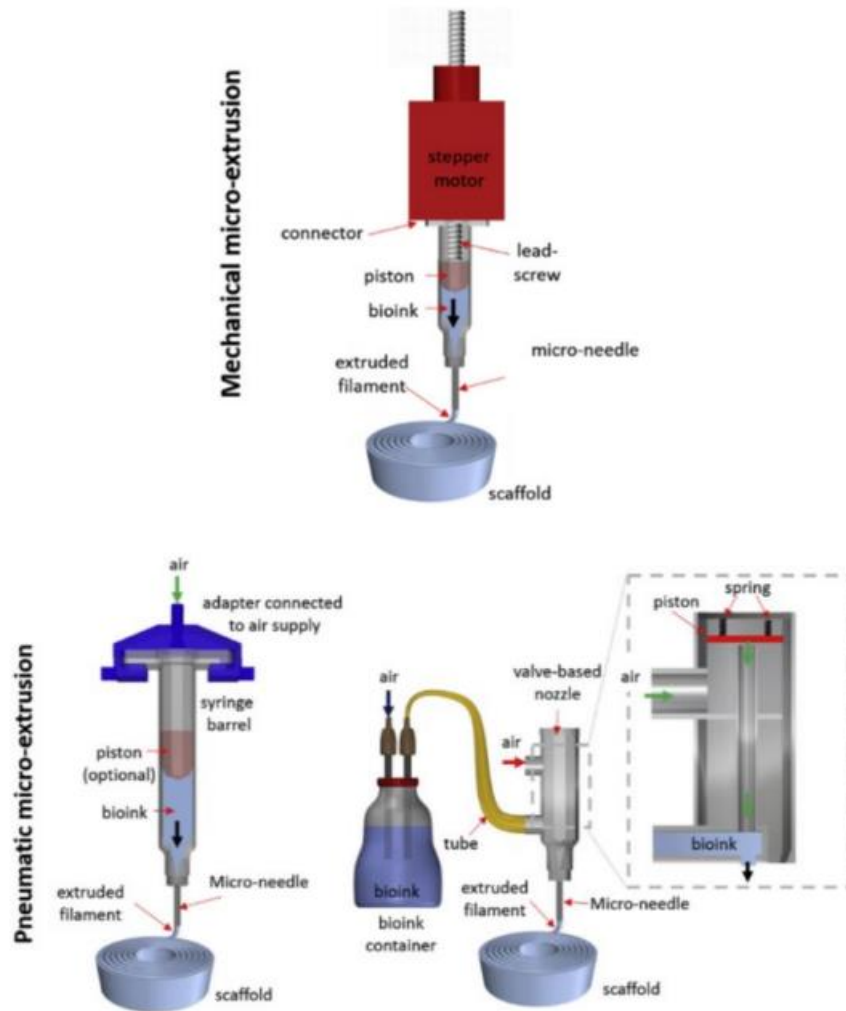
Figure 18. Mechanical and pneumatic micro-extrusion systems (Ibrahim et al., 2016)

An immediate advantage of this technique in pharmaceutical compounding is the simplicity in the loading of active ingredients, as the drug and excipients can be added directly to a gel base. In fact, the content of excipients and APIs can be

controlled much more easily than other techniques, because it reflects the concentration of the added compounds into the soft feed (Firth et al., 2018). The real potential of semi-solid extrusion lies in the low printing temperature and mild processing conditions, thus allowing the use of a wide range of APIs inoperable with FDM (Khaled et al., 2015).

One of the limitations of SSE compared to other 3DP techniques is the low printing resolution of the final product, because this process exploits orifices of relatively large dimensions (400-800 µm) in order to accommodate and extrude viscous material (Vithani et al., 2019).

Nevertheless, SSE technology has demonstrated the possibility of creating complex formulations (Conceição et al., 2019) with the opportunity of being customized not only for the dose (Cui et al., 2020; Yan et al., 2020) but also for the release profiles (Khaled et al., 2018) (Figure 19) and patient acceptability.
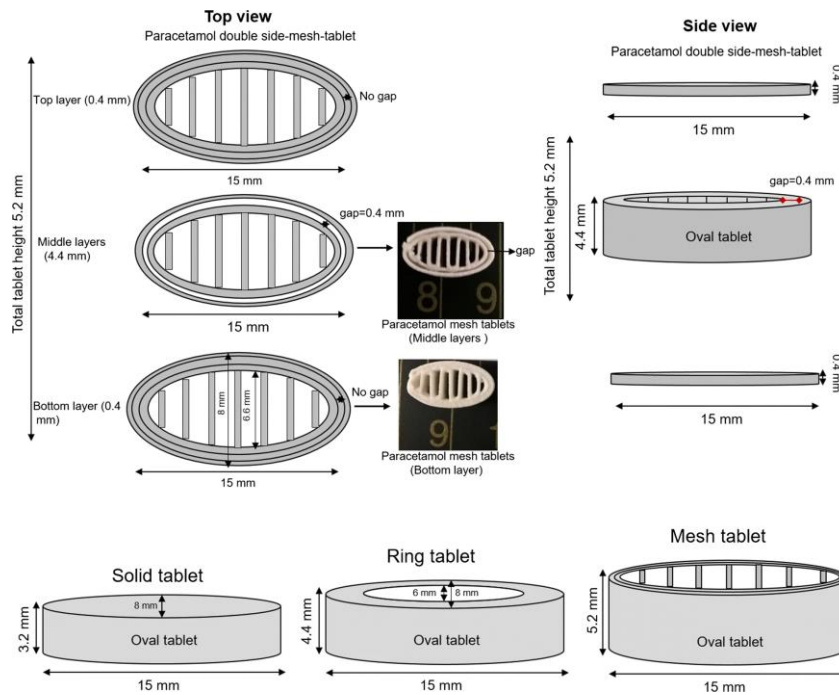
Figure 19. Schematic structures of paracetamol tablets obtained via SSE 3DP using different geometric shapes (developed by Khaled et al., 2018)

Regarding small-scale pharmacy applications and patient compliance of SSE 3D printed forms, in 2019 the first single-centre clinical study was conducted on pediatric patients in the Pharmacy Department of the Clinic University Hospital in Santiago de Compostela (Spain).

Particularly chewable formulations with different dosages, colours and flavours have been administered to children from 3 to 16 years old for the treatment of maple syrup urine disease.

This study demonstrated not only the enhancement of these printed products in controlling the target blood concentration of the active, but also the high

acceptability of the SSE dosage forms in the hospital setting for niche applications (Goyanes et al., 2019).

Hence, the applicability of SSE 3D in the medical arena is now becoming a pragmatic and suitable approach to prepare compounded medicines with improved properties.

1.6.1 Alginate vs semi-solid extrusion

SSE technology, although in its infancy in the pharmaceutical field, has been extensively adopted in other health sectors. Significant signs of progress have been achieved in bioengineering, over the past decade, exploiting the SSE advantages in the biological area for regenerative medicine applications and for tooling of *in vitro* studies (Costantini et al., 2019).

In fact, bioprinting is an additive manufacturing process based on the extrusion of soft feeds containing cells and biomaterials, often referred to as bio-inks. Compared to classical culture strategies, bioprinting is an alternative approach that offers the possibility of distributing several cell types in the desired spatial organization and with the necessary structural complexity (Holzl et al., 2016). In order to achieve an optimal 3D deposition, the inks require a rapid sol-gel transition or an *in situ* transition from fluid to a solid gel state.

For this aim, alginate-based inks have been broadly used mainly deposited in a solution of calcium chloride, or *vice versa*, to induce an immediate ionic crosslinking (Figure 20).
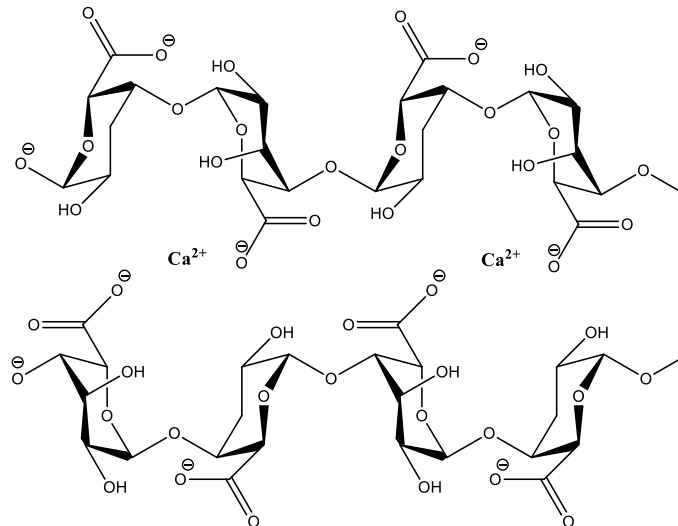
Figure 20. The three-dimensional network after ionotropic gelation of β-l-guluronate blocks of SA and divalent cations, as Ca^{2+}

Recently, a new approach that allows simultaneous and separate extrusion of the alginate-ink and crosslinking gels, coming into contact at the final tip of the print head, has been optimized (Colosi et al., 2016). The extruder consists of two coaxial capillaries filled separately and, with respect to the configuration of the feeds, a bulk or a hollow filament can be obtained (Zhang et al., 2016). An advantage of the coaxial approach is the decoupling of the rheological properties of the feed material from its printability. However, even deepened in the biological domain, to date, this technology has not been still investigated in the pharmaceutical compounding, opening perspectives for novel applications of alginate in co-axial extrusion for solid dosage forms.

2. SECTION I

The effect of polymer particle size on process efficiency: production of customizable 3D printed tablets via fused-filament-fabrication-3D-printing technology from hot melt extruded poly(vinyl alcohol)-Ciprofloxacin filaments
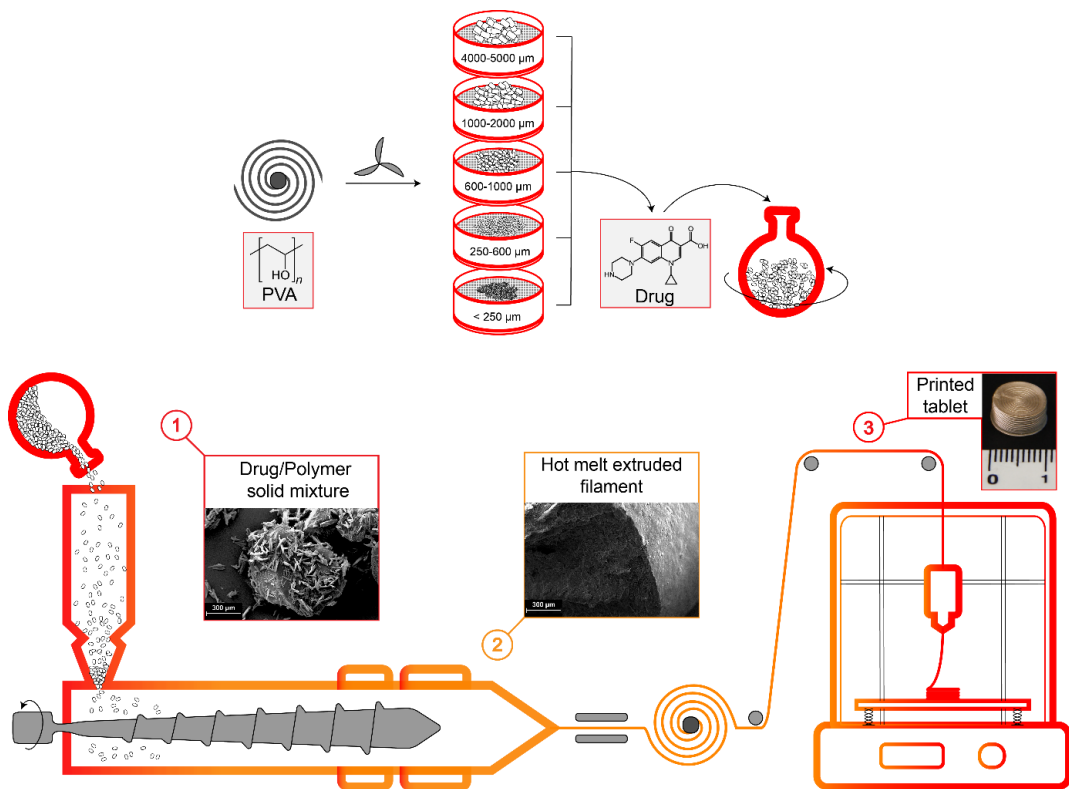
Based on the article

Saviano M., Aquino R.P., Del Gaudio P., Sansone F., Russo P.*, Poly(vinyl alcohol) 3D printed tablets: The effect of polymer particle size on drug loading and process efficiency*, International Journal of Pharmaceutics, Volume 561, 20 April 2019, Pages 1-8

2.1 Scientific background and research aim

Continuous advances in FFF 3DP technology are expected to induce improvement in medical and health outcomes, with new challenges, especially in drug manufacturing and pharmaceutical compounding.

FFF can be considered a rapid technique for the development of innovative personalized drug delivery systems, named printlet[TM] in case of oral drug dosage forms (Goyanes et al., 2017). Formulating medicines by FFF is a challenge due to the impact of 3D technology on physicochemical properties of drugs (mainly thermal stability), thermoplastic polymers and excipients, drug-excipient interactions and polymorphic changes which must be studied on a case-by-case basis.

The main bottleneck for applying this process in pharmaceutical production is the lack of biocompatible and biodegradable polymers in form of API laden filaments. Thus, one of the most delicate steps of the whole process is the drug loading of the thermoplastic polymers to obtain the filament used as feedstock for FFF 3D printers, together with weak information about the effect of design and processes variables on the final product and on drug release patterns.

There are countless approaches for the mixing step of the polymer and the drug, but on the contrary only two main methods can be used to obtain drug-loaded filaments: hot melt extrusion (HME) and the soaking method. The HME is a process where heat and pressure are applied to melt thermoplastic materials and force it through a die, under controlled condition (Tan et al., 2018). This technique has been recently used by the pharmaceutical laboratories for the production of oral dosage forms and drug-device combination products, especially coupled with FFF for advanced delivery systems (Korte and Quodbach, 2018; Musazzi et al., 2018). The

soaking method involves the soaking of polymer filament in a drug-saturated solution (Beck et al., 2017; Goyanes et al., 2015a), in order to allow the drug to diffuse into the polymer. This method, even if easier and less expensive compared to the HME, leads to lower and not very reproducible drug amounts in the filament.

Among the polymers used in 3DP, PVA is a water-soluble support material, helping the print of intricate geometries with a good thermal stability and a good adhesion to several polymeric materials. Moreover, the common use of PVA as a safe excipient in drug formulations makes this polymer a proper candidate for the production of drug-loaded filament.

For these reasons, PVA has been already used for drug filament production, both using the soaking method with very low amount of drug loaded (1750 ± 230 µg/g and 0.06%-6.25% w/w) (Tagami et al., 2017; Goyanes et al., 2015b) and the HME methods (Palekar et al., 2019; Tagami et al., 2018) with higher results (up to 46% w/w) (Pietrzak, Isreb & Alhnan, 2015).

In these studies, adequate attention has not been paid to the particle size of the polymer, that can influence both the adhesion of the drug and the extrudability of the drug/polymer mixture.

In most cases, a commercial spoil of PVA has been simply cut into small pieces (~2 or 1 mm), milled and sieved through a 1000 mesh sieve (Goyanes et al., 2015c; Li et al., 2017), reaching a maximum drug loading of 9.5% w/w. Moreover, even if the drug amounts loaded into the PVA filament *via* HME are sensibly higher compared to the passive diffusion approach, they are still inadequate in the case of thermolabile APIs and high dose drugs.

As the production of oral pharmaceutical formulations using 3DP technologies has been intensively investigated over the past years in terms of

geometry, shape and infills, the methods for material preparation or drug loading have varied in different studies. Thus, a standardized method for the loading of APIs into a polymeric carrier for 3D printing purposes is not available yet (Shaqour et al., 2020).

In this work, in order to identify the optimal polymer particle size able to improve the process efficiency and to maximize the versatility of the 3DP essential for personalized therapies, a systematic study on the influence of polymer size distribution on the mixing-extrusion-printing steps was conducted. Thus, the aim of this study was to investigate the potential of hot melt extrusion of APIs and PVA batches (with different particles size and drug concentrations) to produce drug-loaded filaments, coupled with FDM-3DP technology for printing customized oral drug delivery systems (or rather printlets[TM]).

Several batches of PVA with different size distributions were obtained by cryomilling of the polymer and diverse solid mixtures were prepared, using the obtained five PVA batches (sieves range: 4000–5000 μm, 1000–2000 μm, 600–1000 μm, 250–600 μm, <250 μm) and Ciprofloxacin hydrochloride as active compound in different ratios ratio (from 10% to 35% w/w of API). Then, these solid mixtures were extruded as filaments *via* hot melt extrusion technique. Operative specifics and printer's parameters were tuned and refined for an optimal print of drug-loaded filaments into the desired dosage forms, i.e. cylindrical printlets[TM], fully characterized in terms of homogeneity, process efficiency, physical properties, drug content and release kinetics.

The Ciprofloxacin hydrochloride was selected for its widespread use to treat different types of bacterial infections and for its high melting and degradation temperatures, which should ensure the drug stability after thermal treatments typical

of extrusion and 3D printing. Moreover, being an antibiotic administered at rather different dosages both in paediatric and in geriatric patients (from 10 to 20 mg/kg up to 1 g for controlled release formulations), Ciprofloxacin was a good candidate for the design of customizable oral drug delivery FFF-3D printed systems.

2.2 Materials and Methods

2.2.1 Materials

Ciprofloxacin hydrochloride (CipHCl) was kindly donated by Genetic S.p.A., Fisciano, Italy. Poly(vinyl alcohol) (Natural PVA, Ultimaker filament for 3DP, density 1.23 g/cm3, Ultimaker, Netherlands) was used to form solid dispersions/physical mixtures with CipHCl; Dibutyl Sebacate (technical grade CAS 109-43-3, Sigma- Aldrich, Italy) was used as oily plasticizer. NaCl (CAS 7647-14-5) and HCl 37% w/w (ACS reagent, CAS 7647-01-0) used for the dissolution medium were obtained from Sigma-Aldrich, Italy. Acetonitrile, Super Gradient Reagent Ph. Eur., USP, ACS (CAS 75-05-8, VWR Chemicals, France), orthophosphoric acid 99% (CAS 7664-38-2, Carlo Erba Reactifs, Italy) and triethylamine (CAS 121-44-8, Carlo Erba Reactifs, Italy) were used as mobile phase for high performance liquid chromatography.

2.2.2 Solid mixture production

Starting from dried Ultimaker 99% natural poly(vinyl-alcohol) spool, several batches of PVA with different size distributions were obtained by milling spool segments after a 5-minute stay in dry ice and sieving the obtained material. The polymer batches obtained and analysed were: 4000–5000 μm, 1000–2000 μm, 600–1000 μm, 250–600 μm,<250 μm. These granules were manually mixed in a 250 mL balloon with the drug, at different drug/polymer ratios (from 10% w/w to 35% w/w of CipHCl) using 0.20% w/w of dibutyl sebacate to promote powder adhesion on pellets/powders surface and to aid the extrusion process and the FFF 3DP.

2.2.3 Hot melt extrusion of drug-loaded filaments

Fifteen grams of each of these physical blends were heated and mixed using a single-screw filament extruder (Noztek Touch HT, Noztek, England) at a working temperature of 160 °C–175 °C and a rotational speed of 30–60 rpm, depending on the processed material. These parameters have been optimized for hot melt extruders with a single screw (the configuration of the screw is shown in figure 1.1) and with a pre-heater band at the end of the mixing zone and a second heating chamber before the nozzle (exit diameter of 0.30 mm).

Fig. 1.1: Screw configuration of the single-screw extruder

The rotational force (torque force) applied by the rotating screw on the fused material causing its acceleration was 8.10·Nm at the highest motor speed (60 rpm). Only the drug-loaded filaments with a diameter of 2.85 ± 0.15 mm were used as feedstock for the FFF 3DP process. The total yield of the extrusion process (Y_{Tot}) and the yield in printable filament (Y_{3DP}, i.e. with a diameter of 2.85 ± 0.15 mm) obtained after the loading of 15 g of drug/polymer mixture into the extruder were calculated as reported in Eqs. (1) and (2), respectively.

$$(1) \ Y_{Tot} = \frac{\text{g of filament extruded}}{\text{g of drug/polymer mixture loaded}} \ x \ 100$$

$$(2) \ Y_{3DP} = \frac{\text{g of printable filament extruded}}{\text{g of drug/polymer mixture loaded}} \ x \ 100$$

2.2.4 Digital modelling and 3D printing

Templates for FFF-3DP were designed with CAD software Rhinoceros 5 (Robert McNeel & Associates, McNeel Europe); model geometries were exported as stereolithographic files (.stl) and then processed by the slicing software Cura 3.2.1 (Ultimaker, Netherlands), creating the gcode file used by the 3D printer (Fig. 1.2). Printlets were obtained using a commercial FFF 3D printer Ultimaker 3 (Ultimaker, Netherlands). Printer's parameters and operative specifics were refined to obtain an optimal print of the drug-loaded filaments and the best resolution. The designed flat faced cylindrical printlets were 10×10×5 mm in size.
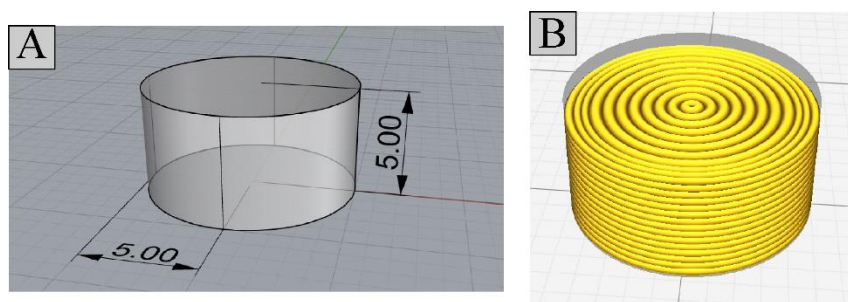
Fig. 1.2. A) Printlets digital template (CAD model); B) sliced model (CAM model).

2.2.5 Drug content analysis of solid mixtures, drug-loaded filaments and printlets

Ultraviolet–visible spectrophotometry (Evolution 201 UV–vis Spectrophotometer, Thermo Fischer Scientific Inc.) was used to monitor the drug content throughout the extrusion and printing process, in physical blends, drug-loaded filaments and printlets. Quartz cells with a 1 cm optical path length were used for all measurements and UV absorbance was measured at 272 nm. The linear relationship of absorbance *vs* CipHCl concentration was verified both in water and in dissolution medium in a range of concentration between 2.0 and 10.0 μg/mL.

For drug content analysis, about 150 mg of drug/polymer mixture, 175 mg of filament segment or 1 printlet (about 350 mg) were precisely weighed and dissolved in 50 mL of distilled water. The drug content was evaluated in different sections of the filament (every 10 cm for the non-printable filament; at the beginning and at the end of the filament segment selected for the print). The solutions were opportunely diluted and analysed by UV spectroscopy.

Aiming to investigate the stability of the drug after the high temperature exposure during the extrusion and the 3D printing processes, an HPLC qualitative and quantitative analysis was run in printlets obtained extruding 250–600 μm PVA and 35% w/w CipHCl, after a 6 months storage at room conditions. The drug concentration was evaluated according to the method described by the European Pharmacopoeia 9th Edition. Briefly, 20 μL of samples were injected in octadecylsilyl silica gel column Nucleodur® C18 Gravity, Macherey-Nagel GmbH & Co. KG, Germany (pore size: 5 μm, length: 0.25 m, diameter: 4.6 mm), using as mobile phase 13 volumes of acetonitrile and 87 volumes of 2.45 g/L solution of phosphoric acid, previously adjusted to pH 3.0 with triethylamine. The mobile

phase was pumped at a flow rate of 1 mL/min (Agilent 1100 Series HPLC, Agilent Technologies, USA) and the UV detector was set at 272 nm. The printlets (about 350 mg) were completely dissolved in 100 mL of distilled water. The solution was then filtered (45 μm filter Chromafil RC-45/25, Macherey-Nagel, Germany) and opportunely diluted with mobile phase prior to HPLC injection.

Finally, a comparison between a 0.9 mg/mL CipHCl solution and the undiluted dissolved printlet solution (about 0.9 mg/mL CipHCl) was made, in order to highlight any differences in the chromatographic peaks, prolonging the run time up to 2.3 times the CipHCl elution time as recommended by European Pharmacopoeia 9th Ed.

2.2.6 Morphological analysis

The diameter of drug-loaded filaments and the physical dimensions of the printlets were measured with a digital calliper (resolution: 0.01 mm; accuracy: ± 0.03 mm). Scanning Electron Microscopy (SEM) (Carl Zeiss EVO MA10 SEM, SMT GmbH, Oberkochen, Germany) (Manniello et al., 2017) allowed observing the surface interaction between drug and PVA pellets/ powder as well as the microarchitecture of the drug-loaded filaments and printlets. Moreover, filaments and printlets were photographed with a single-lens reflex camera (Canon EOS 600D; parameters: f-stop: f/6.3, shutter speed: 1/5 s, ISO 200) to obtain macroscopic and realistic images of the process products.

2.2.7 Particle size analysis of CipHCl

Laser Light Scattering (Beckman Coulter LS 13 320, Beckman Coulter Inc., Indianapolis, USA) was used to analyse CipHCl particle size. The drug was placed in dichloromethane under constant stirring, using the micro liquid module; 60 s analyses were conducted in triplicate.

2.2.8 Thermal characterization

Differential Scanning Calorimetry (DSC) of raw materials, physical blends, drug-loaded filaments and printlets was performed with a DSC 822e (Mettler Toledo, Germany). Measurements were carried out from 25 °C to 350 °C at a heating rate of 10 °C/min (Cerciello et al., 2017); when necessary, a dehydration cycle was performed. Nitrogen was used as an inert purge gas with a flow rate of 150 mL/min for all the experiments and TA standard aluminium pans (40 µL) and predrilled lids were used with an average sample mass of 8–12 mg. Data were collected with Mettler Toledo STARe software and analysed using Thermal Analysis Instruments; all the curves were interpolated to obtain the enthalpy of transformations related to the area under the peaks and to characterize thermal events and degradation profiles of materials.

2.2.9 Porosity of the printlets microstructure

Helium Intrusion porosimetry (AccuPyc II 1340 Gas Pycnometer, Micromeritics, Georgia, U.S.A.) was used to define the density and the porosity of printlets internal structure. Printlets deriving from 250-600 µm PVA batches and 35% w/w of API were analysed using helium as inert gas and displacement medium

for measuring accurately the void fraction of the 3D printed structures. Data were collected in triplicate and the average of porosity was expressed as percentage.

2.2.10 FT-IR analysis

Solid State Fourier Transform Infrared Spectroscopy was performed using Perkin Elmer FT-IR/NIR Spectrometer (Perkin Elmer Inc., USA) equipped with Spectrum Software version 10.5.2. Spectra of raw materials, drug-loaded filament and printlets were acquired at room temperature, recorded in a spectral range over 600-4000 cm^{-1} with background subtraction; resolution of 2 cm^{-1}, scan number of 128 and scan speed of 0.2 cm/s.

2.2.11 Dissolution tests

The dissolution medium was prepared according to European Pharmacopoeia 9th Edition, adding 250 mL of 0.2 M sodium chloride to 425 mL of 0.2 M hydrochloric acid, then mixed with distilled water up to 1000 mL. Finally, the pH was adjusted at 1.2 with HCl 12 N. Drug release profiles from filaments and printlets were obtained using a USP dissolution apparatus I (for printlets) and II (for filaments segments) (AT7 Smart Dissolution Tester, Sotax Corporation). In each assay, the samples were placed in the basket or directly into the vessel under constant stirring at 75 rpm in 750 mL of medium with controlled pH 1.19 ± 0.06 at 37 °C $\pm$ 0.5 °C. Tests were conducted in triplicate and 5 mL medium aliquots were taken at specified time lapse; drug concentration was monitored via UV/vis-spectrophotometry at 272 nm.

2.3 Results and discussion

2.3.1 Hot melt extrusion of drug-loaded filaments starting from solid mixtures

With the aim of studying the influence of PVA particle size on the drug loading and on the mixture-extrusion-printing processes, the first step of this research was the production of several solid mixtures, starting from five PVA batches (4000–5000 µm, 1000–2000 µm, 600–1000 µm, 250–600 µm,<250 µm) and CipHCl (particle size distribution determined with Laser Light Scattering: 21.43 ± 1.68 µm) at the concentration of 10% or 35% w/w.

Before the milling process, PVA was kept in dry ice for 5 min in order to prevent the overheating of the polymer. The physical blends CipHCl/PVA were produced by manually mixing the polymer pellets and the crystalline API in presence of the plasticizer (dibutyl sebacate) to enhance the adhesion of the API on the polymer surface and to facilitate the extrusion of the solid mixtures *via* HME.

All these solid mixtures were extruded into filaments using a single-screw filament extruder. The temperature and motor speed values have been optimized (Table 1.1) for a hot melt extruder with two heating chambers: the temperature T_2 was set at 175 °C, while the pre-heater temperatures T_1 were modulated according to the PVA sizes, and the motor speed was defined according to the different compacting properties of the processed mixture. In the case of the finest fraction there was no sufficient torque force to promote the extrusion process. Therefore, this PVA size range was excluded from the successive steps, but it should not be discarded the possibility of using finest powder (less than 250 µm) with a double

screw extruder having higher extrusion torque force, in order to explore the homogeneity of the deriving filament in terms of diameter and composition.

Table 1.1: Temperatures and motor speed used in the extrusion process of solid mixtures with different PVA particle size and with 10% and 35% w/w of CipHCl

PVA particle size	T_1 Pre-heater band (°C)	T_2 (°C)	Motor Speed (RPM)
4000-5000 µm	170	175	30
1000-2000 µm	165	175	30
600-1000 µm	165	175	40
250-600 µm	160	175	50
< 250 µm	No extrusion		

All the printable extruded filaments with a diameter of 2.85 ± 0.15 mm were used as a feedstock for the FDM-3DP process; the yield of the extrusion process starting from 15 g of drug/polymer mixture is represented in Table 1.2.

Table 1.2: Total yield and yield in printable filament (i.e. with a diameter of 2.85 ± 0.15 mm) after the extrusion of 15 g of solid mixtures with different PVA particle size and with 10% and 35% w/w of CipHCl

PVA particle size	Total Yield (%)	Yield in printable filament (%)

	10 % CipHCl	35 % CipHCl	10 % CipHCl	35 % CipHCl
4000-5000 µm	30.8 ± 0.8	-	15.4 ± 0.4	-
1000-2000 µm	27.2 ± 0.5	39.1 ± 9.0	14.1 ± 0.3	13.7 ± 3.1
600-1000 µm	31.0 ± 0.3	45.2 ± 7.0	16.0 ± 0.2	16.1 ± 2.5
250-600 µm	25.4 ± 0.6	38.4 ± 7.2	12.2 ± 0.3	13.9 ± 2.6

2.3.2 Digital modelling and FFF 3DP of drug-loaded filaments

First of all, blank printlets with the commercial PVA spool were produced to define the correct parameters for the printing, and then slicing and printer's parameters were refined for an optimal print of the drug-loaded filaments and the best resolution in terms of layers adhesion and of accuracy and preciseness in the printed objects, compared to the digital model (Table 1.3).

Table 1.3: Slicing parameters and operative specifics of the FDM-3DP process

3D-Printer parameters		**Slicing parameters**	
Nozzle diameter	0.40 mm	Layer Height	0.30 mm
Printing Temperature	195°C	Line Width	0.35 mm
Build Plate Temperature	80°C	Wall Thickness	1.00 mm

Print Speed	8.00 mm/s	Number of shells	3
Travel Speed	150 mm/s	Infill Percentage	100%
		Infill Pattern	Concentric

The same printing file was then used for all the printlets; a concentric pattern was used for its fitting the printlet digital shape and an infill percentage of 100% was set to obtain the highest density and, therefore, the highest dosage. The wall thickness used was 1 mm with 3 shells to give to the printlets a dense shell modulating API release and the erosion of the inner polymer matrix.

The printing temperature was maintained at 195 °C throughout the printing step, below the degradation temperatures of the PVA matrix and the CipHCl; while the building plate temperature was set at 80 °C to enhance the adhesion of the first layer on the plate and to let the layers partially melting together in the Z dimension. The printing process was performed on a paper support and print cooling was enabled to maintain the printing at the right temperature. The print speed was set at 8 mm/s and the speed-while-traveling was set at 150 mm/s, so the speeds and the accelerations of the print core were refined for printing small models of dosage forms.

2.3.3 Drug content analysis of solid mixtures, drug-loaded filaments and printlets

The PVA particle size greatly affected the ability of the polymer to load the drug. Finest fractions allowed a drug loading more efficient than the millimetric fractions, leading to mixtures that were more homogeneous. Furthermore, coarse or

moderately fine PVA powders (600–1000 µm and 250–600 µm) showed better processability during the extrusion process, reducing the drug loss during both the drug/ polymer mixing and the extrusion processes. The extruded filaments showed a growing trend in the uniformity of CipHCl dispersion in the finest polymer with size reduction, at both percentages of drug (Table 1.4).

Table 1.4: Drug content analysis for 10% and 35% w/w CipHCl batches throughout the manufacturing process (UV spectroscopy data)

10% w/w batches			
PVA particle size	**CipHCl content (%)**		
	Mixtures	Filaments	Printlets
4000-5000 µm	9.67 ± 1.42	6.74 ± 1.12	Discarded
1000-2000 µm	8.91 ± 0.75	8.42 ± 0.74	7.72 ± 0.07
600-1000 µm	9.22 ± 1.13	8.50 ± 0.68	7.30 ± 1.86
250-600 µm	9.55 ± 0.46	9.15 ± 0.24	8.17 ± 0.33
< 250 µm	8.84 ± 0.78	No extrusion	-
35% w/w batches			
PVA particle size	**CipHCl content (%)**		
	Mixtures	Filaments	Printlets
4000-5000 µm	Discarded	Discarded	Discarded
1000-2000 µm	28.9 ± 8.90	26.4 ± 3.15	26.3 ± 0.18

600-1000 µm	33.8 ± 3.97	31.1 ± 1.37	26.5 ± 0.71
250-600 µm	31.2 ± 1.74	28.9 ± 1.25	27.1 ± 0.64
< 250 µm	Discarded	Discarded	Discarded

Printlets obtained from the finest fractions had highest drug amounts and lowest standard deviations, highlighting that the most processable mixture, in terms of drug content, extrudability and printability was the 250–600 µm API/PVA mixture.

Concerning drug stability issue, the HPLC analysis did not show any qualitative differences in the chromatographic peak between the drug raw material and the CipHCl contained in the 3D printed tablets (figure 1.3).
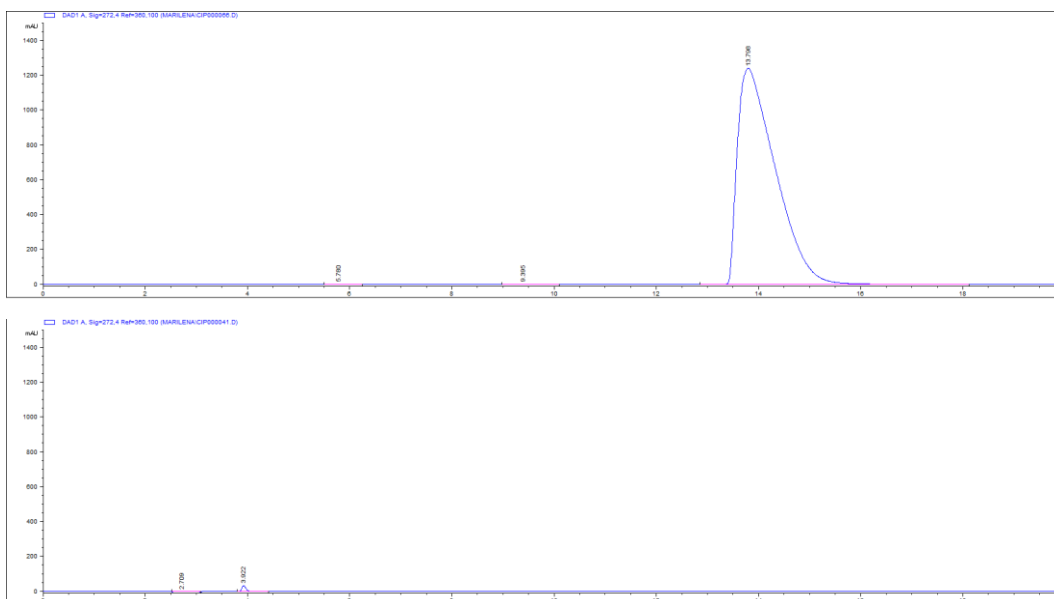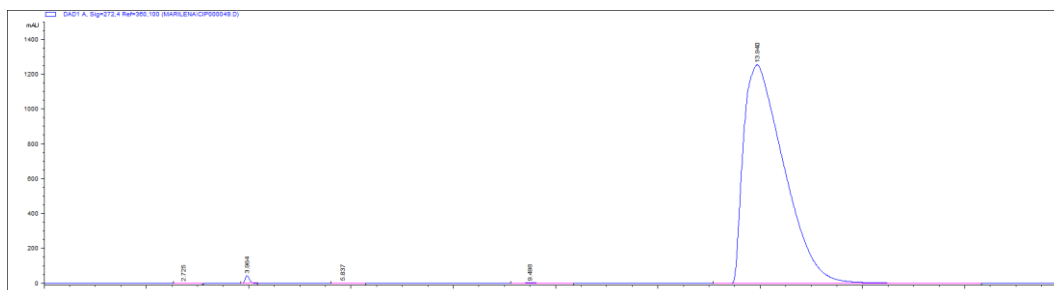
Figure 1.3. Chromatograms of (from top to bottom): CipHCl neat material, blank printlet of PVA, printed PVA 250-600 μm with 35% w/w of CipHCl solubilized and opportunely diluted

The chromatogram acquired from the CipHCl reference solution was used to identify the drug peak, with a retention time of 14 minutes. The blank PVA printlet showed a single weak peak at 4 minutes, and the drug-laden printlet showed both peaks without any changes. Moreover, two other peaks with very low AUC were detected in the loaded printlet and they were related to the presence of two impurities deriving from CipHCl due to the thermal processing of extrusion and printing. Particularly the peaks were ascribed to the defluorinated and the decarboxylate derivatives of the API (impurities B and E, as reported by European Pharmacopoeia 9th Edition, considering the relative retention with reference to CipHCl). Both impurities were considerably under the disregard limits identified by Eu. Pharmacopoeia, or rather less than 0.05% of the principal peak of the drug in the chromatogram.

Moreover, the amount of CipHCl of the DDS found after six months of storage, at room temperature and repaired from light, was practically identical to the amount detected immediately after the printlets production (HPLC $25.8 \pm 0.14\%$ *vs* UV $25.1 \pm 1.2\%$).

These results detected *via* HPLC highlight the correctness of the UV analysis about drug content in the printlet (and in all the intermediate products), and the high stability of the drug dispersed in the polymeric PVA matrix in these oral formulations.

2.3.4 Morphological analysis

The quantitative results were also confirmed by SEM micrographs. The adhesion of drug onto the polymer increased with the reduction of PVA granulometry, due to the increase in the surface area, both with low and high amount of drug. As clearly shown in Fig. 1.4, a great quantity of free drug is evident in coarse batches, while in the finest fraction a uniform coating of drug crystals on the surface of the polymer was observed.
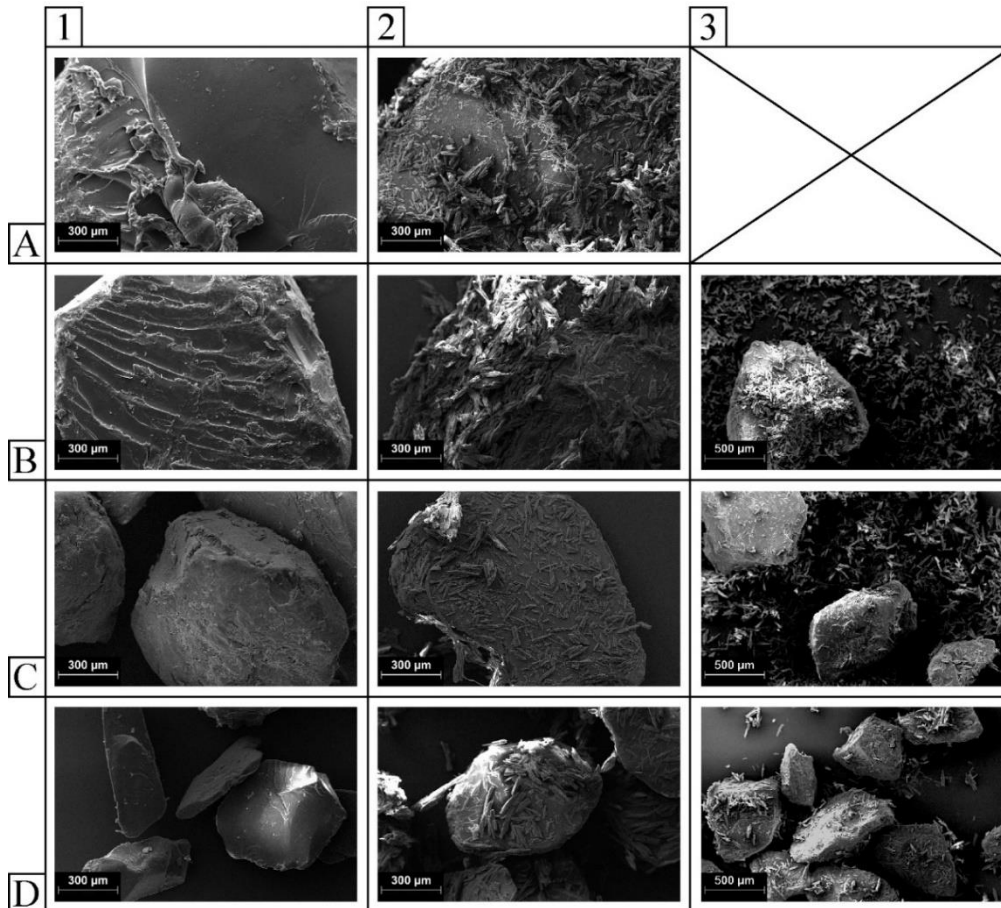
Fig. 1.4. Micrographs of different PVA particle size: A) 4000–5000 µm; B) 1000–2000 µm; C) 600–1000 µm; D) 250–600 µm) of: 1) PVA raw; 2) solid mixtures with 10% w/w of CipHCl and 3) solid mixtures with 35% w/w of CipHCl

Regarding the drug-loaded filaments (Fig. 1.5), the growing trend in the uniformity of the solid dispersion within the reduction of PVA particle size was confirmed by micrographs (Fig. 1.6); moreover, the API homogeneous dispersion can be clearly seen in the finest fraction analysed (see magnification, Fig. 1.6).
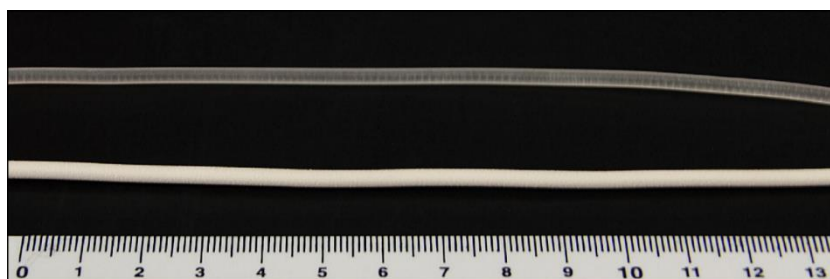
Fig. 1.5. Macroscopic images of PVA raw commercial filament (up) and drug-loaded filaments obtained from solid mixtures with 250–600 µm PVA and 35% w/w CipHCl (down)
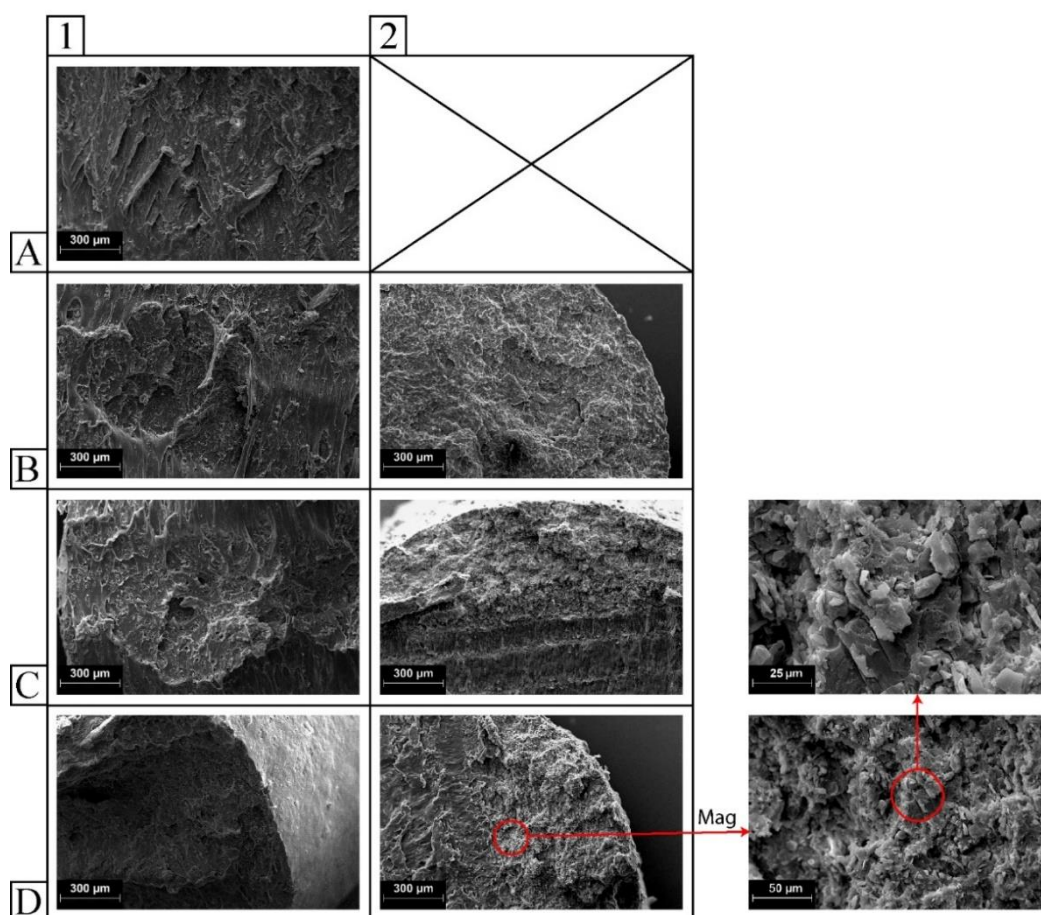
Fig. 1.6. Micrographs of drug-loaded filaments obtained from solid mixtures A): 4000–5000 μm; B) 1000–2000 μm; C) 600–1000 μm; D) 250–600 μm with 1) 10% w/w CipHCl and 2) with 35% w/w of CipHCl

Macroscopic images and micrographs showed some differences in the layers adhesion along the XY and the Z dimensions among different printlets. In particular, the layers were completely fused together for the finest extruded batches; on the contrary, for the other batches, an incomplete fusion of the deposited layers and a lower printing resolution characterized the printlets (Fig. 1.7).
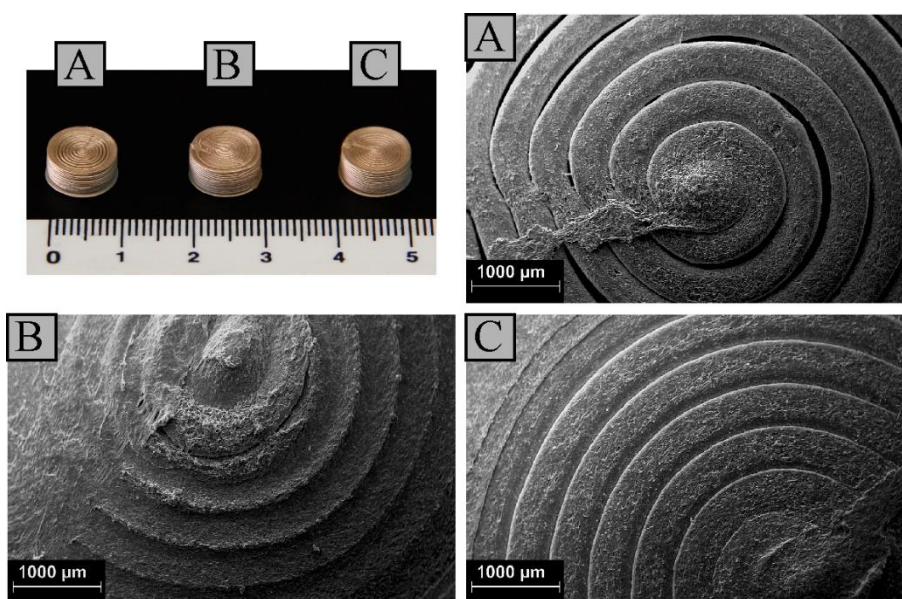
Fig. 1.7. Photographic and SEM acquisition of printlets obtained from solid mixtures with 35% w/w CipHCl and with A) 1000–2000 μm PVA; B) 600–1000 μm PVA; C) 250–600 μm PVA after metallization

The cross section obtained by printlets cryofracture displayed the complete homogenization of the drug into the polymer; only few niches of drugs are present

into the hollows of the printlet microarchitecture (Fig. 1.8). Indeed, the finest batch 250-600 μm with 35% w/w of API had a percentage of porosity of 18.49 ± 0.81, highlighting again the optimal adhesion of the lines in the same layer and between adjacent layers of the obtained printlets from the finest powder, giving also adequate consistency for their potential stocking and handling.
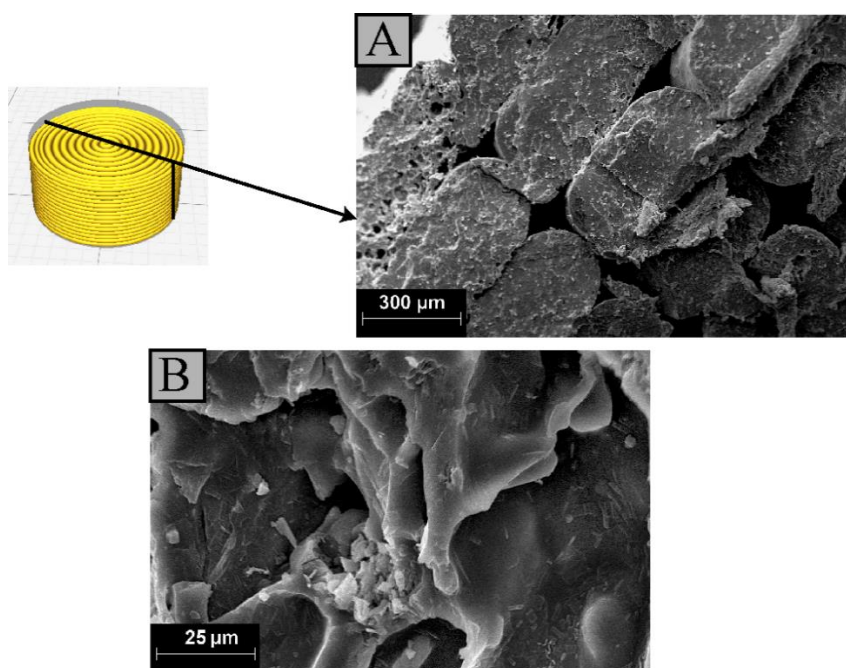
Fig. 1.8: Micrographs of cross sections of printlets obtained from 250 to 600 μm PVA and 35% CipHCl A) magnifications 200X and B) 2500X

The obtained printlets retained the designed dimensions along X and Y axes (10×10 mm), with low standard deviations, particularly for the finest mixtures (600–1000 μm and 250–600 μm). However, along the Z axis, a height reduction was experienced due to a partial overlap of the deposited fused layers, as expected for objects created via FFF-3DP technology (Table 1.5).

Table 1.5: Analysis of the dimensions along the X, Y and Z axes of the printlets and their average mass

Printlets 35% w/w CipHCl	X (mm)	Y (mm)	Z (mm)	Mass (mg)
1000-2000 µm	9.70 ± 0.35	9.77 ± 0.26	4.67 ± 0.16	326.98 ± 26.23
600-1000 µm	10.18 ± 0.25	10.21 ± 0.24	4.72 ± 0.02	419.93 ± 49.61
250-600 µm	10.20 ± 0.13	10.19 ± 0.15	4.67 ± 0.10	367.74 ± 37.53

However, this variation in the Z dimension ($\sim 6.3\%$) for all the obtained printlets could be taken into account and anticipated when designing the digital model. Moreover, for all the printlets obtained from the analysed fractions, mass values showed high standard deviations and did not comply with the uniformity of mass test described by the Pharmacopoeia for conventional tablets. Therefore, the mass has to be considered as a critical point; nevertheless, the correct mass for the dosage forms could be successfully reached starting from drug-loaded filaments with a narrower diameter variation than the selected one (2.85mm ± 0.15 mm), to obtain a constant flow of melted material for the printing process.

2.3.5 Thermal characterization

Differential Scanning Calorimetry of raw materials and products was performed to characterize thermal events and degradation profiles throughout the manufacturing process. All the thermal profiles obtained from different PVA fractions mixtures, filaments and printlets were superimposable. Hence, as an example of thermal analysis of solid mixtures, filaments and printlets, the 600–1000 µm batch thermograms were reported (Fig. 1.9).
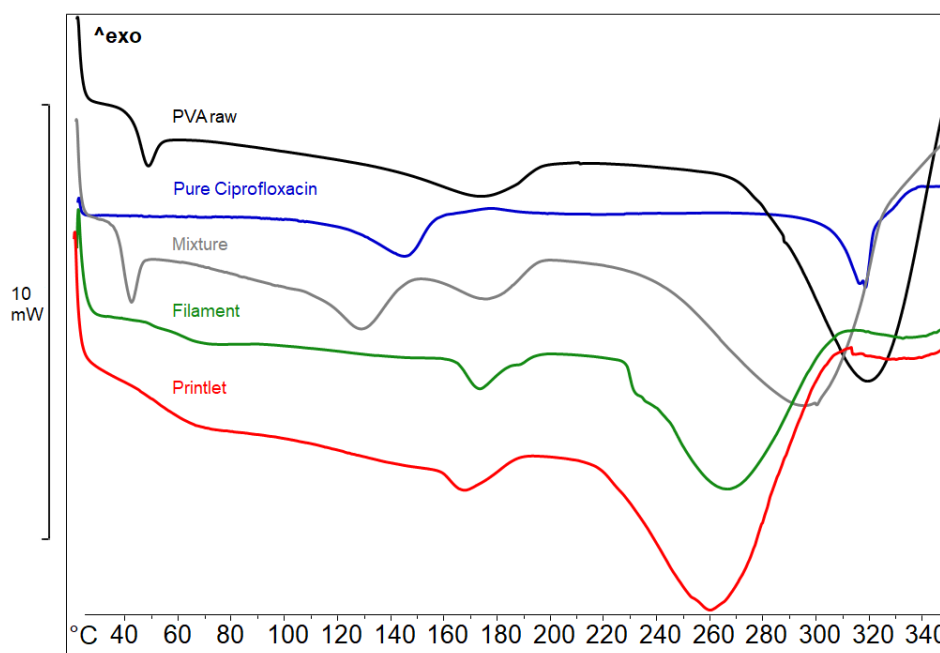
Fig. 1.9. Thermograms of (from top to bottom): PVA raw; Blue: pure Ciprofloxacin hydrochloride; Grey: PVA 600-1000 µm/CipHCl mixture; Green: PVA 600-1000 µm/CipHCl filament; Red: PVA 600-1000 µm/CipHCl printlet.

Thermal analysis of PVA raw material indicated that its glass transition temperature T_g had a range from 40°C to 55°C, whereas the melting range T_m was

from 170°C to 185°C; moreover, the decomposition of PVA started above 280°C, pointing out the high thermal stability of the selected polymeric carrier.

Neat CipHCl showed the loss of water of crystallization at 147 °C and a melting temperature at 320 °C.

In solid mixtures, the overlapping of the melting peak of CipHCl, shifted to lower temperature (at about 300 °C), with the PVA degradation peak underlined that the drug and the polymer had good interaction by the first step of this process, i.e. the mixtures production. The T_g peaks reduction of PVA in filaments and printlets displayed that the extrusion process led to a relatively reduction in the plastic behaviour of the material, nevertheless the filaments exhibited in all the cases good printability. Moreover, both drug/polymer mixing and the extrusion process led to a shift to lower temperatures of the degradation peaks (up to 260°C), highlighting the reduction in the linkage of repeating units of PVA consequent to the mechanical milling of PVA spool. This shift to lower temperatures of the degradation peaks was not troublesome, since during the extrusion and the printing the operative temperatures were always lower than the degradation ones.

2.3.6 FT-IR analysis

All the PVA batches produced by milling showed in their IR spectra same profiles (Fig. 1.10), underlining that the drying process preserved the inner structure of the polymer even after the mechanical grinding step.
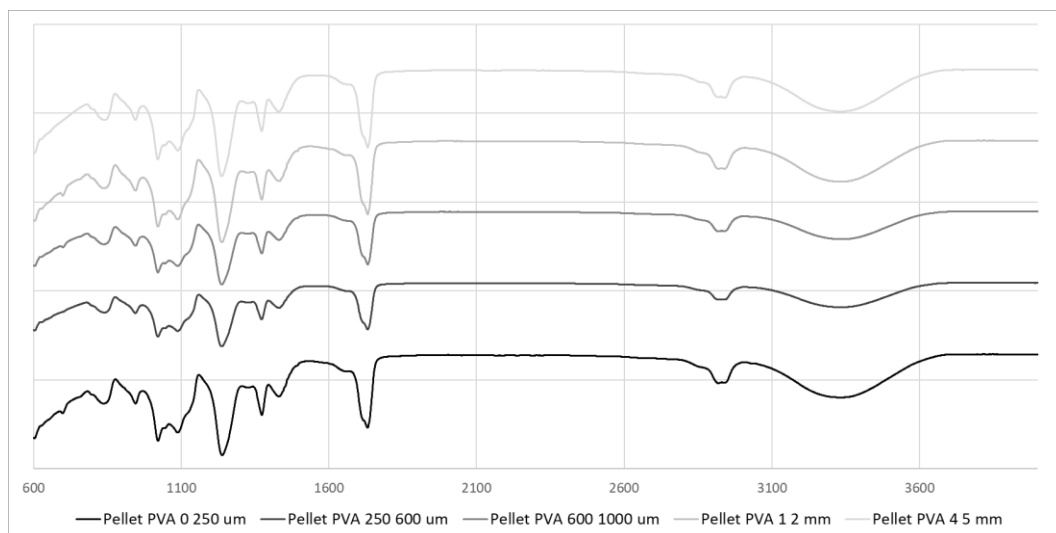
Fig. 1.10. IR spectra of PVA with different particle size ranges

Particularly, in all the batches, characteristic bands of PVA are detected as shown in table 1.6:

Table 1.6. Region of absorption of all neat PVA batches obtained via cryo-milling

Functional group	Region (cm^{-1})	Comments
Hydroxyl O-H	3230-3590	Broad band of stretching vibrations, as usually for solids, liquids, and concentrated solutions with intermolecularly hydrogen bonded O-H groups
CH$_2$	2900-2990	Asymmetric stretching vibrations
Carbonyl C=O	1715-1740	Typical band
Vinyl group -CH=CH$_2$	1645-1650 1650-1740	Stretching vibrations slightly visible
C-H	1300-1440	Deformation vibrations
O-H	1260	In-plane deformation vibration gives rise to a sharp, narrow band

Alcohol C-O group	1000-1090	Stretching vibration; hydrogen bonding and chain branching have the effect of slightly decreasing the frequency of this band
C-C-O	800-900	Stretching vibration with a band of medium intensity

Analysing bands derived from O-H deformation vibrations, alcohol C-O groups region and C-C-O stretching vibrations, it can be deduced that the used PVA is a blend of different grades of PVA with low molecular and high molecular weight (M_w 30000-150000 Da). This mixture is usually used in 3DP to improve the thermal/degradation stability and printability, with a degree of hydrolysis around 80-90%.

Regarding CipHCl (Fig. 1.11, 1.12 and 1.13), characteristic regions of vibration detected in the spectrum of the unprocessed drug are summarized in table 1.7.

Table 1.7. Region of absorption of neat CipHCl

Functional group	Region (cm^{-1})	Comments
Hydroxyl group O-H	3525	Stretching vibrations of intermolecular hydrogen-bonding
N-H	3300-3500	One stretching band which is weak as usual for secondary amines
N–H	3375	Stretch of piperazinyl moiety
Aromatics cyclic enes =CH bonds (Ar-H)	2950-3085	Stretching vibrations as four peaks
Hydrohalide N-H$^+$	2250-2700	Amines with CNH$^+$ have absorption of medium intensity as a group of sharp bands; amine stretching vibrations
Carboxylic acid CO	1705	Stretching vibrations as narrow peak

N-H	1610-1620	Bending vibrations of quinolones
Conjugated aromatic ring	1600	Observed as a doublet
C=C, CN and C=O of quinoline	1575-1625	Substituents directly conjugated to the ring increased the intensity of this doublet
Ring -C=C-	1430-1625	Carbon-carbon stretching vibrations, with three bands due to skeletal vibrations
Carbonyl group C-O	1450	The strongest band of vibration
C-N	1265-1380	Double band for tertiary aromatic amines
O-H	1260	Bending vibrations indicated the presence of carboxylic acid
piperazinyl groups C-N	1170-1190	Secondary aliphatic amines with two bands of medium-weak intensity; stretching vibrations
Carbon-halogen C-F bond	1025	Vibration of fluorine group, stretching
Aromatic group quinoline	900-1290	Aromatic in-plane C-H deformation vibrations, sharp bands of weak intensity C-C, C-O stretching vibrations
	780-860	Strongest absorptions of =C-H vibrations out of the plane of the aromatic ring

In all the spectra of the different solid mixtures (Fig. 1.11), all the peaks of ciprofloxacin were clearly visible such as the PVA frequencies.
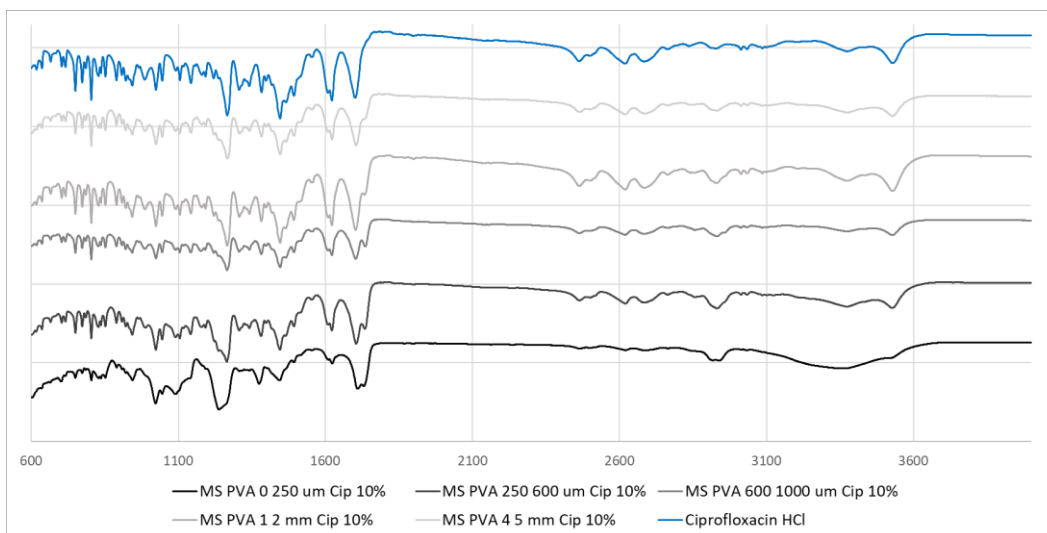
Fig. 1.11. IR spectra of PVA-CipHCl solid mixtures

Though the band widening at around 3360 cm^{-1} underlined a better intermolecular H-bonding interaction between the matrix and the drug for the finest batches, particularly for polymer mixtures with particles size less than 250 µm. This band became broader in all the filaments and printlets spectra (Fig. 1.12 and 1.13) and, for both processes products, a gradual combination of bands and change in relative intensity in the range 1700-1740 cm^{-1} was visible, where the stretching vibrations of ciprofloxacin carboxylic CO and of PVA carbonyls are present. These two events further highlighted the advancement in the dispersion of the solid drug in the polymeric matrix during the extrusion and printing process.

Considering the spectra set of the hot melt extruded filaments starting from diverse solid mixtures batches (Fig. 1.12), the Ciprofloxacin spectrum was easily recognizable, however a difference can be seen in the range 2500-3050 cm^{-1}, may due to the loss of the hydrochloride moiety caused by the thermal processing during extrusion, where several peaks rose.

92
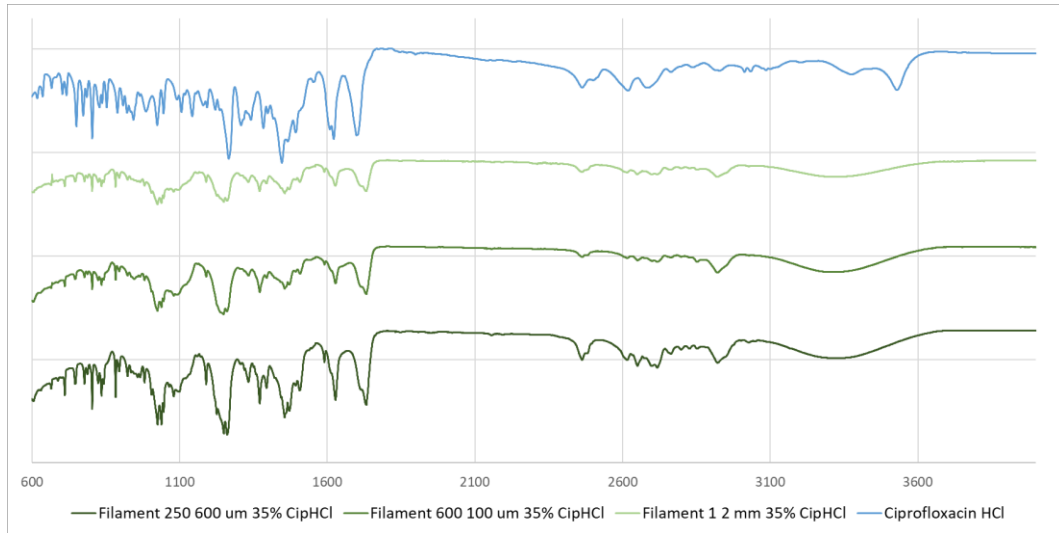
Fig. 1.12. IR spectra of PVA-CipHCl filaments

In all the printlets spectra (Fig.1.13), ciprofloxacin bands were slightly visible, sign of the best homogeneity of the final product of the process.
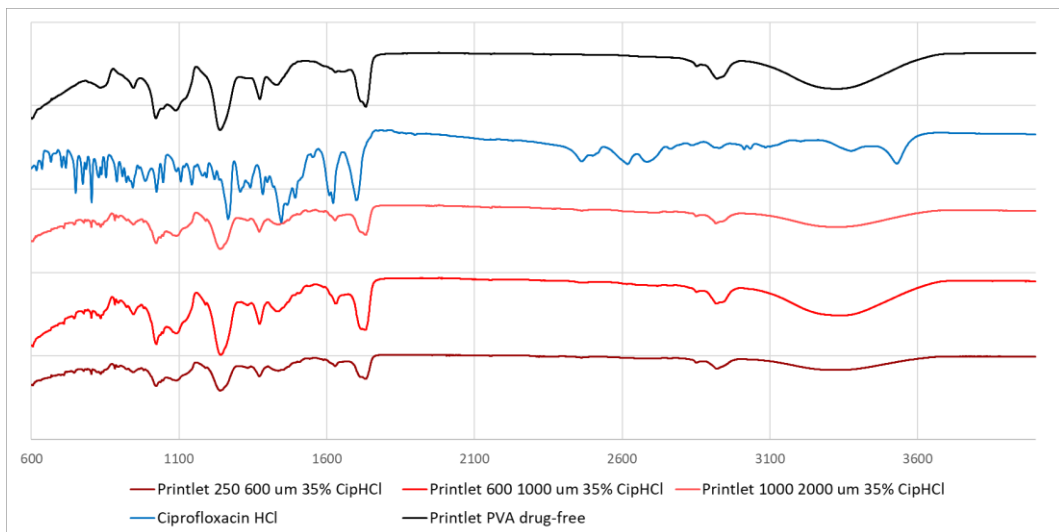
Fig. 1.13. IR spectra of PVA-CipHCl printlets

Although, avoiding the overlapping wavenumbers, the main characteristic bands of the active compound were recognizable:

- N-H bending vibrations of quinolones at 1620 cm^{-1};
- the ring carbon-carbon stretching vibrations -C=C- at 1430-1625 cm^{-1};
- the C-N stretching vibrations of piperazinyl groups at 1170-1190 cm^{-1};
- =C-H vibrations out of the plane of the aromatic ring quinoline at 780-860 cm^{-1}.

Particularly, the ring vibration at 1430-1625 cm^{-1} and the piperazinyl groups C-N peaks at 1170-1190 cm^{-1} are undoubtedly still visible in all the obtained printlets, confirming the presence of the ciprofloxacin without degradation occurred after thermal processing. While the other bands are partially covered from the PVA absorption, confirming the optimal dispersion of the drug into the printouts, comparing with mixtures and filaments.
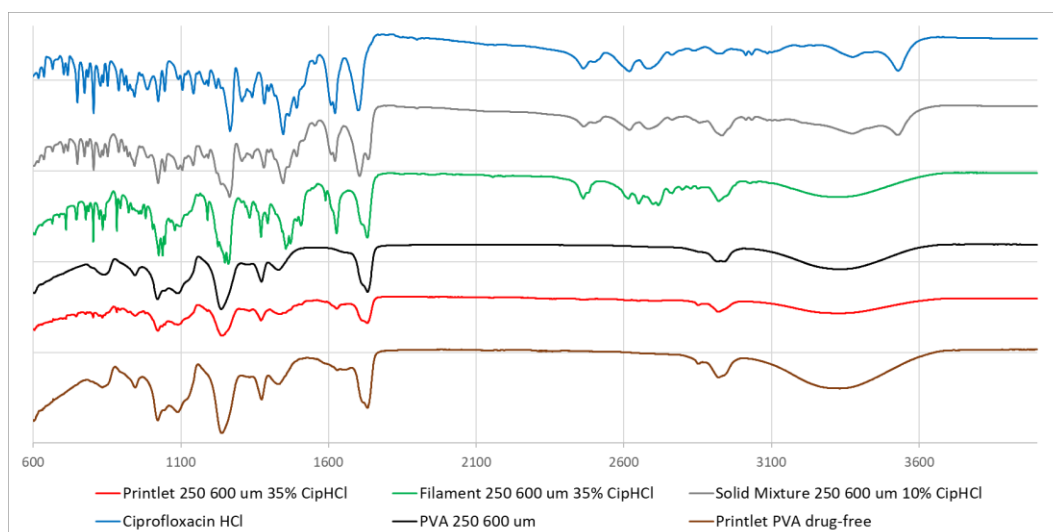
Fig. 1.14. Comparison of IR spectra of raw materials and products of the whole manufacturing process

Finally, the FT-IR analysis (Fig. 1.14) further confirmed the stability of the Ciprofloxacin to the thermal processing for producing FFF 3D printed PVA oral formulations.

2.3.7 Dissolution tests of filaments and printlets

Dissolution tests were firstly performed on segments of filaments with 10% w/w of API and the drug release followed a zero order kinetic up to 90 min. Filaments obtained from coarse and moderately fine PVA powders (Fig. 1.15) showed almost the same drug release profile with lower standard deviations, underlining the homogeneity of finest mixtures (PVA 600–1000 μm and PVA 250–600 μm).

The drug release profiles obtained from printlets produced using 10% and 35% of drug in the mixtures (Fig. 1.16) showed a complete release of the CipHCl in 270 min. This delay in the API release was to ascribe to the additional material fusion during the printing process that led to a stronger interaction between polymer and drug.

Moreover, all the printlets showed similar profiles of dissolution underlining the possibility of loading different amount of drug with almost no changes in the release profiles of printlets.
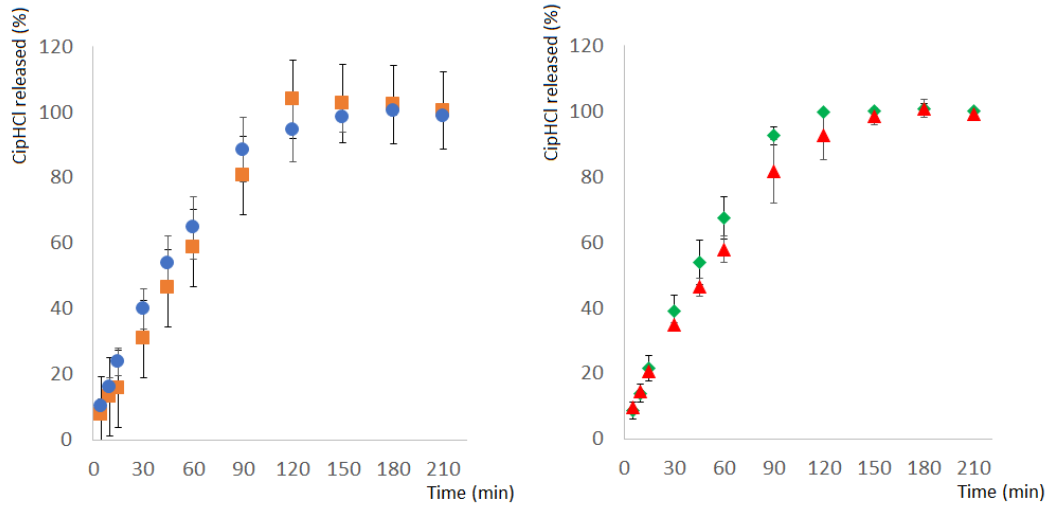
Fig. 1.15: Dissolution profiles of filaments obtained from 10% w/w of CipHCl batches (■ PVA 4000-5000 μm; ● PVA 1000-2000 μm; ◆ PVA 600-1000 μm; ▲ PVA 250-600 μm)
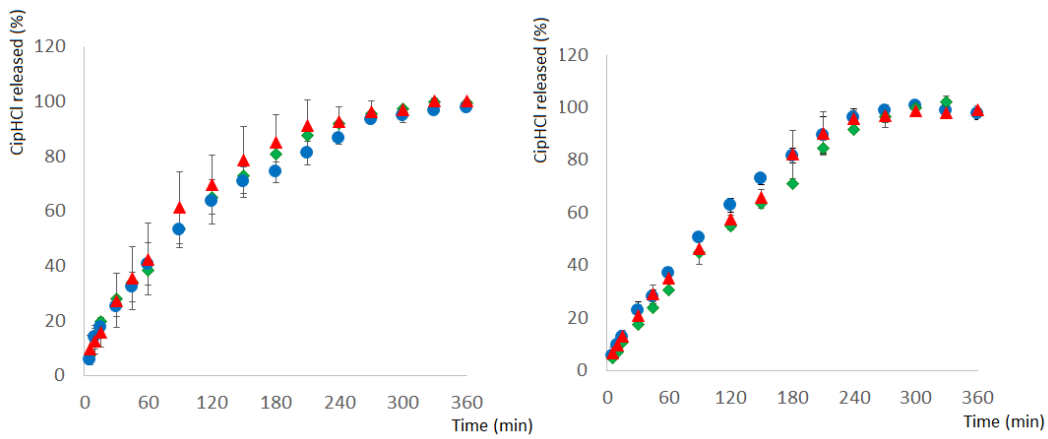
Fig. 1.16: Dissolution profiles of printlets obtained from 10% (left) and 35% (right) w/w of CipHCl batches (● PVA 1000-2000 μm; ◆ PVA 600-1000 μm; ▲ PVA 250-600 μm)

2.4 Conclusions

In conclusion, the scientific research herein described demonstrates the possibility of producing low and high dosage oral drug delivery systems exploiting the novel features of Fused Filament Fabrication 3D printing in pharmaceutical compounding. Particularly, PVA filaments loaded with different amount of thermostable API, i.e. Ciprofloxacin Hydrochloride, were manufactured and used as feedstock for 3D printing, starting from the production of solid mixtures drug/polymer with different size distributions. Thus, all the parameters of the whole manufacturing process, such as formulation variables (concentration and characteristics of polymeric carrier, drug and excipients) and extrusion of filaments (printability, yield and loaded percentage of drug) and their printing in form of printlets^{TM} (characterized in dissolution kinetics), have been analysed, deepened and optimized.

In this research, the importance of polymeric particle size distribution has been demonstrated not only on drug adhesion on the polymer during the preparation of solid mixtures with different ratio of API, but also on the extrusion and printing processes. Indeed, the PVA particle size affected the polymer ability to form homogeneous mixture with the drug and the efficiency of the extrusion and printing processes.

The systematic analysis of the effect of different size distributions on mixing-extrusion-printing steps showed better results in drug content and printability for moderately fine particles (250–600 μm), that allowed a complete adhesion of the drug on the polymer surface and a greater homogeneity of both filaments and obtained final printlets. Thus, finest powder batches of polymeric carriers are

indispensable for a great processability and for the reduction of drug loss during the drug/polymer mixing and the extrusion process.

Drug-loaded filaments with different drug concentrations, 10% w/w and 35% w/w of CipHCl, as model thermostable API, and optimal drug distribution were successfully printed, and the obtained printlets^{TM} showed high resolution and superimposable drug release profiles, regardless the filament drug content used for the printing step.

Hence, these results can be used as starting point to discover the freeform 3D modelling of oral drug delivery systems made of PVA, thanks to the optimal printability, chemical and thermal stability of this polymer, loading different thermostable APIs, and re-tuning the critical process parameters here identified.

Finally, protocols for the production of personalized oral drug delivery systems have been developed and optimized for the manufacturing of pharmaceutical forms with thermoplastic biocompatible polymers, taking an important step for the future application of 3D-printing manufacturing process in personalized galenic formulations and revealing potentialities of hot melt extrusion coupled with Fused Filament Fabrication 3D printing in dose customization according to the patients' needs and dosage regimen.

3. SECTION II

Development and analysis of a novel post-loading technique for FFF 3D printed systems: microwave-assisted impregnation of gastro-retentive PVA capsules-in-capsule models
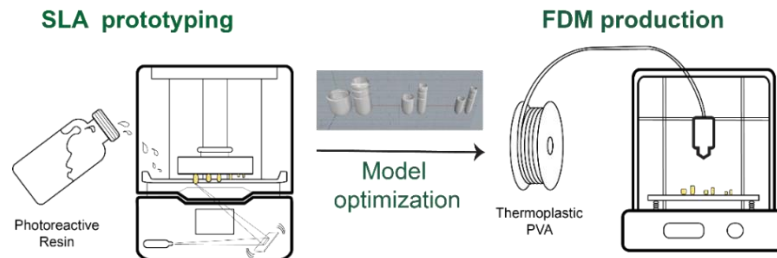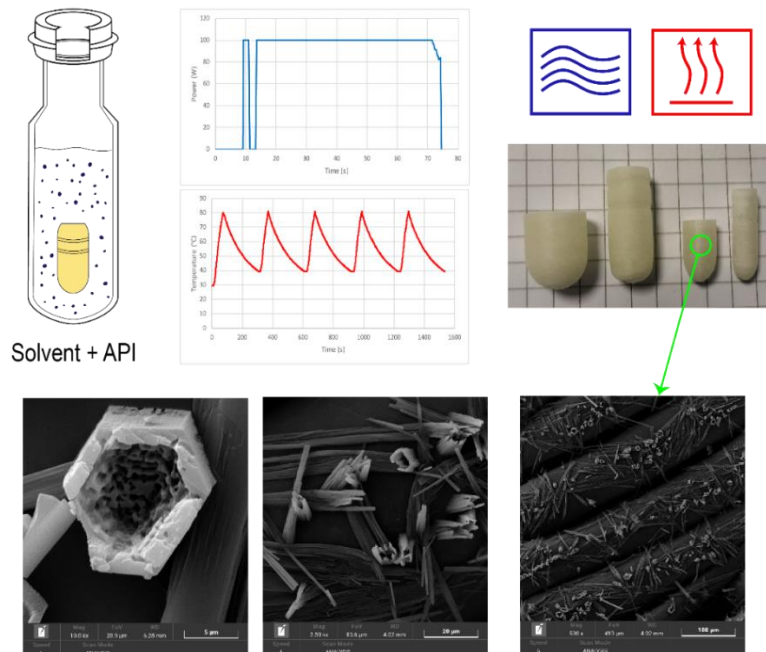
In collaboration with

Dr Stephen Hilton and colleagues, Research Department of Pharmaceutical and Biological Chemistry, UCL (University College London) School of Pharmacy, London, UK

3.1 Scientific background and research aim

Stereolithography 3D printing offers greater accuracy and reproducibility compared to the more prevalent filament deposition modelling 3D printing (M.R. Penny & S. Hilton, 2020). Thus, SLA technology could be exploited for the rapid prototyping of functional tools and preliminary models, in order to obtain the highest resolution during their production.

FDM/FFF manufacturing is one of the most used techniques in the pharmaceutical field for the development of drug delivery systems. In fact, extensive studies have been conducted on the potential use of FDM for the production of medical devices and printed tablets, with bespoke geometries, sizes and release profiles (Pietrzak K., Isreb A & Alhnan M.A., 2015; Kempin W. et al., 2017). However drug-loaded filaments for FDM3DP are not available yet, therefore FFF must be coupled with other technologies, i.e. pre-loading *via* hot melt extrusion, in which the APIs undergo thermic processing (Goyanes A. et al., 2017), or soaking post-loading, where the polymeric matrix is loaded through the immersion in a drug-solution, with poor results in terms of loading efficiency (W. Jamróz, et al., 2018).

Microwave radiations are characterized by high and rapid penetration power which has a significant effect particularly on polar compounds. Microwave irradiation of polymers has proved to be an economical, fast and green technique for chemical synthesis, structural cross-linking and drug incorporation (L. J. Waters, S. Bedford & G. M. B. Parkes, 2011).

However, the microwave systems have not been deepened as a post-loading technique of printed structures, thus studies need to be conducted to highlight the potentiality of this method in enhancing the loading of drugs into the polymeric

matrix. Therefore, microwave assisted drug-loading approaches need to focus on the characterization of the impact of the radiations on the chemical and physical properties of polymeric scaffolds and on the stability of the used drug.

In fact, the microwave systems have superior heating features which are based on the quick achievement of high temperatures (up to 300°C) and pressures (up to 30 bar) beyond traditional reflux heating. These characteristics could be applied in the pharmaceutical compounding with the adequate analysis of their effect on the final drug delivery system.

Under the effect of ionizing irradiation, polymers, such as poly(vinyl alcohol), may undergo variations in chemical structure and the polymer chains could go through cross-linking or chain scission, depending upon the radiation power, chemical structure, crystallite size and the environment of the analyte (H.F. Afzal et al., 2020).

In this research project, the effect of the impregnation with the model drug Caffeine *via* microwave irradiation of PVA floating systems, printed *via* FFF3DP, was evaluated in terms of drug-loading efficiency, thermal and chemical stability of components, and morphology of the drug and the processed printouts.

Moreover Polyethylene glycol (PEG) (with a melting range of 33-40°C), one of the safest organic cosolvents and pharmaceutical excipient, (IIG limits for oral administration: up to 1.5197 mg) (A.A. D'souza & R. Shegokar, 2016) has been added to improve the post-loading process, exploiting its enhancing properties on the absorbing performances of systems subjected to microwave processing (L. Liu et al. 2012).

Hence, the aim of this research is to develop and characterize a novel method for the post-loading of FFF printouts, facilitating the transition from traditional methods, such as solvent casting or soaking, to microwave enhanced techniques.

3.2 Materials and Methods

3.2.1 Materials

Clear Resin (photopolymer resin, Formlabs, Massachusetts, USA) was used for the SLA 3D printing of caps-in-cap prototypes. While poly(vinyl alcohol) (Natural PVA, Ultimaker filament for 3DP, density 1.23 g/cm3, Ultimaker, Netherlands) was used as pristine PVA for the FDM 3D printing of drug-free models.

Fluorescein sodium salt (Fluka Analytical) was employed for a preliminary analysis of solute distribution after the microwave processing. Anhydrous Caffeine 99% (Sigma-Aldrich, aqueous solubility 21.6 mg/mL, 25°C, pH 7.0) (Yalkowsky S.H. et al., 2010) was chosen as model drug to load the PVA blank models of caps and bodies.

For the microwave-assisted impregnation, different solvents were selected for the preliminary analyses: Ethyl alcohol, Acetone, 2-propanol (IPA), Ethyl Acetate purchased from Sigma-Aldrich. Moreover, Poly(ethylene glycol) PEG 1000 (BioUltra, Sigma) has been added to the acetonic carrier solutions.

For the mobile phase preparation Tetrahydrofuran, Acetonitrile, Sodium Acetate trihydrate (EMSURE®, Merk), and Glacial Acetic acid were utilized.

Materials were used as received without any modification and all other chemicals employed were of ACS reagent grade and solvents were of HPLC grade; all the materials have been used as supplied.

3.2.2 Digital modelling of caps-in cap

CAD models of the caps-in-cap formulations were drawn using Fusion360 (Autodesk, California, USA) and Rhinoceros 6 (Robert McNeel & Associates, McNeel Europe) and then exported as .stl extensions. Graphical designs were then imported to the slicing software:

- o PreForm version 3.3.1 (Formlabs, Massachusetts, USA) prior to printing *via* SLA 3D printer Form3 (Formlabs, Massachusetts, USA);
- o Cura 4.6.0 (Ultimaker, Netherlands), creating the gcode file used by the FDM 3D printer Ultimaker[3] (Ultimaker, Netherlands).

3.2.3 Prototyping via SLA 3DP

With the aim to reduce the material cost of iteration and to obtain prototypes with the highest resolution, the manufacturing fits and the 3D printing tighter tolerances of models have been screened *via* a fast SLA prototyping. For the SLA printing of the final capsules-in-capsule (caps-in-cap) models, a 25 µm resolution was chosen to obtain the highest accuracy in the reproduction of the models, using Clear resin as construction material. A full raft with edited pins of 0.5 mm was created to support the printouts while printing occurred.

Post-processing of 20 minutes in 2-propanol IPA with shaking was required to remove all the uncured resin from the models, and a final post-curing of 30 minutes at 60°C was defined as optimal to obtain the final cured models.

3.2.4 FFF 3D printing of caps-in cap

The SLA fast prototyping led to define as final blank geometries the caps-in-cap showed in figure 2.1.

Figure 2.1: Digital models of the caps and bodies for 3D printing of caps-in-cap systems

The production of the models was then translated in the FFF manufacturing process with minimal changes in sizes considering the thermal expansion of printed PVA (coefficient of thermal expansion PVA 85 µm/(m°C)) with the following printer and slicing parameters (Table 2.1):

Table 2.1. Operative specifics and slicing parameters used for FFF 3DP

FFF 3D-Printer and slicing parameters	
Material	PVA
Nozzle diameter	0.4 mm
Printing Temperature	215°C
Initial Layer Printing Temperature	220°C

Build Plate Temperature	85°C		
Construction Volume Temperature	38°C		
Layer Heigh	0.10 mm		
Outer Wall Line Width	0.19 mm		
Inner Wall Line Width	0.19 mm		
Pattern	Concentric		
Print Speed	Body1 and Cap1-2	Body2	Bodycap3
	20 mm/s	10 mm/s	8 mm/s
Initial Layer Speed	20 mm/s	10 mm/s	8 mm/s
Inner Wall Speed	18 mm/s	9 mm/s	7 mm/s
Outer Wall Speed	15 mm/s	8 mm/s	6 mm/s
Retraction distance	4.5 mm		
Print Cooling	Enabled		
Support Support overhang angle Support XY distance Support Z distance	Generated for model 3 30° 0.38 mm 0.20 mm		

3.2.5 Preliminary analysis of solvents for impregnation and solute distribution via Fluorescence imaging

As a preliminary screening of adequate solvents for microwave post-loading, PVA models have been completely immersed in the solvents for 20 hours (Ethanol, Acetone, IPA, Ethyl Acetate) in steady conditions. Matrix swelling and solvent absorption were monitored acquiring masses and dimensions immediately after the withdrawal from the solvents.

Furthermore, to monitor the adsorption of solutes on the PVA models, Fluorescein sodium salt was added to pure Acetone and stirred for 3 hours prior to use. Then, 15 mL of this solution were used to post-load blank models *via* Biotage Initiator for monitoring the permeation of solutes into the PVA matrix with different wall widths and various microwave cycles of loading.

3.2.6 PVA impregnation via soaking and via microwave-assisted process

Caffeine laden solutions for soaking and microwave processing were prepared gradually adding the predetermined mass of Caffeine (1-2% w/v) to obtain oversaturated solutions in the selected solvent (i.e. Ethanol, Acetone, IPA and Ethyl Acetate) under constant stirring for 24 hours. Additionally, Acetone and 2% w/v of Caffeine solutions have been added with PEG 2% w/v, creating a molecular distribution of drug in the carrier solution.

For the soaking process, blank models (n=6) of PVA were immersed in 15 mL of Acetone and Caffeine 2% w/v. The vials containing the saturated acetonic dispersion of the drug with the models were sealed to avoid the evaporation of the acetone and kept under magnetic stirring for 48 hours at room temperature.

For the PVA matrix microwave-assisted impregnation, microwave heating *via* Biotage® Initiator Microwave Synthesizers (Biotage, Uppsala, Sweden) was used to enhance the load of the model drug into the PVA blank scaffolds. Particularly, for the production of drug-loaded batches, 15 mL of the oversaturated solutions of selected solvents and caffeine (1-2 % w/v) were dispensed into the 20 mL glass vials. Then, immediately before the microwave-assisted loading, the blank model (one cap or one body) was added into the vial, sealed and then processed. The solvent temperature during irradiation ranged from 40°C to a maximum 140°C

with and heating rate between 2–5 °C/s depending on solvent and power applied. The power range was screened in the whole range 1–400 W and the magnetron always set to 2.45 GHz of frequency. Absorption level was generally set to normal according to the polarity and conductivity of the used solvents; for Absolute Ethanol and IPA impregnation trials have been carried out also with high and very high absorption levels. Pre-stirring of 30 seconds was set out before the start, while continuous magnetic agitation with a stirring range of 600 rpm was used during the impregnation process.

The contact time between liquid mixtures and solid scaffolds was set between 10 seconds and 20 minutes, or by using cycles of irradiation (i.e. 5 x 10 seconds at maximum temperature). Cooling with pressurized air supply was activated after each cycle of impregnation (> 60 L/min, 2.5-4 bar). Both the soaked and the irradiated models were placed on glass supports and air-dried for 48 hours or dried at 40 ± 2 °C until constant weight was obtained. The drug content of soaked and irradiated samples was analysed *via* HPLC as described below.

3.2.7 Analysis of FFF 3D printed models and processed materials

At least three units for each formulation have been weighted using analytical balance (Analytical Balance Sartorius Research R200D, USA):
- − after the printing process of blank models;
- − immediately after the withdrawal from the solvent for the preliminary screening;
- − after the soaking process and drying;
- − after the microwave impregnation and drying.

The weight acquired after the impregnation or drug loading was calculated and expressed as percentage following the equation:

$$Weight\ acquired\ (\%) = \frac{mg_f - mg_i}{mg_i} * 100$$

mg_f represents the mass of the formulation after loading and drying, while mg_i represents the initial mass of the sample.

All the blank, soaked, impregnated and drug-loaded formulations have been accurately measured with a digital external micrometre to obtain the dimensions of the blank printouts and the post-loading morphological modifications in terms of height, diameter and width, following the equation:

$$Dimensions\ acquired\ (\%) = \frac{d_f - d_i}{d_i} * 100$$

d_f represents the dimension of the formulation after loading and drying, while d_i represents the initial dimension of the sample.

The printed systems were photographed with a commercial camera (in sRGB, using focal length 4 mm, f-stop f/1.9, exposure time: 1/25 s, ISO speed 320) to obtain macroscopic acquisitions of the loaded models.

Raw materials, dried caffeine powder form acetonic solution (pre and after MW processing), blank models and post-loaded dried formulations were also observed in their macro- and micro- architecture by using Scanning Electron Microscopy (Tescan Solaris, Tescan Orsay Holding, Czech Republic), after metallization *via* Leica EM SCD005, Leica-microsystem, Italy.

3.2.8 HPLC quantitative analysis of Caffeine-loaded printouts

Caffeine quantization from drug-loaded samples was conducted *via* HPLC (Agilent Technologies 1200 series, 1260 Infinity II) equipped with vial autosampler, degasser, quaternary pump, and thermostat column compartment (Agilent Technologies, Cheadle, UK).

The stock solutions were diluted in the mobile phase to prepare various concentrations of Caffeine and the calibration curve was performed in a range of 12 – 450 μg/mL (regression coefficient value R^2 0.999980). Particularly, drug-loaded samples (caps and bodies) were dissolved individually in the adequate volume of mobile phase with continuous stirring at 300 rpm and room temperature, when necessary, sonication cycles (maximum total time of ultrasonic exposure: 2 minutes) were performed to enhance the erosion speed of the PVA matrix until complete dissolution. Hence appropriate dilutions were prepared in the mobile phase for the HPLC analysis to be in the range of the calibration curve.

The analysis was performed using Infinity Lab Poroshell 120 EC-C18 column (Agilent Technologies, Cheadle, UK) with 150 mm length, 3 mm internal diameter and 2.7 μm particle size. The mobile phase was prepared as recommended by European Pharmacopoeia 8th Edition, and consisted of 20 volumes of tetrahydrofuran, 25 volumes of acetonitrile and 955 volumes of a solution containing 0.82 g/L of anhydrous sodium acetate previously adjusted to pH 4.5 with glacial acetic acid. Before its use, the mobile phase was degassed (Ultrasonicator VWR International, Lutterworth, UK).

The flow rate of the mobile phase was 0.5 mL/min; the column temperature was set at 30°C and the chromatograms were acquired at a wavelength of 275 nm. Volumes of 10 μL diluted samples were injected for a total run time of 10 min. The Caffeine peak/retention time was evident at 5-6 min.

The drug content (DC) was expressed as percentage w/w considering the mass of the caffeine ($mg\ Caffeine$) obtained for the single formulations *via* HPLC analysis and the mass of the post-loaded formulations after drying (mg_f), according to the equation:

$$DC\ (\%) = \frac{mg\ Caffeine}{mg_f} * 100$$

3.2.9 Buoyancy tests

The buoyancy tests (n=3) of blank formulations have been carried out on the complete caps-in-cap model (caps and bodies 1, 2 and 3), manually closed and placed in 70 mL of distilled water at 37°C under constant magnetic stirring (50 rpm). The lag time and the floating time have been visually detected and reported in hours.

Buoyancy tests on drug-loaded models (body2 and cap2 enclosed in body1 and cap1) have been carried out following the same protocols above but replacing the distilled water with acidic medium (dissolution buffer 0.1 M HCl solution).

3.2.10 FT-IR analysis

Solid State Fourier Transform Infrared Spectroscopy was performed via FT-IR/NIR spectrophotometer (Perkin Elmer Inc., Spotlight 400N FT-NIR Imaging System, USA) equipped with the Universal ATR accessory crystal plate and Spectrum Software version 10.5.2. All the raw materials, dried caffeine powders pre and post microwave, and blank/loaded printed formulations were analysed in a spectral range of 600-4000 cm^{-1}; moreover, resolution of 1 cm^{-1}, scan number of

128 and scan speed of 0.2 cm/s were used in specular reflectance sampling configuration.

3.2.11 Thermal Analysis via TGA/DSC

Pristine chemicals and dried caffeine powders obtained from the acetonic solutions (pre and post microwave processing) have been analysed *via* Differential Scanning Calorimetry (DSC822e Differential Scanning Calorimeter, Mettler Toledo, Germany) to highlight thermal events. Each sample was accurately weighted in a 40 µL aluminum pan and sealed by a predrilled lid. The thermal cycle set was: a dynamic segment from 25 °C to 400 °C, with a heating rate of 10 °C/min and 70 mL/min of nitrogen as inert gas. The analysis of the data was conducted by STARe Evaluation software v16.20.

Thermogravimetric Analysis (Discovery TGA, TA instruments) was conducted on raw materials, air-dried samples and heated-dried samples with an average mass of 7 mg in TA pans and using a controlled temperature program, from ambient temperature to 400°C, with a temperature of scanning rate of 10°C/min, using N_2 as inert sample purge gas to control the sample environment (20 mL/min). The analysis of the data was conducted by TA Instruments Trios V5.1.1.46572.

3.2.12 Dissolution tests

Drug release profiles were obtained placing the loaded formulations (caps and bodies 2 enclosed in 1) in 750 mL of acidic dissolution medium (0.1 M HCl) and using USP Dissolution Tester TDT-06L (Electrolab), configuration 1 (baskets) at 75 rpm and 37 °C, coupled with 850-DS Dissolution Sampling Station (Agilent

Technologies). For all drug loaded formulations, the withdrawal times were 5';
every 15' minutes until the first hour and then every 30 minutes up to 6 hours. The
samples were quantized undiluted *via* HPLC technique. For all batches analysed,
mean values and standard deviations were reported.

3.3 Results and discussion

3.3.1 Model geometries development and mass/morphological analysis

The modelling of capsules-in-capsule geometries was defined for the possibility of enclosing models in decreasing size consecutively one inside another, as a matryoshka of capsules. Particularly, in all the building steps the models maintained floating behaviour until complete dissolution. This was due to an optimal fraction of the volume of voids over the total volume, even when models are grouped altogether. The developed geometry was configured for having also a great flexibility in terms of number of capsules needed, and for the filling of some of the void volumes with liquid or semi-solid drug vehicles when necessary.

In this research, the capsules shells were used together without any fill.

The prototyping for the FFF 3D printing of caps-in cap was carried out with the aim of obtaining, using a 0.4 mm nozzle, the thinnest wall width for the smallest models (model 3), gradually increased for the largest ones (models 2 and 1).

A fast analysis of the model's geometries and fitting was realized *via* SLA 3DP, taking advantage of the high resolution of this technology and the rapidity of development (printing time for the whole set of capsules: SLA 40 min with the highest resolution; FDM 1 hour with standard resolution).

While SLA printouts usually undergo not noteworthy shrinkage after curing, the FDM printouts are subject to slight swelling after printing, thus during the design process it is essential respecting the tolerances for the 3D printed parts to be accurate, regarding the used technology.

To determine realistic tolerances, the designer in the 3D printing manufacturing process should define tolerances for the design dimensions, as for

plastic injection moulded parts. In fact, in all the manufacturing processes, dimensions are required for the functionality of the prototype and/or correct fit in an assembly. In this case, the assembly requirements are high due to the tiny geometry of the caps-in-cap models.

Considering as fundamental the transition fit, or rather the spacing between two printed parts when no motion between parts is needed, digital models for SLA 3D printing were developed with 250 µm of gaps for the keying-push fit (this fit requires force to join and remove the parts, but allows for easy assembly and disassembly by hand).

The models were rapidly SLA printed until the prototypes with the desired morphological characteristics were reached (figure 2.2 left).
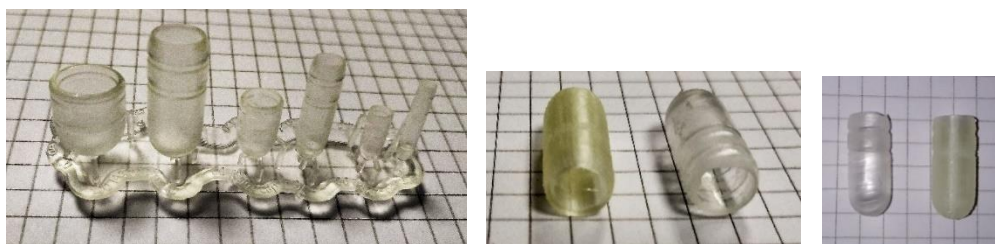
Figure 2.2. From left to right: Final models of caps-in-cap printed via SLA 3DP; comparison between SLA and FDM printouts obtained from the same digital models in which the PVA width expansion can be easily seen

Once selected the opportune model's geometries, during the translation to the FDM 3DP, a re-tuning of the models (figure 2.2 right) was necessary for compensating PVA expansion, moreover the capbody 3 has been developed as a single hollow structure rather than separated cap and body due to the relative lower printing resolution of FDM Ultimaker[3] (XYZ accuracy 20-200 micron using 0.4 mm nozzle) compared to SLA Form3 (XYZ accuracy 25 µm).

116
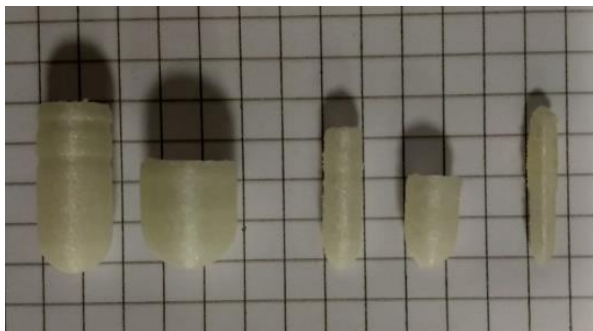
Figure 2.3. Printed caps and bodies optimized for FFF 3DP

The total exposed area, calculated *via* software on the digital models, was about 3000 mm^2, remarkably higher compared to floating models with the same dimensions and low infill percentage for the floating necessity (Giri el al., 2020; Vo et al., 2020). The average total mass of the whole formulation (figure 2.3) was about 1133 mg. Weighted units underlined the FFF high printing reproducibility as confirmed by the low standard deviations of masses (table 2.2).

Table 2.2. Mass analysis of FFF printouts

Model (n=6)	Average mass (mg) ± SD
Cap 1	370.07 ± 16.26
Body 1	374.82 ± 15.26
Cap 2	125.64 ± 9.66
Body 2	150.87 ± 13.63

BodyCap 3	114.43 ± 3.09

The total height of the closed model was 23.00 ± 0.10 mm (digital output: 22.875 mm), and the obtained dimensions of the biggest model 1 (that enclosed the tiniest models 2 and 3) were comparable to the 00 capsules size. Moreover, the general shape of the formulations is related to the well-known geometry of capsules, thus this should suggest high patient compliance and treatment adherence for these 3D printed novel products.

Analysing the dimensional data set of 12 caps-in-cap from 2 batches (6 each) produced with slightly different widths, predictive linear relationships between the digital and the real models has been found (figure 2.4). This result paves the way for an easily re-tuning of the heights, the diameters and the widths of the models, for the purpose of personalization of the shape, dimension and release profiles, according to the patients' dosage needs and swallowing capabilities.
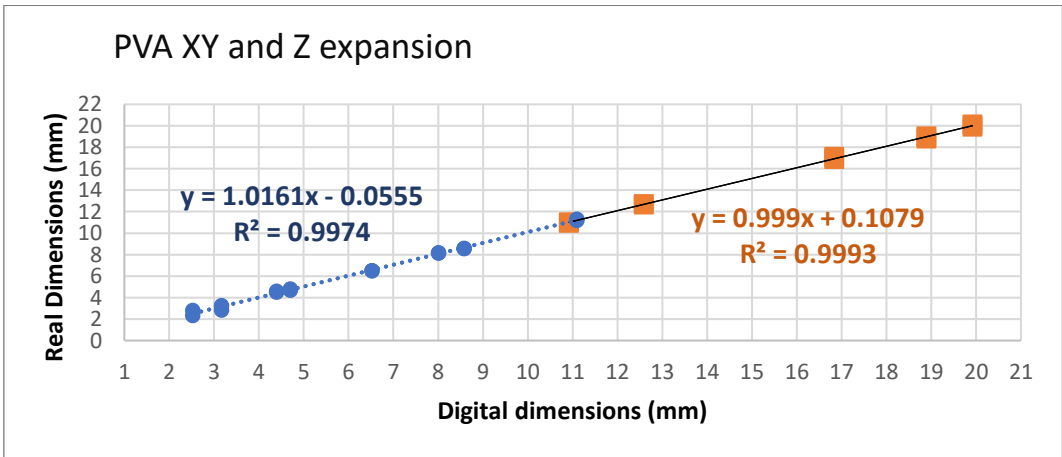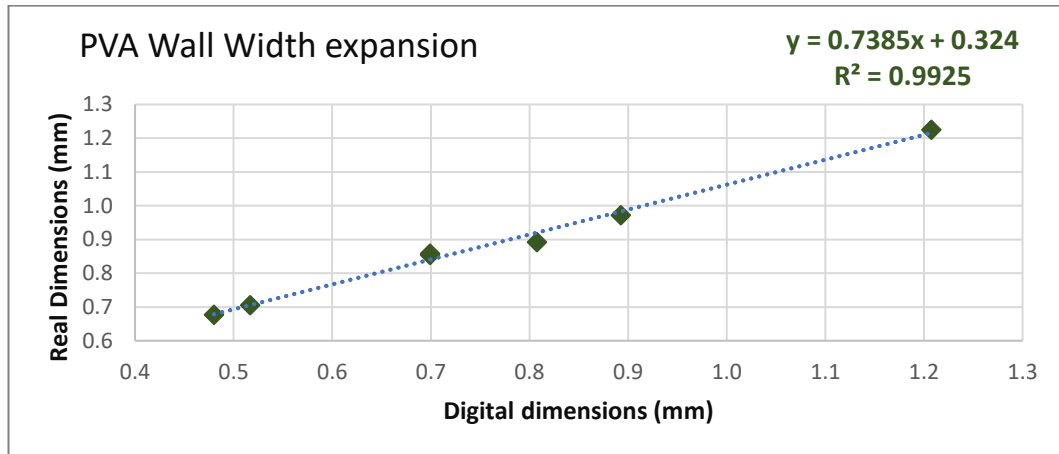
Figure 2.4. Digital-real dimensions linear relationship of PVA printed blank batches: (top) along XY axes (circles) and Z axis (squares); (bottom) along width (diamonds); with related equations on charts

Particularly, considering the PVA expansion along the three axes XY and Z, the digital-real correlation resulted in an accurate prediction for obtaining the desired dimensions of the printouts. For the wall width expansion, the linear relationship was less accurate (R^2: 0.9925), but still realistic, probably due to the bigger nozzle diameter compared to the tiny dimensions of the prints. The accuracy of the prediction could be easily enhanced using nozzles with reduced diameters, such as 0.2 mm, in order to improve the resolution of small models and reduce the variability of widths during printing. Finally, the predictive relationship has been considered fundamental for the thinnest models, to whom the absolute value of the difference between digital and real dimensions was higher than for the biggest models.

3.3.2 Preliminary analysis of solvents for impregnation

All the selected solvents (table 2.3) for the preliminary screening of PVA-solvent interaction (in terms of mass acquired and variation of dimensions in static conditions) belong to the class 3 solvents with low toxic potential, as specified in the EMA document: *"ICH guideline Q3C(R6) on impurities: guideline for residual solvents"*.

Solvent	*Boiling Point (°C)*	*% mass acquired*	*% external diameter acquired*	*% width acquired*
Ethanol	78	43 ± 3	12 ± 1	12 ± 3
Acetone	56	19 ± 3	9 ± 2	8 ± 1
2-propanol	83	3 ± 1	0 ± 0	0 ± 2
Ethyl Acetate	77	0 ± 1	0 ± 0	2 ± 1

Table 2.3. Mass and dimensional analysis of soaked models in different solvents

Considering the percentage of acquired dimensions, the interaction between PVA and solvents was considered high for Ethanol and intermediate for Acetone, while for the other two solvents, 2-propanol and Ethyl Acetate, an irrelevant interaction was found.

The amount of mass acquired, analysed immediately after the withdrawal from the solvent, is certainly related to the boiling point of the used solvent, even if the trend was similar to the percentage of dimensions. Both data set resulted therefore in a confirmation of better interaction for Acetone and Ethanol with PVA.

Theoretically, in fact, the more the solvent power of the medium, the more should the solvent enhance the drug diffusion into the matrix, but more probable will be disruption of the models during impregnation. Indeed, the plasticizing effect

of Acetone and Ethanol was significant, leading to relative softening of the models for the former, and extreme pliability for the latter. Moreover, for Ethanol often the process led to delamination and breakage of the soaked model (Fig. 2.6).

3.3.3 Preliminary analysis of solute distribution via fluorescence imaging

As a preliminary screening of drug penetration into the blank PVA matrix, different microwave cycles were used to load with fluorescein all the three models. As an explanatory example of fluorescent models, printouts loaded in Acetone (the most promising solvent in terms of matrix interaction) using cycles of 5 x 10'' from 40 to 80°C with gradual power have been shown (figure 2.5).
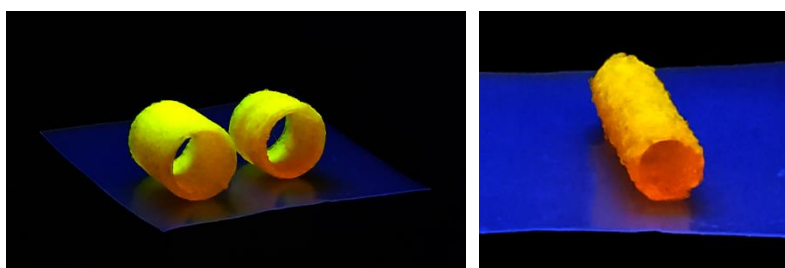
Figure 2.5. Images of fluorescent cross sections of body1 (left) and body2 (right) loaded using 5 x 10'' from 40 to 80°C with gradual power

However, all the images of loaded printouts acquired after the different loading cycles displayed a high adhesion of the solute on the external surface of the matrix, particularly visible for tiny models (figure 2.5 right). But a less homogenous penetration of the solute into the thin walls and in between the area of the adhesion of the layers along Z was always evidenced (figure 2.5 left).

3.3.4 PVA matrix microwave-assisted impregnation

PVA has been chosen for its absorbing properties in the microwave system (Salimbeygi G. et al., 2013) thanks to its good polarity; while Caffeine, categorized into the class I of the Biopharmaceutics Classification System (BCS), was chosen as model drug due to its solubility and high permeability in hydrophilic matrix.

The magnetic stir bar with a pre-stirring of 30 s and a stir rate of 600 rpm of the system allowed the mixture to be continuously blended, promoting homogenous heating throughout.

After the preliminary screening of solvents for microwave post-loading, to confirm the capacity of high interactive solvents in loading higher amounts of solutes, all the four selected solvents and two mixtures (2-propanol:Acetone 50:50 or Ethyl Acetate:Acetone 80:20) were used to load caffeine into the blank printouts, and the results were collected in table 2.4.

Oversaturated solutions with the drug were prepared in relation to the caffeine solubility in these organic solvents (Kulathooran Ramalakshmi & B Raghavan, 1999).

Samples were air dried for 48 hours before mass, dimensional and quantitative analyses.

Table 2.4. Mass, dimension and quantitative analysis of models loaded using different organic solvents, percentages of Caffeine and microwave cycles (in Italic are highlighted samples underwent delamination or breakage)

Time	Temperature	Acquired Mass	Acquired Height	Acquired Diameter	Acquired Width	Drug loading
min or s	*°C*	*%*	*%*	*%*	*%*	*% w/w*
Acetone 2% w/v						

2'	60	4.7	2.2	1.2	0.0	2.40
20'	60	5.0	3.0	1.4	21.5	2.44
5 x 10"	40-60	4.8	2.5	1.0	8.7	2.33
10 x 10"	40-60	6.1	2.6	0.7	3.4	2.62
5 x 30"	40-60	6.0	2.2	0.1	5.6	2.66
10 x 30"	40-60	6.0	2.4	-0.1	2.2	2.58
5 x 10"	40-80	6.1	7.0	-0.7	1.2	2.94
Acetone 1% w/v						
10"	100	-	-	-	-	1.98
10'	100	-	-	-	-	2.24
20'	100	-	-	-	-	2.38
2-propanol 1.5% w/v						
2'	60	7.1	6.6	-0.2	5.9	1.13
2'	60 H	7.6	7.0	-1.3	-9.2	1.10
20'	*60*	*8.1*	*6.6*	*-0.5*	*-8.0*	*2.01*
5 x 10"	60	8.0	5.9	-0.8	-7.1	2.00
2'	*100*	*7.4*	*-*	*-*	*-*	*2.90*
Ethyl Acetate 1% w/v						
20'	60	4.0	1.6	2.2	6.9	0.95
5 x 10"	60	3.8	2.7	0.1	4.8	0.96
2'	100	4.2	3.8	1.7	5.6	1.31
20'	100	4.0	3.7	0.5	5.6	1.37
5 x 10"	100	3.9	3.2	0.8	3.4	1.42
2'	140	5.0	5.1	-1.8	0.0	1.49
Absolute Ethanol 1.5% w/v						
2'	*60*	*4.9*	*20.2*	*-3.0*	*15.5*	*1.25*
2'	*60 H*	*4.8*	*-*	*-*	*-*	*1.12*
2'	60 VH	6.1	28.2	-3.7	0.8	1.57
5 x 10 "	*60*	*5.0*	*-*	*-*	*-*	*1.48*
1 x 10"	*60*	*4.7*	*14.3*	*-3.0*	*9.5*	*0.55*
2-propanol:Acetone 50:50 2% w/v						

2'	60	8.6	6.4	-0.8	7.8	1.7
5 x 10"	50-60	9.2	7.3	0.6	-10.2	2.3
5 x 10"	40-60	11.2	5.6	2.8	-1.3	3.5
2'	*80*	*9.0*	*11.4*	*-2.1*	*-1.7*	*2.9*
5 x 10"	*40-80*	*8.3*	*12.1*	*0.9*	*-3.8*	*2.6*
2'	*100*	*8.3*	*-*	*-*	*-*	*2.9*
Ethyl Acetate:Acetone 80:20 1.5% w/v						
2'	60	4.8	2.5	-0.4	4.4	1.3
2'	100	4.4	5.2	0.2	3.9	1.2
2'	120	4.6	9.8	-3.4	4.0	1.5
5 x 10"	40-120	4.7	-	-	-1.6	1.7

*Figure 2.6. Delamination and/or breakage after MW irradiation of bodies2
processed in:
A) IPA:Acetone using (from left to right): 2 min at 60°C; 2 min at 80°C; 2 min at
100°C
B) Absolute Ethanol at 60°C for 2 min and 5x10 s
C) and D) Caps2 processed at 100°C for 5x10 s and 2 min in different solvents*

Considering that the drug content analysis of the soaked samples in Acetone and Caffeine 2% w/v was 0.55 ± 0.04 % w/w, all the processed samples *via* microwave showed a higher drug content in all the solvents and mixtures. This result already highlights the enhancement effect of irradiation in the mobility of the solute and in the adhesion of the drug on the polymeric printouts, thanks also to the dynamic movement of irradiated PVA models, compared to the steady soaking method.

Then, analysing the concentration of the drug in Acetone 2% w/v (oversaturated solution) and Acetone 1% w/v (not saturated solution), the amount of drug used for the preparation of the solutions is fundamental to increase the loading applying the same cycles of loading (time and temperatures). Thus, oversaturated solutions have been chosen to produce all the subsequent loaded batches.

Treated samples in 2-propanol were less laden of drug compared to Acetone, both using normal and high absorbance set; moreover disruption of models and delamination (figure 2.6 C and D) was evident also at low temperatures (i.e. 60°C).

Considering Ethyl Acetate oversaturated solutions, lower drug loading even at higher temperatures was found, but this solvent preserved the shape of the models, probably due to less interaction with PVA.

On the contrary Ethanol, a very high microwave absorbing solvent, induced breakage of all the treated models or high deformation of the scaffolds (figure 2.6 B), for the extreme interaction with microwave radiations and the polymeric matrix.

Mixtures of different solvents have been produced in order to exploit their interactions with the PVA. In fact, 2-propanol was used to improve the propagation of the microwaves of the lone Acetone in ratio 50:50, but no enhancing of the drug

loading was found. While Ethyl Acetate:Acetone 80:20 did not increase the drug amount into the scaffold, even preserving the shape of the caps and bodies.

Moreover, for high temperatures an increase in the amount of caffeine was found for the loaded samples regardless of the solvent used; while no difference in drug-loading was found for long times of exposition (i.e. 10 s, 2 min or 20 min of continue irradiation) (figure 2.7). Besides for long times of irradiation PVA side chain scission was underlined in literature (H. M. Afzal et al., 2019).
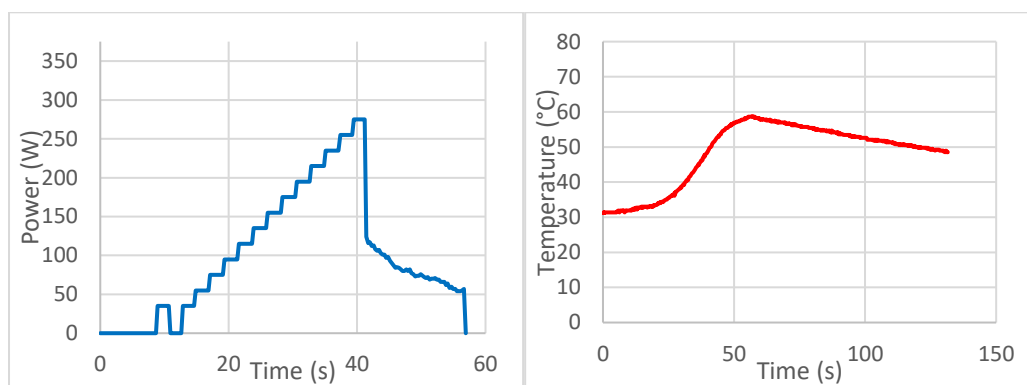
Power and temperature graphs of Acetone and Caffeine 2% w/v 10" 60°C
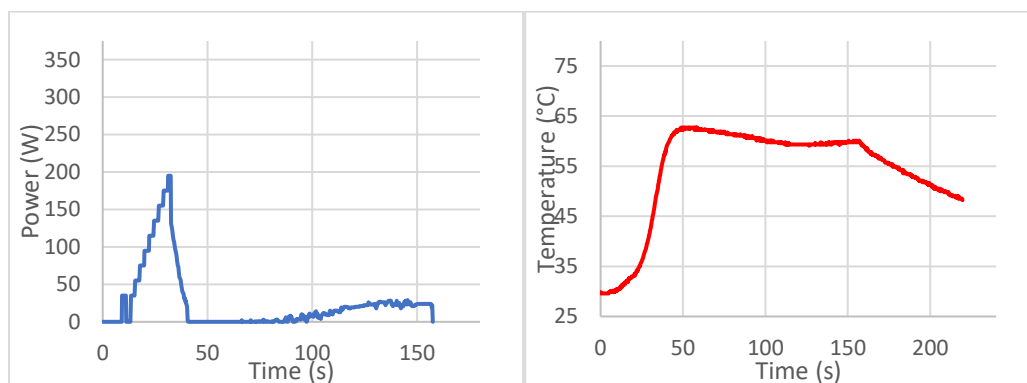
Power and temperature graphs of Acetone and Caffeine 2% w/v 2' 60°C
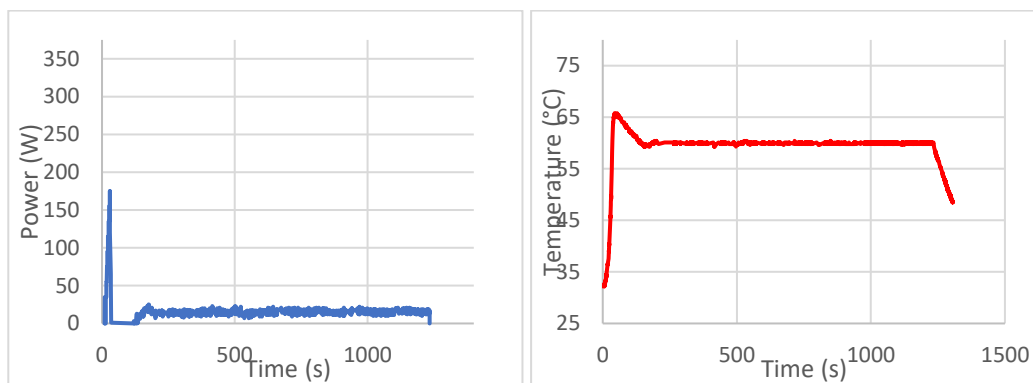
Power and temperature graphs of Acetone and Caffeine 2% w/v 20' 60°C

Figure 2.7. Microwave graphs of different processing steps

Therefore, to avoid the backbone rupture of the PVA polymeric trunk and to improve the shape maintenance of the samples at high temperatures, reduced exposure times of microwaves were considered as optimal.

Particularly, focusing on acetonic solution and cycling pulses, increasing the numbers of cycles (i.e. 5 or 10 pulses with 10 seconds of stay at the maximum temperature), no quantitative enhance was found. Hence 5 short pulses ending with 10 seconds of stay at the final temperature have been selected as the most promising process to load samples at high temperature and to preserve the shape of caps and bodies after the microwave irradiation (5 x 10").

Hence, in this case, Acetone has been finally chosen as appropriate solvent for Caffeine loading, even if the different characteristics of all the screened solvents could be used to modulate the amount of this drug to be loaded in the models. Moreover, these other solvents (interacting with PVA and preserving the shape of the models) could be further exploited for the delivery of APIs with other physicochemical properties or when different ranges of drug amounts are

127

satisfactory (i.e. drug with low therapeutic index or low dosage regimes), adapting the used solvent to the drug, still using PVA as scaffold.

Treating samples with fast pulses and high temperatures (from 40 to 100°C, that also led to a fast increase of the system pressure, >2 bar) still produced deformed caps and bodies, so 80°C was the maximum temperature to be reached during cycles with: 1 bar of pressure developed, lowest effect on the dimensions of the models and highest drug loading.

Finally, heating on a glass plate of loaded samples at 40-42°C was used for all the coming experiments (tables 2.5 and 2.6) to reduce the amount of acetonic residual present in the formulation and speed up the drying process without affecting the shape of the formulations.

Table 2.5. MW cycles effectuated on samples placed in Acetone and Caffeine 2% w/v solutions (in Italic: broken/delaminated samples; in Bold: the best loading cycle using Acetone)

Time	Temperature	Acquired Mass	Acquired Height	Acquired Diameter	Acquired Width	Drug loading
s	•C	%	%	%	%	% w/w
5 x 10"	**40-80**	**4.6 ± 0.8**	**4.0 ± 1.1**	**-1.2 ± 0.8**	**1.9 ± 0.8**	**2.83 ± 0.30**
5 x 10" 100W	40-80	2.1 ± 0.1	2.0 ± 0.5	-0.6 ± 0.9	-1.1 ± 3.1	2.20 ± 0.32
3 x 10"	40-80	6.3 ± 0.4	4.2 ± 0.0	0.2 ± 0.9	1.2 ± 2.1	2.54 ± 0.11
3 x 10" 375 W	40-80	3.1 ± 0.1	4.1 ± 0.3	0.7 ± 0.5	-1.2 ± 2.1	2.47 ± 0.09
5 x 10"	*40-100*	*3.5*	*14.1*	*-4.9*	*8.6*	*3.05*
5 x 10" 100 W	40-100	3.7 ± 0.0	3.0 ± 0.7	-0.9 ± 0.7	-1.1 ± 1.1	2.36 ± 0.44
3 x 10"	*40-100*	*4.1 ± 0.5*	*11.6 ± 1.6*	*-2.9 ± 1.3*	*8.4 ± 6.2*	*2.64 ± 0.16*
3 x 10" 375 W	*40-100*	*4.5*	*-*	*-*	*-*	*2.40*
5 x 10"	50-60	3.9 ± 0.3	2.1 ± 0.6	-0.1 ± 0.5	1.1 ± 7.4	2.20 ± 0.19
5 x 10" 200W	60-80	-	-	-	-	2.23

5 x 10"	60-80	5.5 ± 1.9	2.9 ± 1.3	-0.8 ± 1.2	-2.2 ± 1.9	2.73 ± 0.81
5 x 10"	*70-100*	*7.7 ± 0.7*	*15.6 ± 4.4*	*2.6 ± 2.0*	*-2.4 ± 5.5*	*3.78 ± 0.53*
Multiprocess	60-80	3.9	1.7	3.0	9.7	1.50

In order to reduce the energy released from the microwave system during loading and raise the temperature, a screen of different wattage set was carried out (gradual power from 0 to 375 W, 100 W, 200 W and 375 W). In fact, samples processed at 100 W and 40-100°C range of temperature, did not break or deform excessively. But the amount of drug loaded resulted lower than the processing at gradual power with temperature range 40-80°C. Indeed, 5 x 10" from 40 to 80°C led to the maximum of loadable caffeine of 2.83 ± 0.30 % w/w using only oversaturated Acetone.

Starting from these assumptions, PEG 1000 was added into the acetonic solution (table 2.6), exploiting its capability in enhancing the electromagnetic absorbing properties of the whole system and in reducing the impedance of the medium and, then, the dissipation of microwaves during the irradiation (Li Y. et al., 2018). Moreover, PEG has been added as a suspending agent in order to enhance the homogeneity of caffeine physical dispersion, ensuring de-aggregation of caffeine and thus uniform drug distribution into the oversaturated solution.

Time	*Power*	*Temperature*	*Acquired Mass*	*Acquired Height*	*Acquired Diameter*	*Acquired Width*	*Drug loading*
s	*W*	*°C*	*%*	*%*	*%*	*%*	*% w/w*
5 x 10"	Gradual	40-80	2.5 ± 0.4	4.7 ± 1.9	-0.2 ± 2.5	2.5 ± 4.4	2.41 ± 0.14
5 x 10"	**100**	**40-80**	**3.3 ± 0.3**	**2.1 ± 0.4**	**-0.6 ± 0.5**	**1.2 ± 4.1**	**3.04 ± 0.40**
5 x 10" x3S*	100	40-80	-	-	-	-	1.92 ± 0.34
5 x 10"	200	40-80	2.8	2.9	-0.8	1.2	2.49

| 5 x 10" | 300 | 40-80 | 3.0 | 3.1 | -1.4 | 3.7 | 2.45 |
| 5 x 10" | Gradual | 40-100 | 3.1 | 12.1 | -2.3 | 4.8 | 3.12 |

*x3S: three samples processed together in 15 mL of solution in the same moment

Table 2.6. Cycles effectuated on samples placed in Acetone, PEG 2% w/v and Caffeine 2% w/v solutions (in Bold: the best loading cycle using Acetone-PEG)

Particularly, the addition of PEG allowed to reach 100°C of maximum temperature with gradual increase of power without breaking the models. But in this case, the height acquired was excessive and invalidate the possibility of enclosing the small models (models 2 and 3) into the biggest one (model 1).

Accordingly, discarded the possibility of increasing the temperatures, a screen of different wattage sets led to select as the best process in terms of loading and dimensions maintenance: a cycle at 100 Watts from 40 to 80°C, then 10 seconds at 80°C, and at last a fall from 80°C to 40°C speeded up *via* air cooling, all repeated five times (figure 2.8).
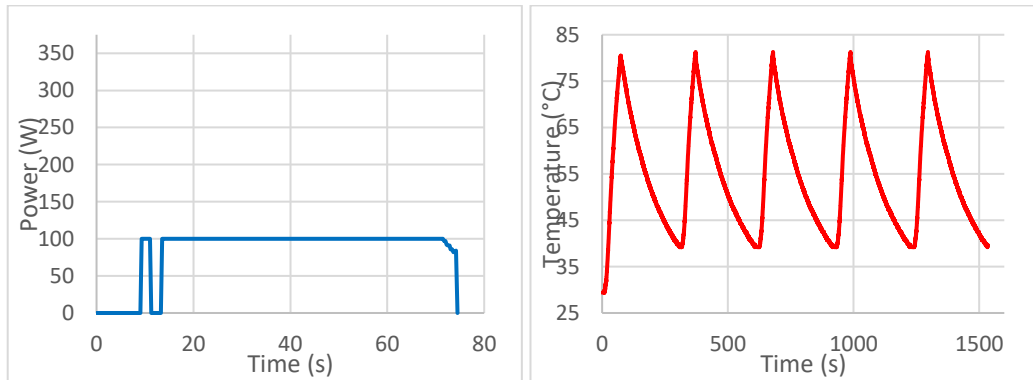
Figure 2.8. Graphs of: (left) power emitted for a single pulse of irradiation; (right) temperature of the five cycles of processing of Acetone PEG 2% w/v and Caffeine 2% w/v (5 x 10" 40-80°C at 100W)

The obtained loaded formulations applying the best selected cycle with PEG are shown in figure 2.9.

Finally, three models were processed together applying the selected cycles, in order to exploit a small scale-up of the process, but resulted in lower drug amount, underlining again the importance of the amount of drug available for the adsorption related to the total mass and surface areas processed.

Figure 2.9. MW drug loaded models in Acetone PEG solution using the best loading cycle with PEG (5 x 10'' 40-80°C at 100W)

In conclusion, the addition of PEG in the oversaturated acetonic solution led to the production of the formulations with the highest drug loading at 100W, corroborating the enhancing properties of PEG in microwave absorbing and in avoiding the attenuation of the waves as it propagates into the absorbing medium. Particularly the effect was related to the set wattage and then to the released energy for molecules vibrations.

A comparison of the amount of drug ($\mu g/mm^2$) adsorbed onto the PVA matrix for some models is shown in table 2.7.

Model	Digitally obtained exposed area mm^2	MW Impregnation in Acetone $\mu g/mm^2$		MW Impregnation in Acetone-PEG $\mu g/mm^2$		Soaking in Acetone $\mu g/mm^2$	
		Average	St Dev	Average	St Dev	Average	St Dev
Cap2	387.022	8.13	0.98	8.85	1.04	1.65	0.14
Body2	452.473	7.05	1.59	-	-	-	-
BodyCap3	349.759	10.27	2.40	-	-	-	-

Table 2.7. Comparison between soaking technique and microwave-enhanced impregnation of the absorbed drug related to the exposed surface area of the models, using the best selected cycles of irradiation

3.3.5 Morphology of processed materials and FFF 3D printed models

Regarding the habit of the caffeine crystals (figure 2.10), unprocessed neat caffeine showed a granular external morphology characterized by irregular cluster of acicular crystals and groups with rough surfaces. All these habits are characteristic of the stable β form (Park & Yeo, 2008).

The organization of the crystals was greatly modified by re-crystallizing before and after the microwave irradiation from the supersaturated solutions, both in acetone and acetone-PEG media.
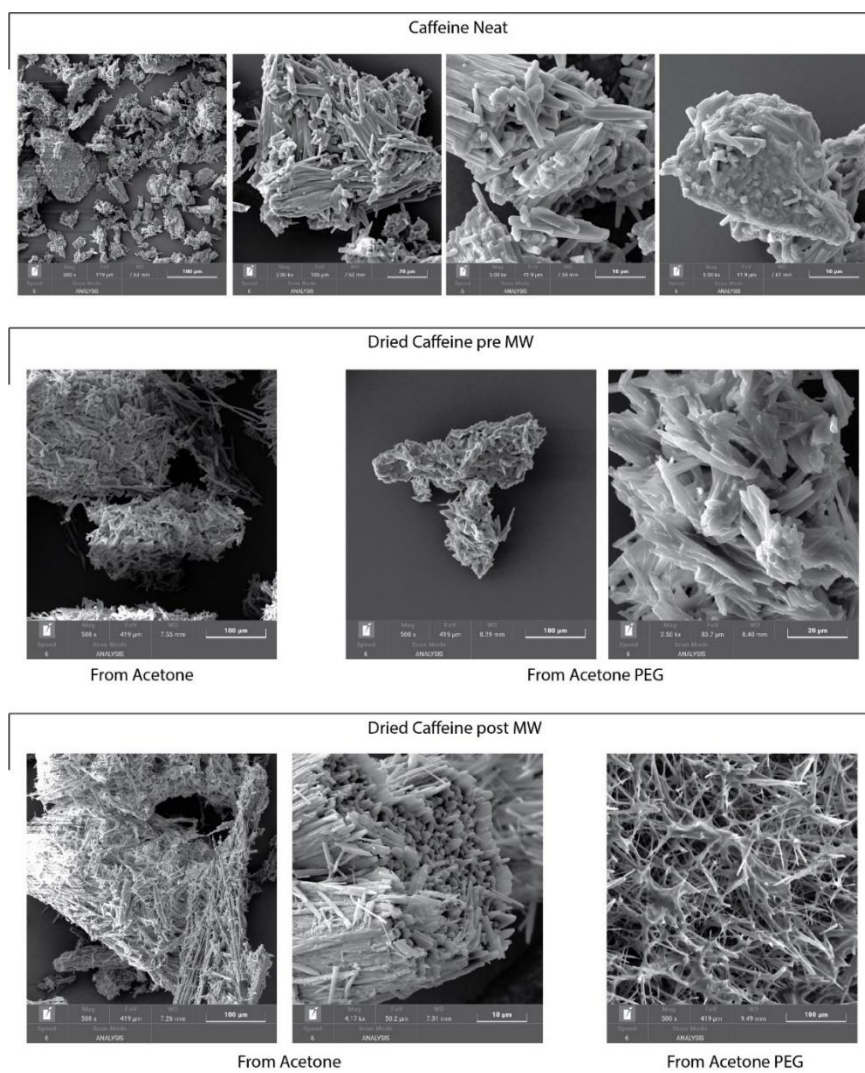
Figure 2.10. Micrographs of neat Caffeine, dried Caffeine obtained from acetone or acetone-PEG solutions before and after the microwave process

All recrystallized caffeine particles from acetone, pre and post microwave, exhibited an acicular and needle-like morphology (a dominant organization of the stable β form). Evident is the presence of extended bundles of parallel laminar β

crystals, assembled in a tubular motif, in which needles pack closely together forming a fibre-like needle wrap (Röthel et al., 2017).

On the contrary, it was found that the presence of PEG led to a significant reduction in bulk size of the caffeine crystallites with particles fused together in uncorrelated islands before the microwave process, while it did not affect the crystal habit, growth again as rod-like crystals. It can be deduced that in the initial stage of caffeine nucleation, PEG induces the formation of a large number of nuclei, and, therefore, the size of each crystal is reduced.

Considering the re-crystallization from acetone-PEG solutions after the microwave, PEG impacted the order and the local morphology of crystals during growth and nucleation. Indeed, a particular habit of the crystals was found, in which caffeine favours the establishment of an interconnected net composed of numerous short and sharp acicular crystals slightly curved.

In this latter case, the length of crystals could be considered limited due to geometrical constraints created by other needles and PEG interfering in extension.

PEG physically stabilized the caffeine in the solution, acting as dispersant. In fact, after the withdrawal from the MW system, the nucleation of crystals was visually slower in the PEG rich solution compared to the rapid recrystallization of elongated and sharp needle-shaped crystals in acetone-caffeine. As highlighted analysing the acquired magnifications (figure 2.10), the formation of smaller crystals in size was evident for caffeine when prepared with the addition of PEG. This evidence could also derive from the stabilization effect caused by PEG, which may reduce the Gibb's free energy of the surface of the crystal during nucleation. Thus, PEG may prevent the crystals from merging into larger ones during the re-

crystallization stage (Wang H. et al., 2002), leading instead to the formation of an interconnected network of small sharp acicular crystals.
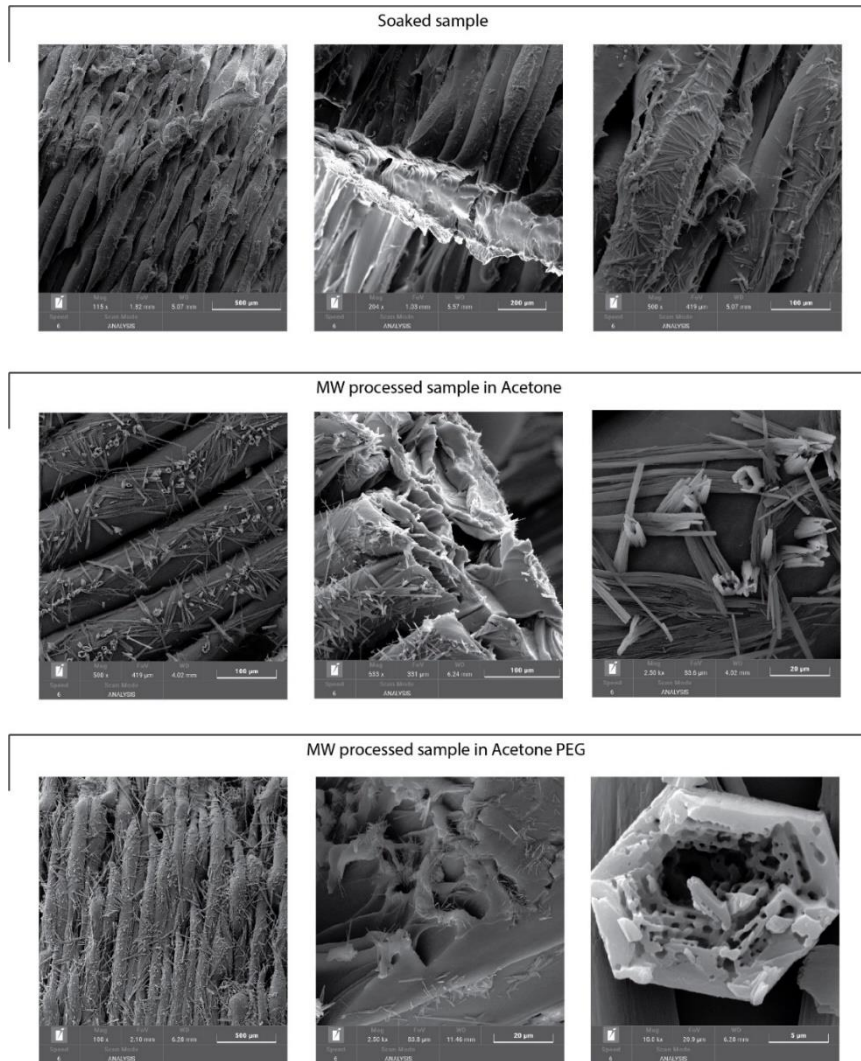
Figure 2.11. Micrographs showing: soaked samples details; samples with the higher drug amount from: acetone and acetone-PEG

Analysing the micrographs of the processed samples (figure 2.11), the PVA models resulted in slightly distorted layers adhesion due to the processes carried out on them. Furthermore, it can be evidenced that the drug adhesion onto the PVA model was more homogeneous for samples processed *via* microwave, compared to the soaked ones.

Moreover, both after soaking and microwaving, the growth behaviour of caffeine crystallites onto the PVA surface followed preferentially a directional growth, favouring a flat-on orientation with respect to the substrate, particularly considering the bundles of packed acicular crystals of β polymorphs. Thus, the orientation of adsorption after nucleation during crystal growth mostly coincided with the long needle axis, regardless of the roughness of the surface.

Particularly, on samples processed in acetone *via* microwave, tubular fashions of the metastable α polymorphs were highlighted. These were organized as slightly disturbed hexagonal or rectangular motifs with a central cavity within the crystals, which favoured instead an edge-on orientation perpendicular to the PVA surface. The cavity in tubular crystals of caffeine forms when the concentration of the residual solution at the centre of the crystal growth face decreases until it is no longer supersaturated. While the edges of the face continue to grow, as it is easier for drug molecules to diffuse to the edges of the rapidly growing hexagonal tubular motif (M.D. Eddleston & W. Jones, 2009a).

Indeed, in literature, the loss of polyhedral stability under these conditions has been reported for a wide range of compounds (C. N. Nanev & A. N. Penkova, 2002).

With regards to samples loaded in acetone-PEG *via* microwave, high organized hexagonal structures of caffeine crystallites were identified,

characteristic of the metastable polymorph α, as further highlighted also by DSC and IR data. This crystal habit occurs when the growth rate of the hexagonal face is greater at the centre than at the edges. Thus, it can be deduced that PEG retarded the drop of acetone solution in evaporating and supersaturation levels increase in the dome of the hexagonal face. This event leads to the diffusion of caffeine molecules in the centre of the cavity in the slowly growing hexagonal crystals, while the growth rate is reduced to the apexes of the structure (M.D. Eddleston & W. Jones, 2009b).

Hence, it can be deduced that β acicular crystals privilege the growth of molecules lying parallel to the surface planes (a flat-on orientation for dominant molecule-substrate interactions). On the contrary, tubular motifs of α forms and hexagonal α polymorphs minimized the interaction area with the underlying substrate, adapting an edge-on molecular orientation (strong molecule-molecule interactions).

Finally, even not penetrating deeply into the polymeric matrix, caffeine accumulated not only on the surface of PVA, but also in the hollow cavities inter and intra layers, existing as thick and short needles grown along random directions, slightly rotated to adjacent needles.

In conclusion, both after soaking and microwave process, caffeine crystallites tended to rearrange in adsorption geometries more energetically advantageous to adapt for the polymeric surface constraints.
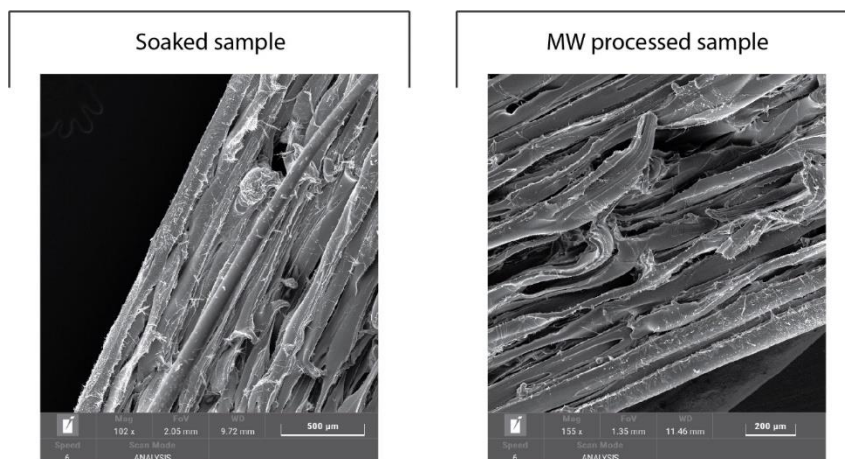
Figure 2.12. Magnifications of soaked and microwaved samples of the inner cavity of the models, showing the reduction of the drug adsorbed on the concave surface of caps and bodies

An interesting aspect of the drug adhesion onto the PVA surface was evidenced by the acquisition of magnifications of the inner part of the caps and bodies (figure 2.12). Here caffeine adsorbed particularly on the initial few layers of the concave area of the models, while on the internal part the drug distribution was not homogeneous and comparable to the outer surface. This resulting in areas with alternating adhesion of Caffeine and interspersed layers missing of API. This occurrence may be explained by the development of Görtler vortices in the boundary layer flows on curved walls, leading to a convective instability of flow and turbulent motions of the liquid into cavity of caps and bodies (Kim et al., 2010). The turbulences prevented the drug to interact and adsorb homogeneously onto the polymeric concave inner surface.

3.3.6 FT-IR analysis
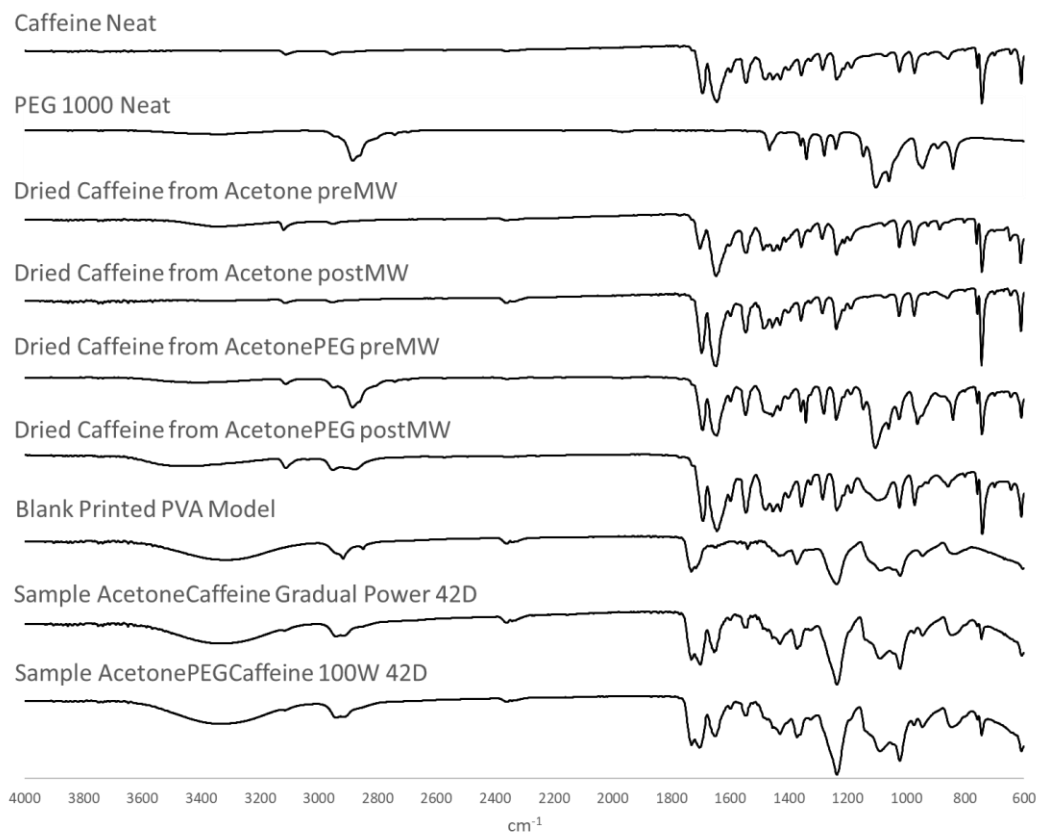
Figure 2.13. FT-IR spectra of raw materials (Neat Caffeine, PEG 1000 and blank printed PVA), dried powders from Acetonic or Acetonic PEG solutions pre and post microwave processing, and heated dried samples treated using 5x10'' cycles 40-80°C (Acetone solution with gradual power; Acetone-PEG solution with 100W)

All the acquired spectra are shown in figure 2.13.

Particularly, in the spectrum of the blank printed PVA model, the intermolecular hydrogen bonded O-H stretching broad band of medium intensity was observed at about 3300 cm^{-1} (3100-3550 cm^{-1}). While the sharp and narrow band visible at about 1260 cm^{-1} was due to the in-plane alcoholic deformation

139

vibrations coupled with CH wagging vibrations. At 600-710 cm^{-1} O-H out-of-p1ane deformation vibrations were present.

The C-O absorbed at 1085-1020 cm^{-1}, stretching vibration frequency of secondary alcohol slightly lowered by the presence of unsaturation and chain branching and showing multiple bands due to coupling. A band of medium intensity in the infrared spectrum at 900-800 cm^{-1} was due to C-C-O stretching vibration.

Bands at 1430-1375 cm^{-1} were associated with CH deformation vibrations of secondary alcohols while 2940-2920-2850 cm^{-1} signals to CH_2 stretching vibrations during interchanging rotational conformations relative to the monomer and its neighbours.

Finally, the frequency of the C=O stretching vibrations was at 1715-1730 cm^{-1}.

Bands highlighted at 2360-2340 cm^{-1} were attributed to diamond plate artefacts and atmospheric CO_2.

PEG 1000 neat vibrational spectrum showed bands near 2885 cm^{-1} and 1465 cm^{-1} due to the CH stretching, deformation and rocking vibrations. Additional bands near 1360-1340 cm^{-1} were associated to the polymeric branching. While in the region 1280-1240 cm^{-1} bands were related to the C-O stretching of epoxides structures of monomers used for PEG synthesis, or onto its chains, confirmed also by the bands at 895-840 cm^{-1} of the ring vibrations.

This saturated aliphatic polyether exhibited strong absorption in the region 1150-1060 cm^{-1} due to the C-O-C asymmetric stretching vibration of the majority of units in the chain core, showing the strongest two peaks for the branched-chain. Weaker bands observed in the region 945-895 cm^{-1} were associated to the symmetric stretching vibration of the C-O-C group.

140

Moreover, a relatively broad band due to the terminal hydroxyl groups was also observed near 3330 cm^{-1}, and probably the band at 1960 cm^{-1} was related to OH bending.

Regarding the pure anhydrous Caffeine spectrum, such as all purines, caffeine showed the characteristic band at 640-610 cm^{-1} probably associated with C-H out-of-plane bending vibrations. The ring stretching vibrations of the C=C and C=N bonds were strongly detected as several bands in the region 1680-1545 cm^{-1}. Other absorptions were also observed at 1480-1430 cm^{-1} and 1025-970 cm^{-1}. At 1695 cm^{-1} the carbonyl stretching vibrations were visible as sharp band; moreover, in the region 3120-3010 cm^{1}, ring =C-H stretching vibrations were highlighted and NCH groups were identified thanks to the methyl groups CH$_3$ symmetric and asymmetric stretching vibrations found at 3000-2815 cm^{-1}.

Considering the air-dried Caffeine obtained from Acetone and Acetone-PEG solutions (pre and post microwave), all the characteristic bands of the drug were found in the spectra.

Before the microwave process, the absorption in the 3500–3150 cm^{-1} region may come from the OH stretch of residual minute quantities of water in pure acetone (> 0.5%) that was trapped in Caffeine crystals (J.J. Max & C. Chapados, 2003), and/or from the formation of organic solvates Caffeine-Acetone in a cocrystal related system (solvent evaporation may give rise to a solvent occlusion into the crystal faces as multicomponent systems) (A.M. Healy et al., 2017). Both phenomena are confirmed by the slight variation of CO stretching vibrations (from 1695 to 1700 cm^{-1}) and of the band characteristic of ring =C-H stretching (from 3110 to 3120 cm^{-1}).

Instead, regarding the air-dried Caffeine obtained from Acetone-PEG solutions, the spectrum obtained before the microwave process, displayed: a slight shift (from 1105 to 1110 cm^{-1}) for the C-O-C asymmetric stretching of PEG, a variation of the band shape in the range 1480-1430 cm^{-1}, and broadening of the band at 3400 cm^{-1}. All confirming the presence of intramolecular non-covalent interactions (such as hydrogen bonding and Van der Waals forces) between Caffeine ring and the PEG trunk and OH terminals. Moreover, in the spectrum of the dried caffeine after the microwave process, a further variation of the C-O-C band was observed, shifting from 1105 to 1095 cm^{-1}. Furthermore, in the range 1340-1360 cm^{-1}, the two bands characteristic of the PEG branching became a single band at 1358 cm^{-1} and a reduction in the relative intensity of PEG bands at 2885 cm^{-1} due to the CH stretching and deformations vibrations was highlighted. From these variations, a re-arrangement of the PEG branching pattern caused by the microwave process may be supposed and the further broadening of the band at 3450 cm^{-1} may suggest a more intimate interaction amid the Caffeine structure and the PEG shaft with reduced segments.

Finally, regarding the samples processed in Acetone (Gradual Power) and Acetone-PEG (100W), both the spectra displayed the typical bands of purines (from 610 to 745 cm^{-1} and 1240 cm^{-1}); besides the CO alcoholic stretching region (1020-1090 cm^{-1}) and CH deformation region (1300-1440 cm^{-1}) of PVA were unchanged. For both processed samples, similar variations in band shifts were underlined, particularly:

- from 1645 to 1655 cm^{-1} of the caffeine ring stretching,
- from 1695 to 1705 cm^{-1} and from 1730 to 1735 cm^{-1} of the carbonyl groups of caffeine and PVA respectively,

− from 2950 to 2940 cm^{-1} of the methyl groups of Caffeine.

Moreover, a broad band at 3330 cm^{-1} increased in relative intensity. All these data highlighted the presence of intramolecular non-covalent interactions between Caffeine structure and PVA, particularly with hydroxylic terminals, enhanced by the microwave processing. Moreover, these shifts highlighted the presence of the α polymorphs of caffeine crystals adsorbed onto the polymeric matrix. The polymorphic transition was therefore mediated by the supersaturated acetonic solution during evaporation and crystals nucleation and growth, as evidenced also by SEM micrographs and DSC analyses.

3.3.7 Thermal Analysis via DSC and TGA
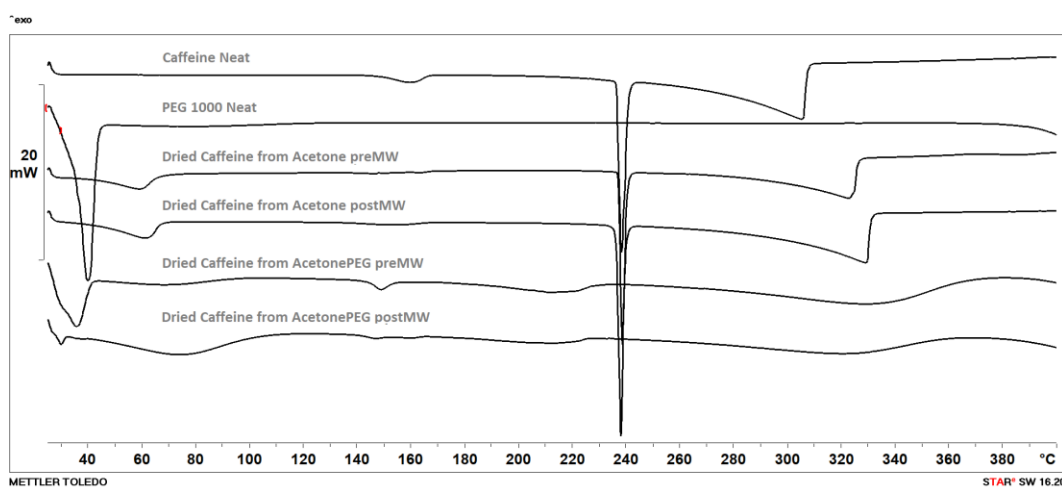
Figure 2.14. DSC thermograms of neat materials and dried caffeine with Y-axis offset for comparison

Starting from the thermogram of pure Caffeine (figure 2.14), the drug, as irregular crystalline particles (figure 2.10, Caffeine Neat) at room temperature, experienced a partial sublimation and recrystallization in the range of temperatures

140-170°C. This endothermic peak of a solid-solid transition (Dong et al. 2017) led to the growth of long needles and rod-shaped crystals (found also after the microwave process, figure 2.14). The melting of the β form of the drug was evident at 240°C, finally the melted product underwent evaporation process from 260 to 310°C (R. Ruiz-Caro1 & M.D. Veiga-Ochoa, 2009). Furthermore, the caffeine did not show thermal events until 140°C, confirming its anhydrous state.

The acquisition of raw PEG 1000 displayed the melting process at 30-45°C and decomposing starting after 380°C.

The thermograms of air-dried Caffeine obtained from Acetone solutions (both pre and post microwaving) showed the evaporation of the residual solvent in the range 30-70°C, with a peak at 60°C, and a slight decrease of the melting peak (237 and 235°C respectively). Moreover the range of evaporation was highlighted at 260-330°C. Minor peaks of recrystallization during solid-solid transition were slightly visible at 155°C, with transition heat in the range -8/-27 mJ. These data confirm the change in the crystalline structure, from irregular particles to needle-like crystals, and the processed crystals are thermally more stable compared to the unprocessed caffeine. Furthermore, the hypothesis derived from FT-IR about the composition of organic solvates Caffeine-Acetone in a cocrystal related system is confirmed.

Finally, the thermograms of air-dried Caffeine obtained from Acetone-PEG solutions corroborated the deduction of the PEG chain scission due to the decrease melting range of PEG at 25-32°C found after the microwave process. Furthermore, for both pre and post microwaving Caffeine, the solvent of crystallization desorbed and evaporated from 45 to 100°C, evidence of the stronger non-covalent interactions with the interstitial acetone trapped into the crystals. The melting range

of the Caffeine turned out in a broader peak starting from 170 up to 230°C, as well as the evaporation process from 270 to 370°C. All these data underlined the probable effect of PEG in the reduction of the Gibb's free energy of the surface of the crystals with the construction of small sharp crystals with improved thermal stability (figure 2.10).
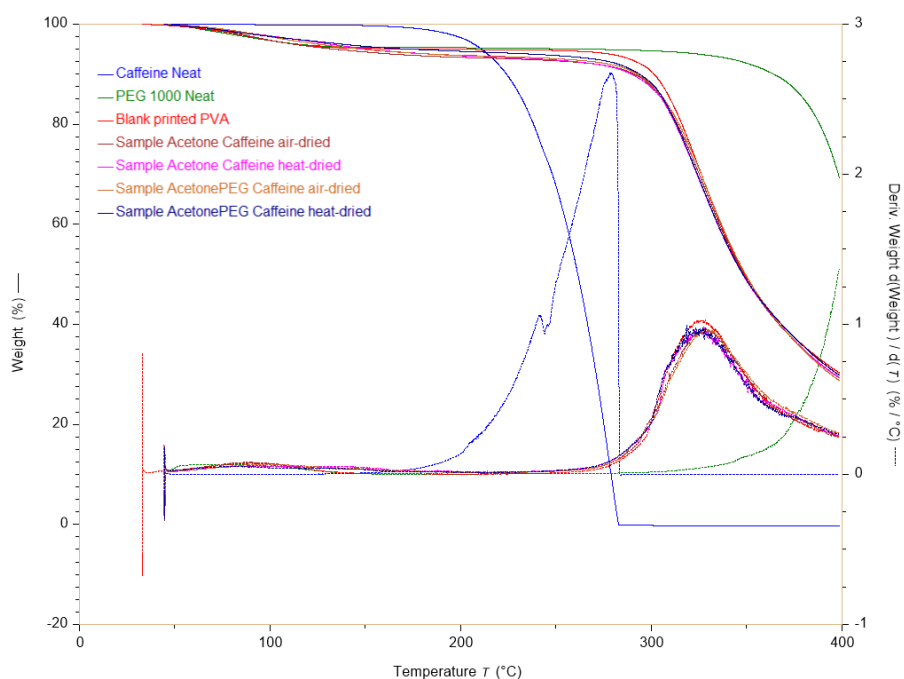
Figure 2.15. TGA thermograms of: neat materials (Caffeine Neat, PEG 1000 neat and printed blank PVA); samples from Acetonic (using gradual power) or Acetonic-PEG solutions (using 100W) post microwave processing, air and heated dried treated using 5x10'' cycles 40-80°C. The solid lines are the weight loss curves and the dashed lines are their respective derivatives

The thermogravimetric analysis (figure 2.15) of neat caffeine indicated that the compound was stable up to 200ºC. Then the onset when the weight loss began

of the melting event took place at 245-283°C and the total mass loss occurred in a single step. The peak of the first derivative indicated at 278°C the point of greatest rate of change on the weight loss curve, thus the inflection point with 100% weight loss confirmed the total evaporation of the drug.

Regarding the unprocessed PEG 1000, the onset of the pyrolysis was found at 391°C, and from 85 to 173°C a 4.6% of weight loss was evidenced (DTGA), due to the evaporation of residual water and formation of volatile products.

For the blank printed PVA models, the weight loss peak was found at 325°C, beginning at 306°C and ending at 348°C (with 30.3% of residual weight at 400°C corresponding to carbonised products). Furthermore, up to 206°C only 5.0% of weight loss occurred due to residual adsorbed water, underlining the high thermal stability of this thermoplastic polymer used for 3D printing.

The air-dried samples from acetone displayed a peak at 91°C, starting from 50°C, with a weight percent loss of 6.7% of residual adsorbed moisture and/or acetone. While the heated-dried samples from acetone experienced at 85°C, starting from 44°C, just 2.5% of weight loss, highlighting the reduction of residual organic solvent and water after the drying step at 40-42°C. For both samples the step transition occurred at 328°C (onset 302°C, endset 349°C) with a change in weight of 71.8%.

Regarding the samples processed in acetone-PEG solution, the air-dried samples showed a peak at 97°C with a variation in weight of -6.3%; while the heated-dried sample displayed a peak at 84°C and underwent 3.1% of weight loss. These differences in variations underlined again the enhancement of the evaporation of residual solvent of the heated drying process, reducing the potential

toxicity of these floating drug delivery systems when administered during long therapeutic regimen.

The weight change was 72.4 and 71.1% for the air and heated dried samples, with step transition at 328 or 318°C respectively (onset 304°C and endset 350°C).

Peaks at 135°C (weight percentage loss of 3.9%) and at 131°C (weight percentage loss of 2.4%) were found in the thermograms of heated-dried samples deriving from Acetone and Acetone-PEG solutions respectively, due to the partial sublimation of the Caffeine α crystals. Thus, these events further confirmed the presence of the α polymorph derived from the microwave-assisted drug-loading and solvent evaporation at 40-42°C.

3.3.8 Buoyancy tests

Blank formulations and drug loaded formulations (models 1, 2 and 3) showed the same buoyancy behaviour with no lag time during tests in beakers, both in distilled water and acidic medium. The floating time of blank and drug loaded formulations lasted until complete erosion of the PVA matrix (6.0 ± 0.5 hours). Regarding MW post-loaded formulations, after 20 hours a minimal sticky residual mass was slightly visible adhered onto the glass surface of beakers or into the metallic mesh of the dissolution baskets. These data were indeed confirmed visually also during dissolution tests of post-loaded formulations (models 1 and 2) placed in USP dissolution apparatus.

3.3.9 Dissolution tests

Analysing the release kinetics of the samples processed in Acetone or Acetone-PEG (figure 2.16), the caffeine dissolution profiles were considered over imposable. Hence, the impact of small pulses using two different parameters of power set (gradual power or 100W) did not affect particularly the PVA matrix in terms of erosion, even if this assumption should be confirmed for higher wattages (i.e. 200 or 300W). Furthermore, caffeine adsorbed onto the Acetone and Acetone-PEG processed samples displayed the same dissolution behaviour, determining a similar *in vitro* drug release rate. Finally, Acetone-treated samples (AC1) displayed a slight reduction in drug released and dissolution, probably due to the presence of different crystals α polymorph organizations.
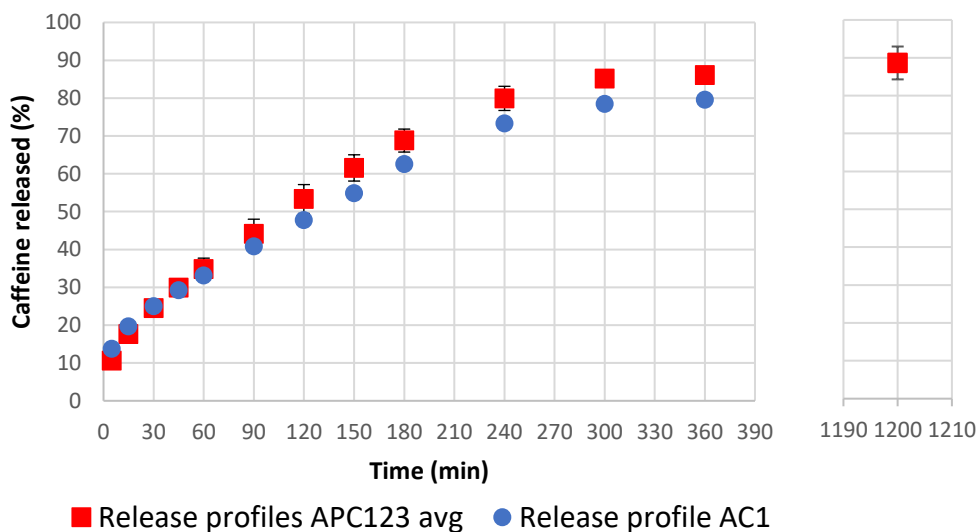
Figure 16. Release profiles in acidic medium of Caffeine from samples processed in Acetone (AP1; n=1) or Acetone-PEG (APC123; n=3)

3.4 Conclusions

In this research, an innovative and unexplored methodology for post-loading of Fused Filament Fabrication 3D printed pharmaceutical formulations, applying microwave irradiation, was analysed and optimized. It is therefore confirmed the potentiality of this process in improving the adhesion of the drug on printed drug delivery models, compared to the traditional soaking technique.

Particularly, Stereolithography 3D printing was used for rapid prototyping of floating systems in order to speed up the freeform fabrications of oral forms, exploiting the high resolution and fast process times of this technology.

Then, the developed models were produced as blank PVA scaffolds *via* FFF3DP and the dimensional outputs were compared to the digital inputs to allow an easily re-tuning of the model's widths and dimensions according to patients needs and swallowing capabilities.

The printed gastro-retentive systems were then subjected to microwave irradiation, screening the effect of oversaturated solutions with the model drug Caffeine, using different solvents with low toxic potential and diverse radiation absorbing properties. Different amounts of drug were found for the selected solvents considering their capability in interacting with the matrix, paving the way for the selective use of solvents for controlling the mass of the drugs in the post-loading process of PVA blank formulations.

Once selected the most promising solvent (Acetone), the methodology was hence fully deepened in terms of parameters (time of irradiation, pulses effect on polymeric models, temperature, pressure and energy released from the system), selecting as best loading process: a cycle at 100 Watts from 40 to 80°C, then 10

seconds at 80°C, and at last a fall from 80°C to 40°C speeded up *via* air cooling, all repeated five times.

All the screened oversaturated solutions displayed a higher amount of Caffeine compared to the soaking technique (5.53 times more for the most promising carrier solution), highlighting the enhancing properties of this methodology in post-impregnation of blank scaffolds.

Moreover, the intensify of drug-loading was found when a biocompatible pharmaceutical excipient with polar characteristics, i.e. PEG, was added to the oversaturated solutions, thanks to the reduction of wave dissipation during irradiation and to the interaction with the selected drug and polymeric matrix.

The best oversaturated solution (Acetone-PEG 2% w/v with 2% w/v of Caffeine) allowed the production of pharmaceutical forms with the highest drug amount, without any changes in physicochemical characteristics and stability of the polymeric matrix.

Moreover, the novel process succeeded in preserving the shape of the loaded oral systems and a deep analysis of the drug adhesion on the developed concave models has been carried out. This highlighted a great adsorption of the API on the external surface and a less homogenous adhesion in the internal cavity of the models, due to turbulence of fluid behaviour in the inner cavities.

Furthermore, modifications in the crystalline habits of the drug were investigated, underlining the formation of different polymorphs after the microwave processing on the loaded formulations. This is a fundamental event to be considered when the physical characteristics of polymorphs lead to modifications in release kinetics.

In conclusion, the novel developed technique for post-loading and impregnation of FFF 3D printed blank polymeric models, enhancing drug adsorption *via* microwave irradiation, could be implemented in clinical settings and manufacturing scale-up for the production of drug delivery systems. These dosage forms can be personalized in amount and types of API, taking into account all the variables and parameters highlighted in this scientific research.

4. SECTION III

Modelling via fused filament fabrication of coaxial semi-solid extruders for the production of tailored floating drug delivery systems by semi-solid 3D printing and extemporaneous alginate gelation
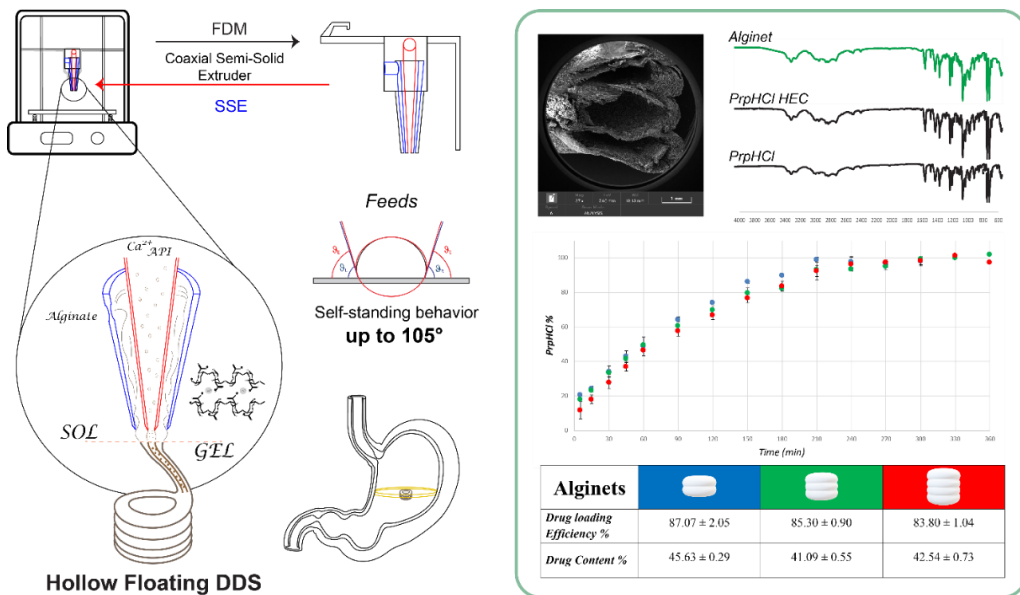
Based on the paper

Falcone G.[1], **Saviano M.**[1], Aquino R.P., Del Gaudio P. , Russo P., *Coaxial semi-solid extrusion and ionotropic alginate gelation: a successful duo for personalized floating formulations via 3D printing,* Carbohydrate Polymers, Volume 260, 15 May 2021, 117791

4.1 Scientific background and research aim

Compared to the notable potentiality of Fused Deposition Modelling 3D printing (FDM 3DP), extremely deepened in prototyping (Boparai, Singh, & Singh, 2016) and recently in the pharmaceutical field (Trivedi et al., 2018; Fina, Goyanes, Rowland, Gaisford, & W Basit, 2020; Maroni et al., 2017; Saviano, Aquino, Del Gaudio, Sansone, & Russo, 2019), Semi-Solid Extrusion 3D printing (SSE 3DP) is an unexplored technology in drug compounding, even belonging to the Material Extrusion techniques as FDM. Lately, SSE has been studied for bioprinting applications (Hölzl et al., 2016), thanks to its mild process conditions in terms of environment settings (room temperature and normal pressure) (Schütz et al., 2010; Townsend, Beck, Gehrke, Berkland, & Detamore, 2019). It is to be considered however that SSE printouts, obtained extruding from a syringe pump system ink gels, usually undergo post printing treatments (i.e. UV or enzymatic crosslinking, chemicals curing) to produce cellular scaffolds or vascular constructs (Hong, Kim, Jung, Won, & Hwang, 2019; Liu et al., 2018; Matai, Kaur, Seyedsalehi, McClinton, & Laurencin, 2020).

Hence, SSE 3DP is a relatively unused technology in the production of drug products, both for the lack of study on the printability of drug loaded gels, and for the critical step of post-processing after printing, that could affect the drug content. In fact, the number of works nowadays present in literature are limited (Goyanes et al., 2019; Khaled, Burley, Alexander, & Roberts, 2014), and particularly, focusing on floating SSE prints, only infill geometries or binding agents have been used to modulate the buoyancy behavior (Li et al., 2019; Wen et al., 2019).

Regarding the production of drug delivery systems, one of the most used natural polymers is sodium alginate (SA), a copolymer containing blocks of (1,4)-linked β-d-mannuronate (M) and β-l-guluronate (G) residues in consecutive or alternate manner (Auriemma et al., 2020). Particularly, it is used for the production of loaded beads obtained by prilling technique (Cerciello et al., 2015; 2017), nanoporous gels enhancing the diffusion of small chemical drugs (Boontheekul, Kong, & Mooney, 2005), nanoparticles (Dodero, Alloisio, Vicini, & Castellano, 2020), and amphiphilic gel beads prepared to modulate the release of hydrophobic drugs (Lee & Mooney, 2012). Nevertheless, to date SA has never been used for the production of drug vehicles *via* SSE.

In detail, the ionotropic gelation is one the most interesting property of SA for novel applications such as SSE. In fact, thanks to its G-blocks, the chemical crosslinking with divalent cations turns into a three-dimensional networks when SA is dispensed into a crosslinker solution (i.e. Ca^{2+}, Zn^{2+}) (Beyer, Bsoul, Ahmadi, & Walus, 2013), also exploiting coaxial extrusion of both components simultaneously (Costantini, Colosi, Święszkowski, & Barbetta, 2018).

In this research, we hypothesized that the ionotropic gelation of SA, in a coaxial semi-solid extrusion printing technique, would lead to novel drug delivery systems (DDS) without further chemical post-processing or crosslinking. Moreover, the suitable pumping of two different feeds into the coaxial extruder in the right configuration in/out would make those DDS able to float. Particularly, the selected fluids were: the SA gel (named ink gel) and a hydroxyethyl cellulose (HEC) gel (Dai et al., 2019) containing the crosslinking agent Ca^{2+} (named crosslinking gel). Finally, theorising the application of this single-step

manufactured DDS in the personalized therapy, the addition of Propranolol Hydrochloride into the SSE formulations was carried out.

4.2 Materials and Methods

4.2.1 Materials

For the FDM 3DP of co-axial extruders, polylactic acid (PLA) was used (Natural PLA, Ultimaker, Netherlands).

All materials for the novel DDSs were used as received unless otherwise noted: sodium alginate European Pharmacopoeia X with β-d-mannuronic:β-l-guluronic acid ratio of 1.3, MW > 200000 g/mol, and 1% aqueous solutions viscosity 65 mPa·s (CAS 9005-38-3, Carlo Erba, Milano, Italy); hydroxyethyl cellulose high viscosity (2100 mPs of 1% aqueous solutions), with a degree of substitution of 1.5 (3 hydroxyls substituted/2 units) (CAS 9004-62-0, ACEF, Italy); calcium chloride (CAS 10043-52-4, VWR International, Milano, Italy); Tween® 85 (Tw, CAS 90005-70-3, Sigma-Aldrich); Propranolol Hydrochloride (PrpHCl, CAS 318-95-9, Farmalabor, Milano, Italy); Hydrochloric acid 37% w/w (ACS reagent, CAS 7647-01-0, Sigma-Aldrich, Italy); Sodium Phosphate (CAS 7601-54-9, Sigma-Aldrich, Italy).

4.2.2 Co-axial extruders production via FDM 3DP

4.2.2.1 Digital modelling and FDM 3D printing

All the extruders were designed using the Computer Aided Design (CAD) software Rhinoceros 6 (Robert McNeel & Associates, McNeel Europe) and adapted to the Ultimaker[3] (FDM 3D printer Ultimaker, Netherlands) printhead. CAD

models were exported as stereolithographic files (.stl) and then processed *via* the slicing software Cura 3.2.1 (Ultimaker, Netherlands) to generate the g-code file read by the 3D printer as commands for the printing process. The refined slicing parameters and operative specifics for the printing of the PLA filament into extruders are shown in table 3.1.

Table 3.1. FDM printing parameters of co-axial extruders

FDM operative specifics		*FDM slicing parameters*	
Material	Ultimaker PLA	**Layer Height**	0.3 mm
Nozzle diameter	0.4 mm	**Infill Line Width**	0.43 mm
Printing Temperature	200°C	**Wall Thickness**	0.5 mm
Build Plate Temperature	80°C	**Top/Bottom Thickness**	1 mm
Infill Print Speed	25 mm/s	**Top/Bottom Pattern**	Concentric
Initial Layer Speed	20 mm/s	**Infill Pattern**	Triangles
Inner Wall Speed	11 mm/s	**Retraction distance**	6.5 mm
Outer Wall Speed	8 mm/s	**Print Cooling**	Enabled
Top/Bottom Speed	11 mm/s	**Support**	Generated

The final prototype of the co-axial extruders is shown in figure 3.1.
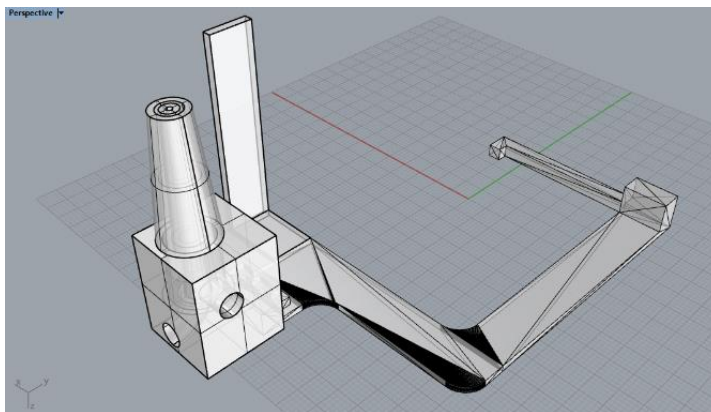
Figure 3.1. CAD model of the coaxial printhead

4.2.2.2 Thermal analysis

Differential Scanning Calorimetry (DSC) of PLA filament and printed PLA extruders was performed *via* DSC 822^e (Mettler Toledo, Germany). Measurements were carried out from 25 °C to 350 °C at a heating rate of 10 °C/min with nitrogen as an inert purge gas with a flow rate of 150 mL/min, in TA standard aluminum pans (40 µL) and predrilled lids; the average samples mass was 10–12 mg. Data were collected with Mettler Toledo STAR^e software; all the curves were interpolated to obtain the enthalpy of transformations related to the area under the peaks and to characterize post-printing modifications and define the working temperatures ranges.

4.2.2.3 Morphological analysis of extruder prototypes

Different extruders were produced varying the digital dimensions of the holes (from 1.05 up to 6.80 mm), and the obtained diameters of the printout prototypes

were measured with a digital caliper. The data acquired were related to the digital dimensions, and the equation of the obtained curve was used to set the digital dimensions, with the aim of producing co-axial extruders with 400-600 µm exit holes.

Then, the final co-axial extruder prototype (n=3) was analysed in dimensions and in weight, according to the FDA guidelines for 3D printed objects "*Technical Considerations for Additive Manufactured Medical Device*", to evaluate the reproducibility of the FDM printing process.

4.2.3 Drug delivery systems design and production

4.2.3.1 Design and development of digital DDS

Templates for the SSE 3DP of blank and drug-loaded formulations were designed with the CAD software Rhinoceros 6. The .stl files of toroidal geometries, selected for the formulations, were processed through the use of the slicing software Cura 4.3.0 (Ultimaker, Netherlands) and sent to the printer as .gcode. The digital dimensions of the printouts are shown in table 3.2.

Table 3.2. Size of the digital models for the different toroidal geometries

Toroidal models	External diameter (mm)	Internal diameter (mm)	Height (mm)	Number of layers	Graphical representation

Drug-free formulations	13.00	7.00	11.75	3	
Drug-loaded formulations	13.00	7.00	7.75	2	
	13.00	7.00	11.75	3	
	13.00	7.00	15.75	4	

4.2.3.2 Composition of the alginate and the crosslinking gel

With the aim to produce floating drug delivery systems *via* SSE, using the custom-made coaxial-extruder, two different gels (referred to ink gel and crosslinking gel) were prepared and their composition optimized:

- Ink gel: SA gel produced with different concentration from 4% to 6% w/v, under constant magnetic stirring, until the complete polymer hydration was reached.

- Crosslinking gel: $CaCl_2$, the crosslinking agent, was solubilized (with different concentration in a range from 0.1 M to a maximum of 0.5 M) in pre-adjusted volume of water; the obtained solution was thickened with 3% of HEC to

obtain an extrudable gel. Furthermore, 0.1% or 0.3% v/v Tw was added to some gels, in order to optimize the shape of the models.

The most promising gels combination (ink gel 6% of SA and crosslinking gel 0.1M CaCl$_2$, 3% w/v HEC and 0.1 v/v Tw), in terms of printing reproducibility and buoyancy properties, was selected for drug loading of PrpHCl. More specifically, the API was added in different ratio (12.5-25% w/w) into the crosslinking gel or into the ink gel, in accordance with drug-polymer compatibility, highlighting its influence on gel extrudability.

4.2.3.3 Analysis of the shape retention of extruded gels

The self-standing behavior of drops of ink and crosslinking gels, pumped individually with the SSE extrusion system, was prior evaluated (Schwab et al., 2020). This preliminary analysis was carried out through a manual points procedure approach. The straight baseline and the drop profile were detected placing points along the drop edges, thus the radius of curvature of the samples was acquired. Finally, the tangent of a fitting curve of the drop profile, both on the left and right side of the drop (ϑ_L and ϑ_R angles) (figure 3.2), was evaluated *via* software analysis.
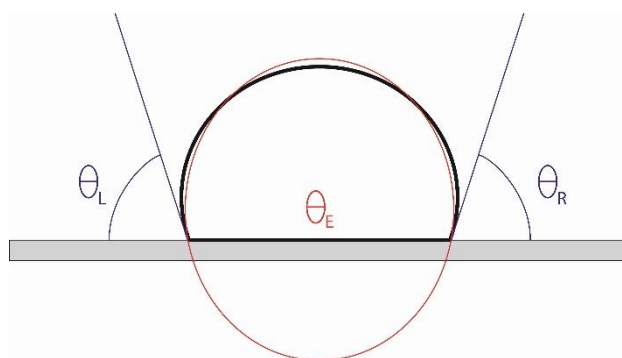
Figure 3.2. Schematic representation of the software evaluation of drop angles

4.2.3.4 Dynamic viscosity measurement

For the ink gels (SA from 4 to 6 % w/v), the dynamic viscosity (expressed in mPa·s), was measured using the viscometer Visco Basic Plus (Fungilab, USA). The measurements were conducted at room temperature with L_3 spindle and 50-1 rpm range. Instead, for all the crosslinking gels, the measurement was effectuated using Visco Smart (Fungilab, USA) with R_6 spindle and 100-20 rpm range. For all the analysed samples, at least seven measurements were acquired at intervals of 10 seconds and 1 minute.

4.2.3.5 Co-axial SSE-3D printing

The DDSs were produced using the printed coaxial extruder connected through tubes to a syringe pump system, Fusion 4000 (Chemix Inc., UK). In particular, the extruder was fixed on the printhead of the Ultimaker³ printer in order to exploit its movements along the axes, while the extrusion occurs (figure 3.3). Specifically, the two gels were loaded in two separate syringes (12.25 mm diameter) to feed the inner and outer channels simultaneously at the same flow rate (150 µL/min; print speed for blank forms 0.25 mm/s; drug-loaded forms 0.225 mm/s). SSE printing took place with no need to heat the nozzle and following the concentric geometry of the drawn toroidal models. The printing parameters were optimized for both drug-free and drug-loaded formulations using an initial layer height of 3.75 mm and then a layer height of 4 mm.

FDM process
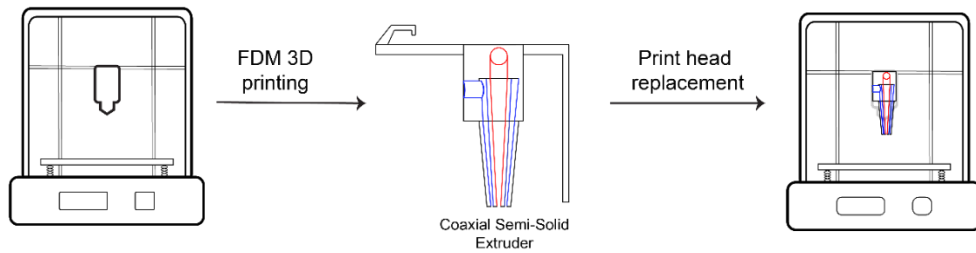
Co-axial SSE process
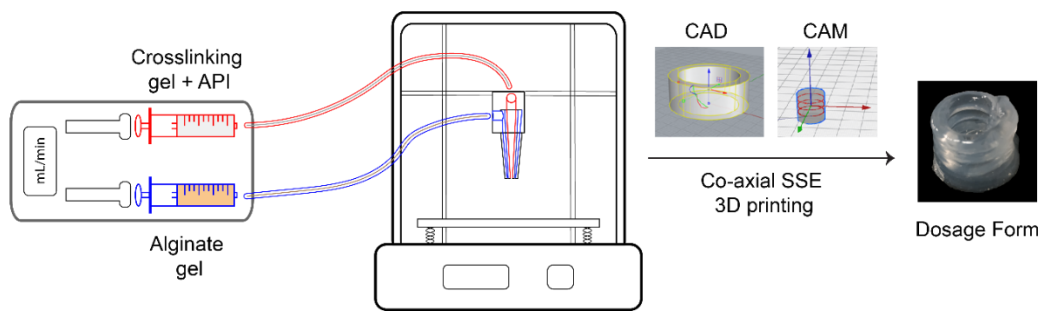
Figure 3.3: Schematic representation of the entire printing process

4.2.3.6 Drying process

The drying methodologies for drug-free and drug-loaded printouts were carried out on F6_0.1 batch. In detail, the processes applied were:

- air drying, with storage at room temperature until constant weight was obtained.
- microwave-assisted drying at 200 W for 15', 300 W for 10' or 400 W for 5'.

- oven drying at 40°C until constant weight was obtained, about 7 hours.

- vacuum drying with vacuum cycles every 30' for 6 hours, and then overnight in desiccator.

4.2.3.7 Dimensional and morphological analyses

The dimensions of all the produced DDSs were measured with a digital caliper, both after printing and after the drying phases, to evaluate the printing process reproducibility and the drying process impact. The change in dimension of the printed forms was compared to the digital models, while the dried formulations were compared to post-printing forms; results were reported as percentage ratio.

The printed systems were photographed with a single lens reflex camera (Canon EOS 600D; parameters: f-stop: f/6.3, shutter speed: 1/5 s, ISO 200). Optical microscopy (Alphaphot-2 YS2, Nikon, Japan), with an objective 4X, was used to acquire images of dried layers details. The drug-free and drug-loaded dried formulations were observed by Scanning Electron Microscopy (Tescan Solaris, Tescan Orsay Holding, Czech Republic) to obtain information about inner microarchitecture of Ca^{++}-alginate matrix and the API distribution.

4.2.3.8 Mass analysis and residual weight

To control the process reproducibility, at least six printed units for each formulation have been accurately weighted after the printing. The residual weight after the drying process was calculated and expressed as the percentage ratio

between the formulation weight after drying and its weight immediately after the printing process.

4.2.3.9 FT-IR analysis

FT-IR analysis was carried out using FT-IR spectrophotometer (Spotlight 400N FT-NIR Imaging System, Perkin Elmer Inc, USA) equipped with an ATR accessory (ZnSe crystal plate). The powders (API and PrpHCl-HEC physical mixture) as well as the printed formulations were analysed using: 128 scans and $1 \, cm^{-1}$ resolution step in the spectral range 4000-600 cm^{-1}.

4.2.3.10 DSC Thermal Analysis

PrpHCl, drug-loaded printed formulation and PrpHCl-HEC physical mixture have been subjected to DSC (DSC 822e, Mettler Toledo, Germany). For all samples, 3-5 mg were weighted in a 40 µL predrilled aluminum pan. The thermal cycle selected included three segments: dynamic from 25 °C to 100 °C at a heating rate of 50 °C/min, isothermal at 100 °C for 10 min, and finally dynamic from 100 °C to 350 °C at 10 °C/min. The latter was reported as thermogram in the results session. The data were analysed by Mettler Toledo STARe software.

4.2.3.11 Buoyancy tests

Buoyancy tests were performed gently placing the dried formulations in acidic dissolution medium prepared according to the method proposed by USP 36

(dissolution 0.1M HCl solution; pH 1.2 ± 0.5). The medium was in constant stirring at 70 rpm and at 37 ± 0.5 °C. The lag time before the buoyancy and the floating time of the single samples were visually evaluated and reported in hours.

During the tests, at specific time points (every 30 minutes) the formulations were withdrawn and the water excess was carefully wiped off using filter papers, the weight was measured using the analytical balance. Then, the percentage of weight acquired due to the medium absorbance by the alginate matrix was calculated using the following equation (1):

$$\% \, Weight \, acquired = \frac{mg_t - mg_{t0}}{mg_{t0}} * 100$$

(1)

mg_t represents the mass of the formulation at specific time points, while mg_{t0} represents the initial mass of the sample.

4.2.3.12 Drug content analysis and drug-loading efficiency

All the formulations (n ≥ 3) loaded with different concentrations of PrpHCl and obtained from different digital models were evaluated for drug content (DC) and drug loading efficiency (DLE) values. Samples were placed in PBS (100 mL, pH 6.8) and treated with ultrasonic cycles of 30' each, until complete solubilization. The PrpHCl content was obtained by UV–vis Spectrophotometer (Evolution 201 UV–vis Spectrophotometer, Thermo Fischer Scientific Inc.), setting the wavelength (λ) at 288 nm, and using PBS calibration curve (concentration range: from 10.3 µg/ml to 63 µg/ml). The DLE (Eq 3) has been calculated as:

$$DLE \, (\%) = \frac{Mass \, of \, PrpHCl \, observed \, (mg)}{Mass \, of \, PrpHCl \, predicted \, (mg)} * 100 \qquad \text{Eq (3)}$$

and the DC (Eq 4) according to:

$$DC \ (\%) = \frac{Mass \ of \ PrpHCl \ observed \ (mg)}{Mass \ of \ dried \ formulation \ (mg)} * 100 \hspace{2cm} \text{Eq (4)}$$

4.2.3.13 Dissolution tests

Dissolution tests were performed with USP dissolution Apparatus II (AT7 Smart Dissolution Tester, Sotax Corporation): paddle configuration, 70 rpm stirring, 37 °C, using as dissolution medium 0.1M HCl, according to USP 36. For all drug loaded batches, the absorbance values at different times were measured and related to the concentration of PrpHCl through an acidic calibration curve (in a range of concentration from 10.5 µg/ml to 65 µg/ml). For all batches analysed, mean values and standard deviations were reported.

4.2.3.14 In vitro release studies and release kinetics

In order to evaluate the release mechanism from different formulations, fitting analysis was performed *via* software using the method proposed by Del Gaudio and colleagues (Del Gaudio et al., 2015). Particularly the fitting analysis was performed using two different kinetic models: Higuchi's model (Eq. 5) and Peppas-Korsmeyer's equation (Eq 6).

$$Higuchi's \ model: M_t = A\sqrt{D(2C_0 - C_S)t} \hspace{2cm} \text{Eq (5)}$$

where M_t is the drug cumulative amount released at time *t*, *A* represents the surface area, *D* the diffusivity of the drug through the matrix, and C_0 and C_s the initial drug concentration and drug solubility respectively

$$Peppas - Korsmeyer's\ equation: \frac{M_t}{M_\infty} = kt^n$$

Eq (6)

where M_t is the drug cumulative amount released at time t, M_∞ is the drug amount released at infinity, k is a constant, and n is a diffusion coefficient, which depends on geometry of the system and on the release mechanism.

4.3 Results and discussion

4.3.1 Co-axial extruder production via FDM 3DP and characterization

The polymer selection for the FDM 3D printing of coaxial extruders fell on PLA, deriving from organic and renewable sources, which allows the creation of high-resolution parts with good surface quality and good mechanical strength. PLA filament as received was analysed *via* DSC (figure 3.4) to define the range of the working temperature not affecting polymer properties.

Particularly, PLA thermogram (figure 3.4, black profile) showed an exothermic event at around 150°C attributable tho the polymer melting, with no further peak up to 320°C when degradation begins; consequntely, the printing temperature was set at 200°C to make sure that the polymer is in the molten state in the conveying canal and to avoid nozzle clogging. Printed PLA was equally evaluated via thermic analysis (figure 3.4, red profile) and the thermogram displayed a flattening of the glass transitions peak, due to a reduction of PLA plasticity after the printing process. However, this reduction did not affect the mechanical resistance of the printed prototypes during handling.
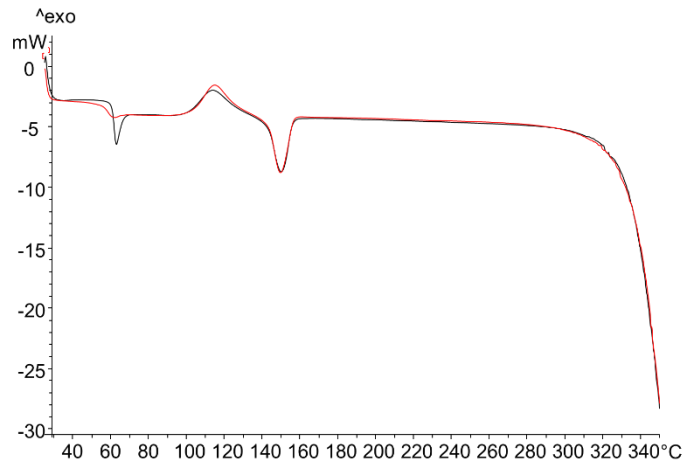
Figure 3.4. Thermograms of PLA raw filament (black profile), printed PLA (red profile)

A preliminary analysis of the natural swelling of the printed PLA was carried out on different extruders in order to define the shrinkage entity of the co-axial exit holes (figure 3.5). The measurements highlighted a linear relationship (y = 1.07x - 0.8738; R^2 = 0.9994) between the digital inputs and the real hole diameters. This helped to foresee the material changes and, therefore, to tune the dimensions of the extruder CAD models to the desired micrometer-scaled diameters, accordingly.
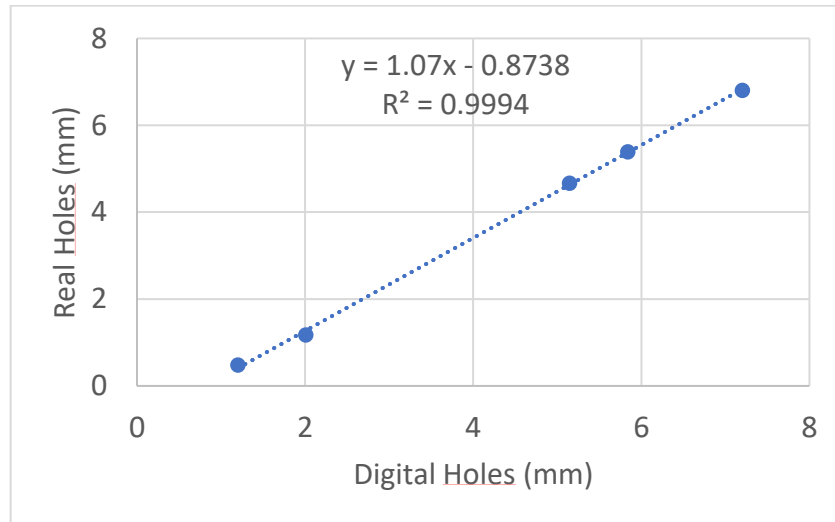
Figure 3.5. Analysis of the shrinkage of PLA holes after printing in relation to the digital models

Moreover, the co-axial extruders were designed in size and dimensions along XY axes for a perfect installation on the Ultimaker³ printhead and into the radial/axial fans bracket, without hampering the normal movement of the printer. The holes for the insertion of the two feeding tubes were designed to fit with them (tubes with a diameter of 3 mm), while the exit holes were designed for a satisfactory resolution of SSE extrusion, taking into account the viscosity of the processed solutions.

The operative specifics were set for an optimal print of PLA filament while the slicing parameters were optimized considering the digital dimensions defined *via* CAD software.

In particular, to promote the adhesion of the first layer, the initial layer printing temperature was set five Celsius degrees above the printing temperature of the whole model; whereas the build plate temperature was set up at 80°C (10

degrees above the recommended one) for avoiding the model detachment from the plate during the z construction movements.

The print speed was gradually decreased from the infill to the inner and outer wall speed, as a compromise between the layers resolution along the z-axis and the XY resolution of tiny parts such as holes and canals.

The slicing parameters, i.e. layer height, wall line width, wall thickness, and the infill line distance, were improved to obtain a solid and completely filled object, with the aim of preventing the gels diffusion through the extruder layers.

Analyzing the morphological and mass data (figure 3.6) of the printed extruders, the result showed that the FDM printing process was highly reproducible in terms of prototypes weight and dimensions along the three axes. As expected, the real dimensions obtained differed from the digital model, but the equation used for taking into account the PLA expansion led to exit holes with the desired dimensions.
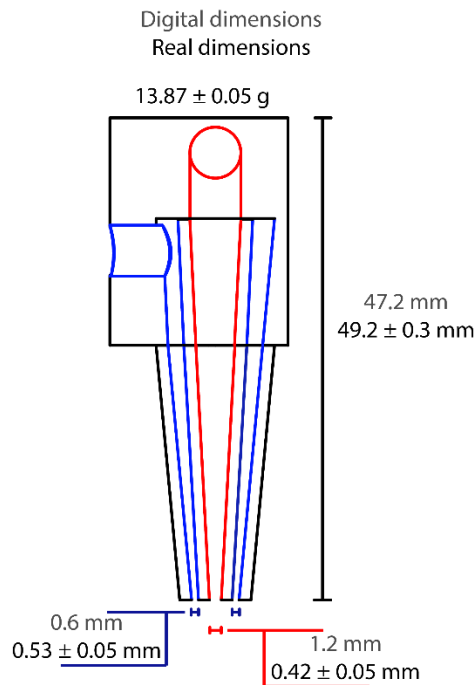
Image 3.6. Dimension and mass analysis of the FDM 3D printed extruders

Furthermore, the lightweight of the extruder did not destabilize the axis center of gravity, ensuring a precise deposition of the gel materials during the printcore movements.

4.3.2 Floating drug delivery systems development via custom-made SSE system

In order to identify the range of concentrations of SA, $CaCl_2$ and HEC allowing for good self-standing behavior after extrusion, the shape retention (ϑ_L and ϑ_R angles) of ink gel and crosslinking gel was monitored (table 3.3). Angles under

175

90° were considered characteristic of printable gel with no spreading onto the plate; angles between 90° and 130° were distinctive of gels with limited spreading onto the surfaces; finally drops with angles over 130° had excessive spreading and consequentially were not printable.

Particularly, it was possible to observe for all the gels analysed that the values of ϑ_L and ϑ_R of the same sample were comparable, demonstrating the good symmetry of the drops after deposition.

Table 3.3. Dynamic viscosity and angle values after extrusion of different ink and crosslinking gels

CaCl₂ (M)	HEC (% w/v)	Tw (% v/v)	SA (% w/v)	ϑ_L (°)	ϑ_R (°)	Dynamic Viscosity (mPa s)
0.5	3	-	-	76 ± 4	74 ± 4	41475 ± 861
0.25	3	-	-	83 ± 11	82 ± 7	14612 ± 2705
0.25	3	0.1	-	79 ± 5	77 ± 7	14133 ± 1075
0.1	3	-	-	84 ± 7	84 ± 3	15200 ± 2335
0.1	3	0.1	-	79 ± 10	74 ± 8	12750 ± 2029
-	-	-	2	130 ± 5	125 ± 6	1128 ± 25
-	-	-	3	117 ± 2	117 ± 3	4473 ± 6
-	-	-	4	115 ± 6	115 ± 9	14267 ± 40
-	-	-	6	105 ± 7	105 ± 7	54661 ± 25

High amount of $CaCl_2$ caused an increase in the solution viscosity, nevertheless all the prepared cross-linking gels were extrudable by the pump. Moreover they showed angles lower than 90°, underlining the possibility to freely change the cross-linker concentration (from 0.1 to 0.5 M) to modulate ionotropic gelation, without affecting the shape retention of these gels.

For ink gels (SA column in table 3.3), despite the increase of concentration from 2 to 6% w/v, all ϑ_L and ϑ_R values were between 100° and 130°, with a lower accommodation after extrusion and deposition for the more concentrated gels. Furthermore, as expected, by increasing the concentration of SA it was possible to observe an increase in dynamic viscosity which did not prevent its extrusion.

As a preliminary study to highlight the interaction between the feeds, two different configurations of extrusion were investigated: the ink gel in the outer channel with crosslinking gel in the inner one and vice versa.

The choice of channel in which gels were pumped affected the structure of the extruded product: pumping the ink gel trough the inner channel, the result after drying was a bulk filament, while if it was pumped in the outer channel, a hollow filament was obtained. According with the aim to develop a new floating system the latter configuration was selected for all the experiments.

Once the optimal ranges of concentration have been identified, in terms of shape retention and extrudability of gels (SA 4 and 6% w/v; HEC 3% w/v with $CaCl_2$ from 0.1 to 0.5M), printing tests were carried out by means of the co-axial extruder fed with different gel compositions, as reported in table 3.4.

Table 3.4. Compositions of extruded gels and weight of the blank and drug-loaded DDSs

177

DDSs	Feeds				Post-printing weight (mg)	Residual weight after drying (%)
	Ink Gel	Crosslinking Gel with HEC 3 %w/v				
	SA (% w/v)	CaCl$_2$ (M)	Tw (% v/v)	PrpHCl (% w/v)		
F4_0.5	4	0.5	-	-	1409.4 ± 141.6	8.90 ± 0.40
F6_0.5	6	0.5	-	-	1570.1 ± 76.8	10.19 ± 0.41
F6_0.25		0.25	-	-	1410.7 ± 101.2	8.24 ± 0.18
F6_0.25_0.1		0.25	0.1	-	1427.9 ± 103.5	7.44 ± 0.31
F6_0.25_0.3		0.1	0.3	-	1604.5 ± 285.4	8.2 ± 0.4
F6_0.1		0.1	-	-	1414.4 ± 52.6	6.62 ± 0.29
F6_0.1_0.1		0.1	0.1	-	1508.0 + 43.8	5.62 + 0.27
F6_0.1_0.1_ 25 (3)		0.1	0.1	25	1815.4 ± 30.7	14.56 ± 0.70
F6_0.1_0.1_ 12.5 (2)		0.1	0.1	12.5	1048.1 ± 29.9	12.15 ± 0.61
F6_0.1_0.1_ 12.5 (3)		0.1	0.1	12.5	1562.5 ± 83.5	12.10 ± 0.31
F6_0.1_0.1_ 12.5 (4)		0.1	0.1	12.5	2097.4 ± 41.6	11.87 ± 0.70

(2) (3) and (4) represents the number of layers

The SSE printing process of all formulations was realized using a print speed slow enough (150 µL/min) to allow the gelling process of the single layer and among following layers.

For the formulation F4_0.5, the poor shape retention of 4% w/v SA (as highlighted by ϑ_L and ϑ_R in table 3.3) was balanced by the presence of a high concentration of $CaCl_2$ (0.5 M), speeding up the gelation rate of polymeric matrix. However, this gelation did not prevent the spreading onto the build plate of part of the outer alginate not involved in the cross-linking process.

Hence, to counteract the leakage of the alginate solution onto the printing plate and to optimize the interaction between the two gels, the SA concentration was increased to 6% w/v, which showed a minimum value of ϑ_L and ϑ_R.

However, F6_0.5 showed poor adhesion between layers due to the immediate hardening of the filament which negatively affected the resolution of final product. Thus, $CaCl_2$ concentration was reduced to 0.25 M (F6_0.25) and 0.1 M (F6_0.1), leading to high-resolution printed products.

The formulation with the lowest amount of crosslinker, F6_0.1, was selected for the reproducibility of the printing phase (table 3.4) to carry out preliminary tests of drying processes.

The microwave-assisted drying, regardless of the wattage and the time of the cycle, brought a general wrinkling of the alginate matrix (figure 3.7)

179
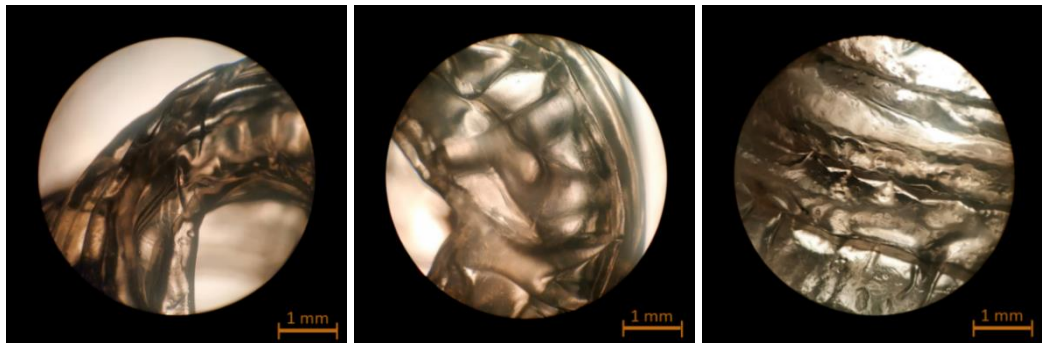
Figure 3.7. Optical magnifications of the formulations F6_0.1 after the microwave-assisted drying process at (from left to right): 200W, 15'; 300W 10'; 400 W, 5'

The separation of the layers and deformation of the toroidal structure were caused by the excessive rapid evaporation of water molecules during microwaving. The oven process browned the formulations, making them glassy and fragile in texture, thus not resistant to handling, and giving them a variable buoyancy behavior. While the vacuum drying affected the hollow cavities of dried forms along the height, impacting the floating behavior of the toroidal channeled filaments. Therefore, the selected process for all the produced batches was the air drying, with the lowest impact on the alginate matrix. Particularly, the air-drying preserved the shape of the printouts without excessive wrinkling; led to an optimal texture of the forms resistant to handling; did not significantly affect the height of the dried forms. Hence this process led to formulations with homogenous cavities and thus reproducible buoyancy.
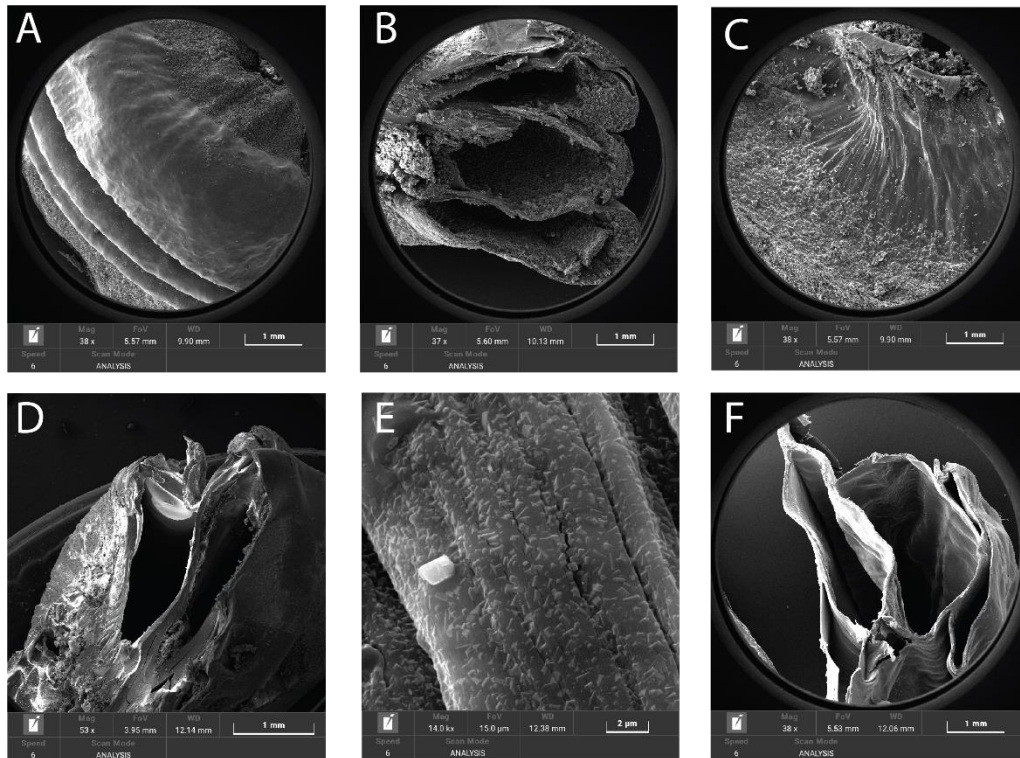
Figure 3.8. SEM acquisition of: (A) external view and (B) longitudinal view of drug-loaded form; (C) a cross section of a drug loaded layer; (D) logitudinal view of blank form; (E) magnification of a blank fibre of the alginate matrix after gelation and drying; (F) a longitudinal view of a polimeric matrix after the dissolution test

However, for both batches F6_0.1 and F6_0.25 an excessive reduction in dimension along the z-axis was observed for the lowest layer, as shown in figure 3.8D and table 4. This evidence was due to a partial collapse of the underlying layers caused form the weight of the upper matrix during the drying, with a decrease of the filament's lumen.

Aiming to reduce this lowering, several experiments were conducted, adding the non-ionic surfactant Tw at different percentages into the crosslinking-gels. The

Tw concentration was above the CMC value (0.00029 mM) (Hait & Moulik, 2001), and reduced the surface tension of the crosslinking gel, promoting the feeds interaction and the formation of a well-structured alginate scaffold (figure 3.8E) (Kaygusuz, Evingür, Pekcan, von Klitzing, & Erim, 2016).

In fact, the addition of the surfactant improved the height retention of the dried formulations, allowing to obtain more homogenous hollow structures at a concentration of 0.1 % v/v. Indeed, printouts deriving from F6_0.25_0.1 batches presented a good printability in terms of shape maintenance and gelation rate (figure 3.10 left). Moreover, F6_0.25_0.1 batch showed a solid alginate matrix, with tunneled filaments and the highest percentage in terms of height retention after the drying process among all the produced formulations (table 3.5).

Table 3.5. Dimensional analysis of blank and drug-loaded DDSs after printing and after air-drying process

DDS	$\dfrac{\textit{Post printing model}}{\textit{Digital model}}$ (%)	$\dfrac{\textit{Post drying model}}{\textit{Post printing model}}$ (%)
F6_0.25	Diameter: 109.8 Height: 82.9	Diameter: 88.2 Height: 19.7
F6_0.25_0.1	Diameter: 105.8 Height: 86.1	Diameter: 70.7 Height: 37.8
F6_0.1	Diameter: 106.7 Height: 88.9	Diameter: 88.7 Height: 17.6
F6_0.1_0.1	Diameter: 111.1 Height: 85.6	Diameter: 75.8 Height: 28.7
F6,0.1,0.1_ 12.5 (3)	Diameter: 111.3 Height: 89.3	Diameter: 92.6 Height: 34.5

F6,0.1,0.1_ 25(3)	Diameter: 113.7 Height: 95.6	Diameter: 81.2 Height: 44.5
F6,0.1,0.1_ 12.5 (2)	Diameter: 111.5 Height: 94.8	Diameter: 87.1 Height: 36.7
F6,0.1,0.1_ 12.5 (4)	Diameter: 111.2 Height: 91.9	Diameter: 86.8 Height: 42.7

Notwithstanding the good results obtained adding 0.1% v/v of Tw, when the surfactant was added in higher concentration, as in F6_0.25_0.3, the formulations presented hollow filaments but, after the drying process, they resulted mealy. The texture was due to a large amount of HEC on the outer wall of the filaments, coming out after the extrusion process. Moreover, alginate matrix was brittle, underlining the effect of the surfactant in hiding part of the negative centers of alginate structure that cannot interact with calcium ions, as evidenced also by Kaygusuz and colleagues (Kaygusuz et al., 2016). F6_0.25_0.3 were then fragile and characterized by porousmatrix, with less Z shape retention after drying, compared to F6_0.25_0.1.

Moreover, the impact of 0.1 % v/v Twon forms produced with the lowest crosslinker concentration (F6_0.1_0.1 with 0.1 M $CaCl_2$) was evaluated. The results showed a slight reduction in height of these formulations compared to F6_0.25_0.1 batches, but these forms displayed a good shape retention coupled with the most promising interaction with medium (figure 3.9).
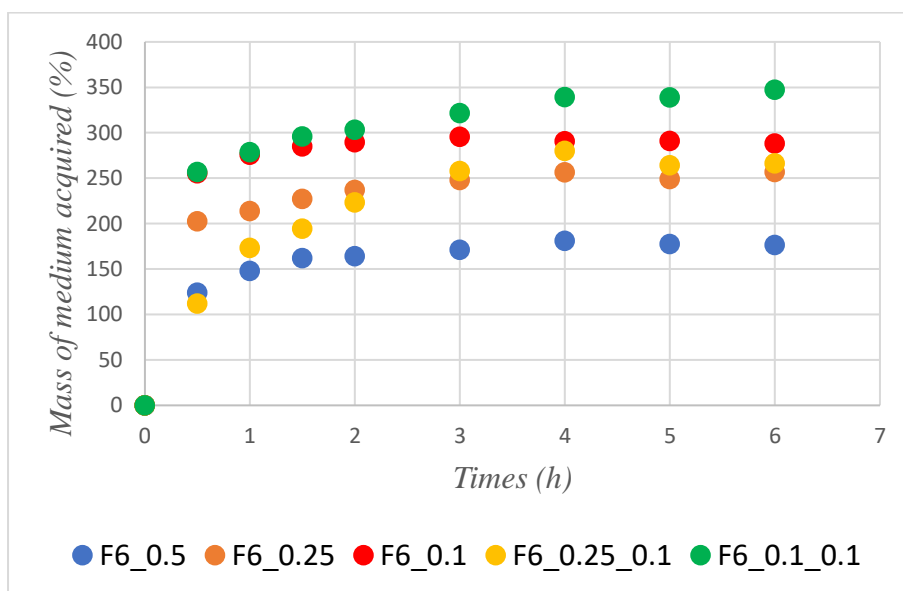
Figure 3.9. Medium uptake values of different batches

Regarding the media uptake (figure 3.9), all the tested batches showed a rapid gain in the weight acquired in the first 30 minutes, that gradually increased during the tests time. This evidences a rapid hydration of the polymer into aqueous solutions that may ease the drug dissolution. A relationship between $CaCl_2$ concentration and medium uptake capacity was highlighted, with a doubling of fluid absorbed by F6_0.1_0.1 compared to F6_0.5. Moreover, the addition of Tw positively affected the medium uptake capacity, in fact the absorption capacity increased from 250% to 350%.

Evaluating the buoyancy properties of the forms, all the high-resolution printouts (blank and loaded) showed a floating time of 5 ± 1 hours without a lag phase. After a complete characterization of blank forms, the most promising combination of gels was selected to be loaded with PrpHCl:

- Ink gel: SA 6% w/v;
- Crosslinker gel: CaCl$_2$ 0.1 M + HEC 3% w/v + Tw 0.1% v/v.

Propranolol, in form of Hydrochloride, was selected thanks to its specific physico-chemical and pharmacokinetic characteristics. To identify in which gels, ink gel or crosslinker gel, it was better to load the drug, the characteristics of all gel components were evaluated. The API loaded ink gel was produced however, during the gel preparation phase, the incompatibility of SA with anionic salts due to precipitation phenomena was highlighted. Therefore, for the following experiments, PrpHCl was added to the crosslinker gel.

Different ratios of PrpHCl were selected in accordance with maximum and minimum daily dosage (25% w/w ~190mg and 12.5% ~95mg, considering a DDS with an average mass of 1500 mg). In addition to the evaluation of the effect of different drug concentrations, batches with 12.5% w/v of drug were produced also with various heights (2, 3 or 4 layers), in order to verify the potential application of the developed SSE 3D printing system in personalized medicine.

The addition of PrpHCl in the crosslinking gel had a positive influence on the shape retention, as underlined by the ϑ_L and ϑ_R values of gel loaded with 12.5% w/v of API (ϑ_L= 57 ± 1; ϑ_R = 59 ± 1). As shown in table 3 and 4, the use of different drug concentrations or different numbers of layers did not affect results in dimension, both after the printing phase and the drying process. While, as expected, a growth of the residual weight has been found for higher drug loaded batches, but not for forms with different heights. Finally, the high reproducibility of printing process of all batches was highlighted by the weight of single layers (535.41 ± 40.00 mg) obtained during the production of different digital models.

Figure 3.10. Three layers model of: (Left) blank DDS; (Right) drug-loaded DDS

To verify the presence of interactions between PrpHCl and the polymers, FT-IR analysis was carried out (figure 3.11b). Particularly, the spectrum of drug-loaded form showed a shift of COO- asymmetric stretch at lower wave-values, compared to neat SA spectrum, as result of the calcium-alginate interaction. Moreover, a large peak in the range 3200-3400 cm^{-1} was evident, due to the extensive hydrogen bonding founded (Daemi & Barikani, 2012). The PrpHCl spectrum showed several characteristic peaks: two peaks in a range 770-797 cm^{-1} identified the α-naphthalene group; at 1072 cm^{-1} the symmetric stretch of C-O-C was observed, as well as the asymmetric stretch at 1266 cm^{-1}; the C-N bond was detected among 1147-1170 cm^{-1}, and finally the O-H and N-H bonds were shown at 3227 and 3032-2968 cm^{-1}, respectively (Farhadnejad et al., 2018). Following the results proposed by Takka S. et al. 2003 regarding the interactions of PrpHCl and anionic polymers, the IR spectra of HEC-PrpHCl physical mixture and drug-loaded formulations were compared with PrpHCl spectrum to investigate eventually additional bands, broadening or alterations in wavenumber position (Takka, 2003). From the comparison between neat API, HEC-PrpHCl physical mixture and drug loaded DDS, all characteristics peaks of PrpHCl were still detected, underlining no chemical interaction among the components of the formulations.
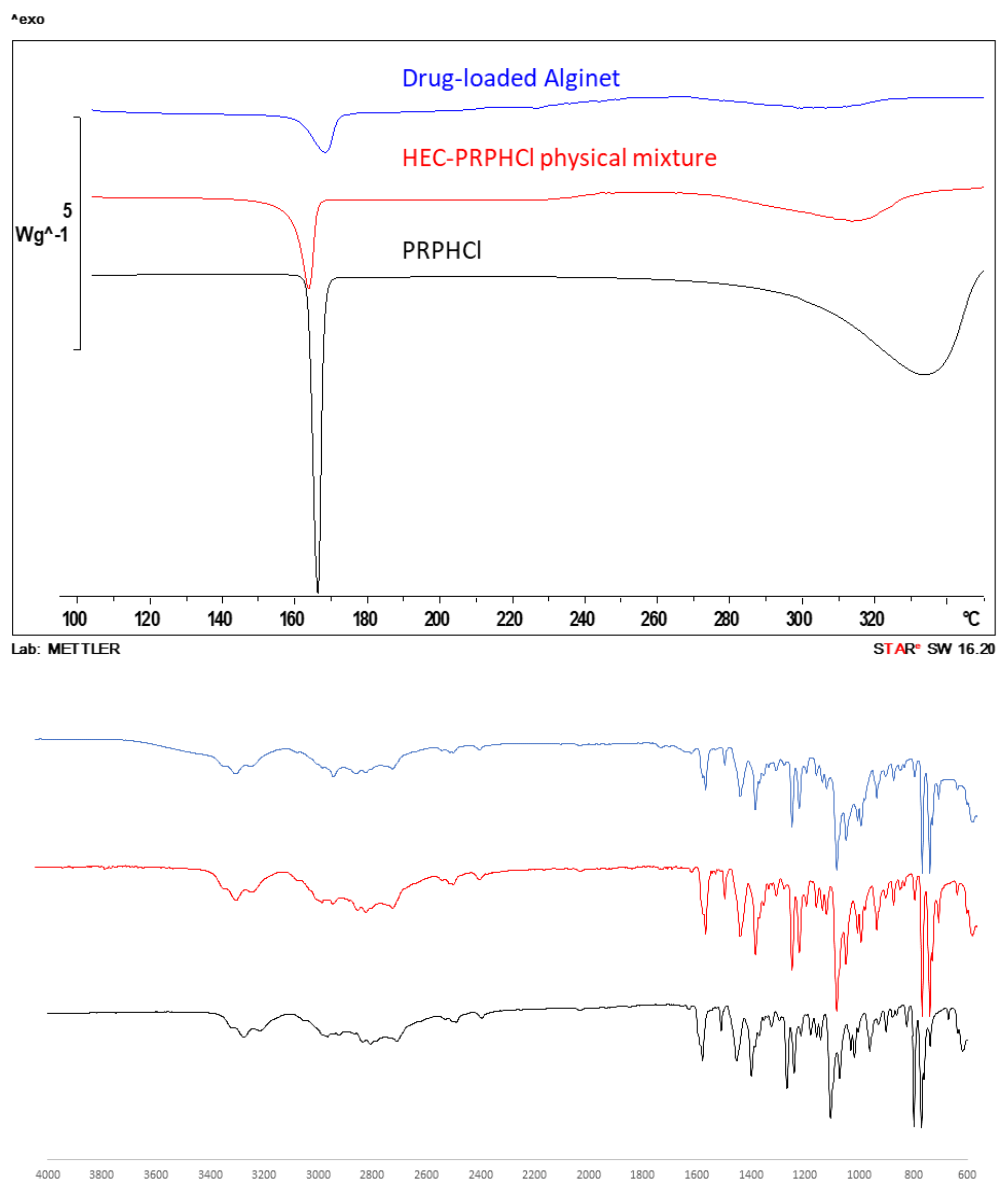
Figure 3.11. Physico-chemical characterization of: (from bottom to top): pure PrpHCl (black), HEC-PrpHCl physical mixture (red) and drug-loaded form (blue)

The data obtained from FT-IR were coupled with DSC thermal analysis (figure 3.11a). The API thermogram showed an endothermic peak at 165°C, representing the melting range of PrpHCl commercially available, in accordance with Bartolomei et al. (1998) (Bartolomei, Bertocchi, Ramusino, & Signoretti, 1998). The same peak was detected in the thermograms of HEC-PrpHCl physical mixture and drug-loaded formulation, proving the absence of physicochemical interactions, and therefore the drug stability, during all processing steps.

DLE and DC were among the most interesting aspects to be analysed for the co-axial SSE 3DP process, in relation with different API concentrations or different digital models. The DLE was significantly lower in printouts with higher amount of API in the crosslinking gel. Matching the data (table 3.6) with SEM micrographs, the reduced loading efficiency and reproducibility of formulations containing PrpHCl 25% w/v were probably due to the elevated migration of the drug into the HEC during the formation and drying of filaments (figure 3.8C), aided by the drug solubility. On the contrary, the variation of digital models in height (at the same drug concentration, 12.5% w/v) did not affect the DLE (table 5).

Table 3.6. Drug loading efficiency and drug content values of different DDSs

DDSs	**Drug loading Efficiency**	*Drug Content*
F6_0.1_0.1_25 (3)	60.84 ± 2.31	50.47 ± 1.60
F6_0.1_0.1_12.5 (2)	87.07 ± 2.05	45.63 ± 0.29
F6_0.1_0.1_12.5 (3)	85.30 ± 0.90	41.09 ± 0.55

F6_0.1_0.1_12.5 (4)	83.80 ± 1.04	42.54 ± 0.73

DDSs obtained from different drug concentrations (12.5% and 25% w/v) or digital models (2, 3 or 4 layers with 12.5% w/v of API) were subjected to dissolution tests (the model with 3 layers after printing is shown in figure 3.10 right; while after drying in figure 3.8 A and B). For all batches, the drug release was complete after 6 hours. Comparing data obtained from drug release, DC and DLE, it is possible to assume that the overlap of 25% w/v curves and 12.5% w/v curves (figure 3.12a) does not mean that the kinetic release was independent from drug concentrations, but probably it was due to the maximum load capacity of the polymeric matrix. While, the release kinetics obtained from F6_0.1_0.1_12.5 batches with (2), (3) and (4) layers (figure 3.12b) were very similar, ensuring the ability to produce , formulations with different drug dosages exploiting the developed SSE process without affecting the drug release.
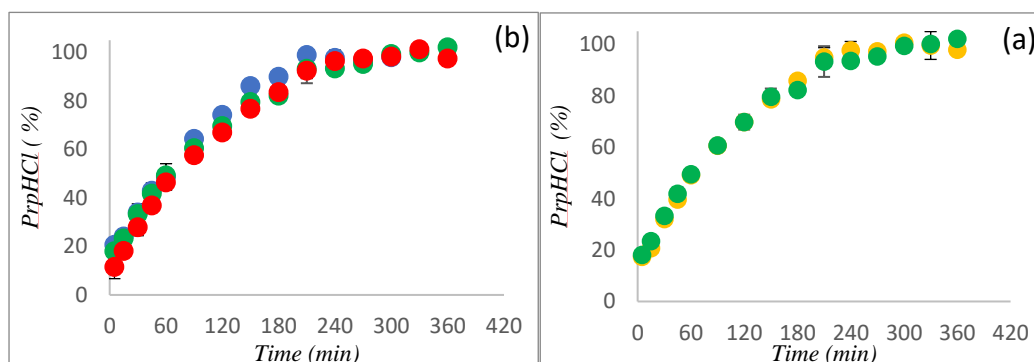
Figure 3.12. Dissolution profile of:
a) DDS produced from feeds with different drug concentration
(green: F6_0.1_0.1_12.5 (3); yellow: F6_0.1_0.1_25 (3))
b) DDS printed with different number of layers
(blue: F6_0.1_0.1_12.5 (2); green: F6_0.1_0.1_12.5 (3); red: F6_0.1_0.1_12.5

(4))

As shown by table 3.7, the Peppas-Korsmeyer's equation (Ritger & Peppas, 1987) fitted well the release data producing $r^2_{adj} > 0.92$ and lower values of reduced χ^2 for all formulations. The Higuchi's model (Higuchi, 1961) showed in all cases poorest performance. Moreover, the values of coefficient *n*, ranging between 0.71 and 0.77, indicate a complex non-Fickian transport mechanism involving matrix swelling depending on the number of layers. In fact, increasing the matrix's layers results in a relaxed matrix (figure 3.8F) in height able to strictly control drug diffusion trough the alginate hydrogel at the boundary of the forms (Peppas and Sahlin, 1989, De Cicco et al 2016). Both *n* coefficient and reduced χ^2 were not significantly influenced by drug concentration in any fitting model leading to the conclusion that drug content do not contribute actively to the release behaviour into the produced formulations.

Table 3.7: Fitting of different kinetic models on the release profiles of different DDSs

Model	Higuchi		Korsmeyer-Peppas		
DDSs	r^2_{adj}	†**Reduced χ^2**	r^2_{adj}	†**Reduced χ^2**	**n (S.E.)**
F6_0.1_0.1_12.5 (2)	0.87204	8.83	0.92026	2.62	0.71±0.04
F6_0.1_0.1_12.5 (3)	0.8367	9.80	0.93521	2.01	0.73±0.07

F6_0.1_0.1_12.5 (4)	0.80342	8.39	0.97201	1.82	0.77±0.04
F6_0.1_0.1_25 (3)	0.83212	8.98	0.93489	2.08	0.75±0.11

* r^2_{adj}:1-[(n-1/n-k-1)(1-r^2)], n: number of data points, k: number of independent variables

†χ^2/DoF as obtained by the Levenberg-Marquardt method

4.4 Conclusions

In this research, the hypothesis of applying the extemporaneous gelation of sodium alginate in pharmaceutical compounding, *via* co-axial semi-solid extrusion 3D printing (technology borrowed from bioprinting scaffolding), was successfully assessed and confirmed.

The ink and crosslinking feeds for the *in situ* one-step production of hollow floating forms were identified respectively in: sodium alginate 6% w/v and calcium chloride 0.1 M, the latter thickened with hydroxyethyl cellulose 3% w/v and added with Tween85® 0.1% v/v. Specifically, HEC was used to obtain a gel with adequate rheological properties for the extrudability of the crosslinking feed. The surfactant addition improved the resolution of dried DDSs (an increase of a further 10% in height) and the medium uptake capacity (~100% more than tween-free forms).

The addition of Propranolol hydrochloride in the crosslinking gel, in two different concentrations (12.5 and 25% w/v), enhanced the extrudability of the gel and the shape retention, by lowering the angle values of the deposited gel. Even varying the digital model of the DDS in terms of number of layers, the elevated reproducibility of the developed process was highlighted in terms of mass of a single layer (average value of 535 mg) and drug content (43% w/w). Furthermore, the optimized process did not affect the physicochemical characteristics of the components, as supported by FT-IR and DSC thermal analyses results.

From the *in vitro* studies data, the buoyancy time of all produced batches was 5 ± 1 hours without lag phase. Furthermore, the drug release kinetics of batches with 12.5% w/v of API but differing in number of layers (2, 3 or 4 layers) were strictly similar and independent from the drug amount.

In conclusion, the herein established manufacturing process of floating DDSs, by using in a pioneering manner the ionotropic gelation of sodium alginate, guides the possible application of co-axial semisolid extrusion 3D printing in the personalization of dosage according to the patients' therapeutic plans.

Bibliography and Webography

Afzal Hafiz Muhammad, Farrukh Shehzad, Mukarram Zubair, Omer Yahya Bakather & Mamdouh A. Al-Harthi, 2020, Influence of microwave irradiation on thermal properties of PVA and PVA/graphene nanocomposites, Journal of Thermal Analysis and Calorimetry volume 139, pages353–365(2020)

Aquino, R.P., Barile, S., Grasso, A., Saviano, M., 2018. Envisioning smart and sustainable healthcare: 3D Printing technologies for personalized medication. Futures 103, 35–50.

Arafat, B., Wojsz, M., Isreb, A., Forbes, R.T., Isreb, M., Ahmed, W., Arafat, T., Alhnan, M.A., 2018. Tablet fragmentation without a disintegrant: A novel design approach for accelerating disintegration and drug release from 3D printed cellulosic tablets. Eur J Pharm Sci 118, 191-199.

Aslam Muhammad, Mazhar Ali Kalyar, Zulfiqar Ali Raza, Polyvinyl alcohol: A review of research status and use of polyvinyl alcohol based nanocomposites, Polymer Engineering and Science, Volume58, Issue12, Pages 2119-2132, December 2018

ASTM. Standard terminology for additive manufacturing technologies. F2792-12a. 2012

Auriemma, G., Russo, P., Del Gaudio, P., García-González, C. A., Landín, M., & Aquino, R. P. (2020). Technologies and formulation design of polysaccharide-based hydrogels for drug delivery. Molecules, 25(14), 3156.

Awad, A., Trenfield, S.J., Gaisford, S., Basit, A.W., 2018. 3D printed medicines: a new branch of digital healthcare. Int. J. Pharm. 548, 586–596.

Azad Mohammad A., Deborah Olawuni, Georgia Kimbell, Abu Zayed Md Badruddoza, Md. Shahadat Hossain and Tasnim Sultana, Polymers for Extrusion-Based 3D Printing of Pharmaceuticals: A Holistic Materials–Process Perspective, Pharmaceutics 2020, 12, 124

Bartolomei, M., Bertocchi, P., Ramusino, M. C., & Signoretti, E. C. (1998). Thermal studies on the polymorphic modifications of (R, S) propranolol hydrochloride. Thermochimica acta, 321(1-2), 43-52.

Beck, R.C.R., Chaves, P.S., Goyanes, A., Vukosavljevic, B., Buanz, A., Windbergs, M., Basit, A.W., Gaisford, S., 2017. 3D printed tablets loaded with polymeric nanocapsules: an innovative approach to produce customized drug delivery systems. Int. J. Pharm. 528, 268–279.

Beyer, S., Bsoul, A., Ahmadi, A., & Walus, K. (2013). 3D alginate constructs for tissue engineering printed using a coaxial flow focusing microfluidic device. 2013 Transducers & Eurosensors XXVII: The 17th International Conference on Solid-State Sensors, Actuators and Microsystems (Transducers & Eurosensors XXVII) (pp. 1206-1209)

Bhupendra Raj Giri, Eon Soo Song, Jaewook Kwon, Ju-Hyun Lee, Jun-Bom Park and Dong Wuk Kim, 2020, Fabrication of Intragastric Floating, Controlled Release 3D Printed Theophylline Tablets Using Hot-Melt Extrusion and Fused Deposition Modeling, Pharmaceutics 2020, 12(1), 77

Boontheekul, T., Kong, H.-J., & Mooney, D. J. (2005). Controlling alginate gel degradation utilizing partial oxidation and bimodal molecular weight distribution. Biomaterials, 26(15), 2455-2465.

Boparai, K. S., Singh, R., & Singh, H. (2016). Development of rapid tooling using fused deposition modeling: a review. Rapid Prototyping Journal.

Cerciello, A., Auriemma, G., Morello, S., Pinto, A., Del Gaudio, P., Russo, P., & Aquino, R. P. (2015). Design and in vivo anti-inflammatory effect of ketoprofen delayed delivery systems. Journal of pharmaceutical sciences, 104(10), 3451-3458.

Cerciello, A., Del Gaudio, P., Granata, V., Sala, M., Aquino, R. P., & Russo, P. (2017). Synergistic effect of divalent cations in improving technological properties of cross-linked alginate beads. International journal of biological macromolecules, 101, 100-106.

Cerciello, A., Del Gaudio, P., Granata, V., Sala, M., Aquino, R.P., Russo, P., 2017. Synergistic effect of divalent cations in improving technological properties of crosslinked alginate beads. Int. J. Biol. Macromol. 101, 100–106.

Chandler Warr, Jonard Corpuz Valdoz, Bryce P. Bickham, Connor J. Knight, Nicholas A. Franks, Nicholas Chartrand, Pam M. Van Ry, Kenneth A. Christensen, Gregory P. Nordin, and Alonzo D. Cook, Biocompatible PEGDA Resin for 3D Printing, ACS Appl. Bio Mater. 2020, 3, 4, 2239–2244

Charoenying, T.; Patrojanasophon, P.; Ngawhirunpat, T.; Rojanarata, T.; Akkaramongkolporn, P.; Opanasopit, P. Fabrication of floating capsule-in-3D-printed devices as gastro-retentive delivery systems of amoxicillin. J. Drug Deliv. Sci. Technol. 2020, 55, 101393

Chia Helena N. and Wu Benjamin M., (2015), Recent advances in 3D printing of biomaterials, Journal of Biological Engineering (2015) 9:4

Collins FS, Varmus H. A new initiative on precision medicine. N Engl J Med. 2015;372(9):793–5.

Colosi C, Shin S R, Manoharan V, Massa S, Costantini M, Barbetta A, DokmeciMR, DentiniMand Khademhosseini A 2016 Microfluidic bioprinting of heterogeneous 3D tissue constructs using low-viscosity bioink Adv. Mater. 28 677–84

Conceição Jaime, Xián Farto-Vaamonde, Alvaro Goyanes, Oluwatomide Adeoye, Angel Concheiro, Helena Cabral-Marques, José Manuel Sousa Lobo, Carmen Alvarez-Lorenzo, Hydroxypropyl-β-cyclodextrin-based fast dissolving carbamazepine printlets prepared by semisolid extrusion 3D printing, Carbohydrate Polymers,Volume 221, 2019, Pages 55-62

Costantini Marco, Cristina Colosi, Wojciech Święszkowski, and Andrea Barbetta, Co-axial wet-spinning in 3D bioprinting: state of the art and future perspective of microfluidic integration, Biofabrication, Volume 11, 11 012001

Council of Europe. European Pharmacopeia, 10th ed.; Council of Europe: Strasbourg, France, 2021.

Cui Mengsuo, Hao Pan, Dongyang Fang, Sen Qiao, Shu Wang, Weisan Pan, Fabrication of high drug loading levetiracetam tablets using semi-solid

extrusion 3D printing, Journal of Drug Delivery Science and Technology, Volume 57, 2020, 101683

Cui Mengsuo, Yuenan Li, Shu Wang, Yuanyuan Chai, Jintong Lou, Fen Chen, Qijun Li, Weisan Pan, Pingtian Ding, Exploration and Preparation of a Dose-Flexible Regulation System for Levetiracetam Tablets via Novel Semi-Solid Extrusion Three-Dimensional Printing, Journal of Pharmaceutical Sciences, Volume 108, Issue 2, 2019,nPages 977-986

Cunha-Filho Marcilio, Ma´ısa RP Araujo´, Guilherme M Gelfuso, & Tais Gratieri, FDM 3D printing of modified drug-delivery systems using hot melt extrusion: a new approach for individualized therapy, Therapeutic. Delivery. (2017) 8(11), 957–966

Daemi, H., & Barikani, M. (2012). Synthesis and characterization of calcium alginate nanoparticles, sodium homopolymannuronate salt and its calcium nanoparticles. Scientia Iranica, 19(6), 2023-2028.

Dai, L., Cheng, T., Duan, C., Zhao, W., Zhang, W., Zou, X., Aspler, J., Ni, Y. (2019). 3D printing using plant-derived cellulose and its derivatives: A review. Carbohydrate polymers, 203, 71-86.

Del Gaudio, P., De Cicco, F., Sansone, F., Aquino, R. P., Adami, R., Ricci, M., & Giovagnoli, S. (2015). Alginate beads as a carrier for omeprazole/SBA-15 inclusion compound: A step dtowards the development of personalized paediatric dosage forms. Carbohydrate polymers, 133, 464-472

Dodero, A., Alloisio, M., Vicini, S., & Castellano, M. (2020). Preparation of composite alginate-based electrospun membranes loaded with ZnO nanoparticles. Carbohydrate polymers, 227, 115371.

Dong J.X., Q. Li, Z.C. Tan, Z.H. Zhang, Y. Liu, (2007) The standard molar enthalpy of formation, molar heat capacities, and thermal stability of anhydrous caffeine, J. Chem. Thermodyn. 39 (2007) 108.

D'souza A.A., Shegokar R., 2016, Polyethylene glycol (PEG): a versatile polymer for pharmaceutical applications, Expert Opinion on Drug Delivery, 17 May 2016, 13(9):1257-1275

Đuranović Marija, Obeid Samiha, Madžarević Marijana, Cvijić Sandra, Ibrić Svetlana, Paracetamol extended release FDM 3D printlets: Evaluation of formulation variables on printability and drug release, International Journal of Pharmaceutics, Volume 592, 5 January 2021, 120053

Eddleston Mark D. and William Jones, (2010), Formation of Tubular Crystals of Pharmaceutical Compounds, Crystal Growth & Design, Vol. 10, No. 1, 2010.

Ehtezazi, T.; Algellay, M.; Islam, Y.; Roberts, M.; Dempster, N.M.; Sarker, S.D. The Application of 3D printing in the formulation of multilayered fast dissolving oral films. J. Pharm. Sci. 2018, 107, 1076–1085.

Eleftheriadis Georgios K., Katsiotis Christos S., Bouropoulos Nikolaos, Koutsopoulos Sotirios & Fatouros Dimitrios G. (2020) FDM-printed pH-responsive capsules for the oral delivery of a model macromolecular dye, Pharmaceutical Development and Technology, 25:4, 517-523

EMA/554262/2018, Committee for Medicinal Products for Human Use (CHMP), Assessment report: Onpattro, 26 July 2018

Farhadnejad, H., Mortazavi, S. A., Erfan, M., Darbasizadeh, B., Motasadizadeh, H., & Fatahi, Y. (2018). Facile preparation and characterization of pH sensitive Mt/CMC nanocomposite hydrogel beads for propranolol controlled release. International journal of biological macromolecules, 111, 696-705.

FDA Center For Drug Evaluation And Research; Application Number: 207958orig1s000, Labeling, Spritam®, 07/2015

Fina, F., Goyanes, A., Rowland, M., Gaisford, S., & W Basit, A. (2020). 3D Printing of Tunable Zero-Order Release Printlets. Polymers, 12(8), 1769.

Firth J., Basit A.W., Gaisford S. (2018) The Role of Semi-Solid Extrusion Printing in Clinical Practice. In: Basit A., Gaisford S. (eds) 3D Printing of Pharmaceuticals. AAPS Advances in the Pharmaceutical Sciences Series, vol 31. Springer, Cham.

Gaisford Simon, and Abdul W. Basit 3D Printing of Pharmaceuticals, Chapter 2, 3D Printing Technologies, Implementation and Regulation: An Overview, (2018), AAPS Advances in the Pharmaceutical Sciences Series 31

Gardan J. Additive manufacturing technologies: state of the art and trends. Int J Prod Res. 2016;54:3118–32.

Genina, N.; Boetker, J.P.; Colombo, S.; Harmankaya, N.; Rantanen, J.; Bohr, A. Anti-tuberculosis drug combination for controlled oral delivery using 3D printed compartmental dosage forms: From drug product design to in vivo testing. J. Control. Release 2017, 268, 40–48.

Gioumouxouzis CI, Katsamenis OL, Bouropoulos N, Fatouros DG. 3D printed oral solid dosage forms containing hydrochlorothiazide for controlled drug delivery. J Drug Deliv Sci Technol. 2017;40:164–71.

Goyanes A, Buanz AB, Hatton GB, Gaisford S, Basit AW. 3D printing of modified-release aminosalicylate (4-ASA and 5-ASA) tablets. European journal of pharmaceutics and biopharmaceutics, eV. 2015; 89:157-62.

Goyanes Alvaro, Usanee Det-Amornrat, JieWang, Abdul W. Basit, Simon Gaisford, (2016), 3D scanning and 3D printing as innovative technologies for fabricating personalized topical drug delivery systems, Journal of Controlled Release 234 (2016) 41–48

Goyanes, A., Chang, H., Sedough, D., Hatton, G.B., Wang, J., Buanz, A., Gaisford, S., Basit, A.W., 2015. Fabrication of controlled-release budesonide tablets via desktop (FDM) 3D printing. International journal of pharmaceutics 496, 414-420

Goyanes, A., Fina, F., Martorana, A., Sedough, D., Gaisford, S., Basit, A.W., 2017. Development of modified release 3D printed tablets (printlets) with pharmaceutical excipients using additive manufacturing. Int. J. Pharm. 527, 21–30.

Goyanes, A., Madla, C. M., Umerji, A., Piñeiro, G. D., Montero, J. M. G., Diaz, M. J. L., Barcia, M. G., Taherali, F., Sánchez-Pintose, P., Couce, M.-L., Gaisford, S., & Basit, A. W. (2019). Automated therapy preparation of isoleucine formulations using 3D printing for the treatment of MSUD: First single-centre, prospective, crossover study in patients. International journal of pharmaceutics, 567, 118497.

Goyanes, A.;Wang, J.; Buanz, A.; Martínez-Pacheco, R.; Telford, R.; Gaisford, S.; Basit, A.W. 3D printing of medicines: Engineering novel oral devices with

unique design and drug release characteristics. Mol. Pharm. 2015, 12, 4077–4084

Gudeman Jennifer, Michael Jozwiakowski, John Chollet, Michael Randell, (2013), Potential Risks of Pharmacy Compounding, Drugs R D (2013) 13:1–8.

Habib WA, Alanizi AS, Abdelhamid MM, Alanizi FK. Accuracy of tablet splitting: comparison study between hand splitting and tablet cutter. Saudi Pharm J. 2014;22(5):454–9.

Hafiz Muhammad Afzal, Farrukh Shehzad, Farrukh Shehzad, Mukarram Zubair, Mukarram, Mamdouh A. Al-Harthi, 2019, Influence of microwave irradiation on thermal properties of PVA and PVA/graphene nanocomposites, Journal of Thermal Analysis and Calorimetry 139(1), 2019-

Hait, S. K., & Moulik, S. P. (2001). Determination of critical micelle concentration (CMC) of nonionic surfactants by donor-acceptor interaction with Iodine and correlation of CMC with hydrophile-lipophile balance and other parameters of the surfactants. Journal of Surfactants and Detergents, 4(3), 303-309.

Hamburg MA, Collins FS. The path to personalized medicine. N Engl J Med. 2010;363(4):301–4.

Hansch C, Leo A, Hoekman D. Exploring QSAR - Hydrophobic, Electronic, and Steric Constants. Washington, DC: American Chemical Society; 1995

Haring, A.P., Tong, Y., Halper, J., Johnson, B.N., 2018. Programming of Multicomponent Temporal Release Profiles in 3D Printed Polypills via Core-Shell, Multilayer, and Gradient Concentration Profiles. Advanced healthcare materials 7, e1800213

Healy Andrew V., Evert Fuenmayor, Patrick Doran, Luke M. Geever, Clement L. Higginbotham and John G. Lyons, Additive Manufacturing of Personalized Pharmaceutical Dosage Forms via Stereolithography, Pharmaceutics 2019, 11(12), 645

Healy Anne Marie, Zelalem Ayenew Worku, Dinesh Kumar, AtifM.Madi; 2017, Pharmaceutical solvates, hydrates and amorphous forms: A special emphasis on cocrystals, Advanced Drug Delivery Reviews, 2017

Higuchi, T. (1961). Rate of release of medicaments from ointment bases containing drugs in suspension. Journal of Pharmaceutical Sciences, 50(10), 874-875.

Hollander Jenny, Natalja Genina, Harri Jukarainen, Mohammad Khajeheian, Ari Rosling, Ermei Makila, Niklas Sandler, (2016), Three-Dimensional Printed PCL-Based Implantable Prototypes of Medical Devices for Controlled Drug Delivery, Journal of Pharmaceutical Sciences 105 (2016) 2665e2676

Hölzl, K., Lin, S., Tytgat, L., Van Vlierberghe, S., Gu, L., & Ovsianikov, A. (2016). Bioink properties before, during and after 3D bioprinting. Biofabrication, 8(3), 032002.

Hong, S., Kim, J. S., Jung, B., Won, C., & Hwang, C. (2019). Coaxial bioprinting of cell-laden vascular constructs using a gelatin–tyramine bioink. Biomaterials science, 7(11), 4578-4587.

Hossam Kadry, Soham Wadnap, Changxue Xu, Fakhrul Ahsan, Digital light processing (DLP) 3D-printing technology and photoreactive polymers in fabrication of modified-release tablets, European Journal of Pharmaceutical Sciences Volume 135, 1 July 2019, Pages 60-67

http://www.ashfordorthodontics.co.uk/

https://3dprint.nih.gov/

https://clinicalgenome.org/

https://formlabs.com/

https://www.3dsystems.com/

https://www.aprecia.com/

https://www.astm.org/

https://www.fabrx.co.uk/

https://www.materialise.com/

https://www.sciencedirect.com/

https://www.spritam.com/#/hcp

Hui Wang, Jin-Zhong Xu, Jun-Jie Zhu, Hong-Yuan Chen, 2002, Preparation of CuO nanoparticles by microwave irradiation, Journal of Crystal Growth Volume 244, Issue 1, September 2002, Pages 88-94.

Hull Charles W., Apparatus for production of three-dimensional objects by stereolithography, US Patent 4575330A, 1984

ICMRA Innovation Project 3D Bio-Printing Case Study: Summary of Discussions and Considerations for the New Informal Innovation Network, Therapeutic Goods Administration (TGA) of Australia; the Agência Nacional de Vigilância Sanitária (ANVISA) of Brazil; the European Medicines Agency (EMA) of the European Union; the Ministry of Health, Labour and Welfare and the Pharmaceuticals and Medical Devices Agency (MHLW/PMDA) of Japan; and the Health Sciences Authority (HSA) of Singapore. 2019

Issa Amalia M., Personalized Medicine and the Practice of Medicine in the 21st Century, Mcgill J Med. 2007 Jan; 10(1): 53–57

Jamróz Witold, Joanna Szafraniec, Mateusz Kurek & Renata Jachowicz, 2018, 3D Printing in Pharmaceutical and Medical Applications – Recent Achievements and Challenges, Pharmaceutical Research volume 35, Article number: 176 (2018).

Jamróz,W.; Kurek, M.; Łyszczarz, E.; Szafraniec, J.; Knapik-Kowalczuk, J.; Syrek, K.; Paluch, M.; Jachowicz, R. 3D printed orodispersible films with Aripiprazole. Int. J. Pharm. 2017, 533, 413–420

Jeroen Water Jorrit, Adam Bohr, Johan Boetker, Johanna Aho, Niklas Sandler, Hanne Mørck Nielsen, Jukka Rantanen, (2014), Three-Dimensional Printing of Drug-Eluting Implants: Preparation of an Antimicrobial Polylactide Feedstock Material, Wiley Online Library.

Johnson Ashley, Akm Khairuzzaman; Suniket Fulzele; Adam Procopio; Yash Kapoor; Derrick Smith. An overview of 3D printing techniques, capabilities, and challenges. AAPS Magazine, March 2017

Kaygusuz, H., Evingür, G. A., Pekcan, Ö., von Klitzing, R., & Erim, F. B. (2016). Surfactant and metal ion effects on the mechanical properties of alginate hydrogels. International journal of biological macromolecules, 92, 220-224.

Karakurta Ilbey, Ayça Aydoğdu, Sevil Çıkrıkcı, Jesse Orozco, Liwei Lin, Stereolithography (SLA) 3D printing of ascorbic acid loaded hydrogels: A controlled release study, International Journal of Pharmaceutics Volume 584, 30 June 2020, 119428

Kempin W, Franz C, Koster LC, Schneider F, Bogdahn M, Weitschies W, et al. Assessment of different polymers and drug loads for fused deposition modeling of drug loaded implants. European journal of pharmaceutics and biopharmaceutics, eV. 2017; 115:84-93.

Khaled, S. A., Burley, J. C., Alexander, M. R., & Roberts, C. J. (2014). Desktop 3D printing of controlled release pharmaceutical bilayer tablets. International journal of pharmaceutics, 461(1-2), 105-111.

Khaled, S. A., Burley, J. C., Alexander, M. R., Yang, J., Roberts, C. J. (2015a). 3D printing of tablets containing multiple drugs with defined release profiles. International Journal of Pharmaceutics 494, 643–650.

Khaled, S.A., Alexander, M.R., Irvine, D.J. et al. Extrusion 3D Printing of Paracetamol Tablets from a Single Formulation with Tunable Release Profiles Through Control of Tablet Geometry. AAPS PharmSciTech 19, 3403–3413 (2018).

Khan, F.A., Narasimhan, K., Swathi, C., Mustak, S., Mustafa, G., Ahmad, M.Z., Akhter, S., 2019. 3D printing technology in customized drug delivery system: current state of the art, prospective and the challenges. Curr. Pharm. Des.

Kim Min Chan, Chang Kyun Choi, Do-YoungYoon, (2010), The onset of Görtler vortices in laminar boundary layer flow over a slightly concave wall, European Journal of Mechanics - B/Fluids Volume 29, Issue 6, November–December 2010, Pages 407-414.

Konta, A.A.; García-Piña, M.; Serrano, D.R. Personalised 3D printed medicines: Which techniques and polymers are more successful? Bioengineering 2017, 4, 79.

Korpela Jyrki, Anne Kokkari, Harri Korhonen, Minna Malin, Timo Narhi, Jukka Seppala, (2013), Biodegradable and bioactive porous scaffold structures prepared using fused deposition modeling, J Biomed Mater Res Part B 2013:101B:610–619

Korte, C., Quodbach, J., 2018. Formulation development and process analysis of drugloaded filaments manufactured via hot-melt extrusion for 3D-printing of medicines. Pharm. Dev. Technol. 23, 1117–1127.

Kulathooran Ramalakshmi Raghavan, 1999, Caffeine in Coffee: Its Removal. Why and How?, Critical Reviews in Food Science and Nutrition 39(5):441-56, 1999.

Kushwaha, S. Application of hot melt extrusion in pharmaceutical 3D printing; Journal of Bioequivalence & Bioavailability 10, 54–57 (3), 2018.

Le Bras, A., 2018. Interventional cardiology: 3D printing of personalized implants for left atrial appendage occlusion. Nature reviews. Cardiology 15, 134-135

Lee, K. Y., & Mooney, D. J. (2012). Alginate: properties and biomedical applications. Progress in Polymer Science, 37(1), 106-126.

Li, P., Zhang, S., Sun, W., Cui, M., Wen, H., Li, Q., Pan, W., & Yang, X. (2019). Flexibility of 3D extruded printing for a novel controlled-release puerarin gastric floating tablet: design of internal structure. Aaps Pharmscitech, 20(6), 236.

Li, Q., Guan, X., Cui, M., Zhu, Z., Chen, K., Wen, H., Jia, D., Hou, J., Xu, W., Yang, X., Pan, W., (2018), Preparation and investigation of novel gastro-floating tablets with 3D extrusion-based printing. International Journal of Pharmaceutics 535, 325–332.

Li, Q., Wen, H., Jia, D., Guan, X., Pan, H., Yang, Y., Yu, S., Zhu, Z., Xiang, R., Pan, W., 2017. Preparation and investigation of controlled-release glipizide novel oral device with three-dimensional printing. Int. J. Pharm. 525, 5–11.

Liravi F., S. Das, C. Zhou, Separation force analysis and prediction based on cohesive element model for constrained-surface Stereolithography processes, Comput. Aided. Design 69 (2015) 134–142

Liu Lei, Rui-Lin Liu, Jing Zhang, Zhi-Qi Zhang, 2012, Study on the PEG-based microwave-assisted extraction of flavonoid compounds from persimmon leaves, Separation Science, Volume35, Issue23, 2012.

Liu, W., Zhong, Z., Hu, N., Zhou, Y., Maggio, L., Miri, A. K., Fragasso, A., Jin, X., Khademhosseini, A., & Zhang, Y. S. (2018). Coaxial extrusion bioprinting of 3D microfibrous constructs with cell-favorable gelatin methacryloyl microenvironments. Biofabrication, 10(2), 024102.

Londono, J., Tadros, M., Salgueiro, M., Baker, P.S., 2018. Digital design and 3D printing of an implant-supported prosthetic stent for protecting complete arch soft tissue grafts around dental implants: A dental technique. The Journal of prosthetic dentistry 120, 801-804

Manniello, M.D., Del Gaudio, P., Aquino, R.P., Russo, P., 2017. Clarithromycin and Nacetylcysteine co-spray-dried powders for pulmonary drug delivery: a focus on drug solubility. Int. J. Pharm. 533, 463–469.

Maroni, A., Melocchi, A., Parietti, F., Foppoli, A., Zema, L., Gazzaniga, A., 2017. 3D printed multi-compartment capsular devices for two-pulse oral drug delivery. Journal of controlled release : official journal of the Controlled Release Society 268, 10-18.

Matai, I., Kaur, G., Seyedsalehi, A., McClinton, A., & Laurencin, C. T. (2020). Progress in 3D bioprinting technology for tissue/organ regenerative engineering. Biomaterials, 226, 119536.

Matijaši´c, G.; Greti´c, M.; Vinˇci´c, J.; Poropat, A.; Cuculi´c, L.; Raheli´c, T. Design and 3D printing of multi-compartmental PVA capsules for drug delivery. J. Drug Deliv. Sci. Technol. 2019, 52, 677–686

Max Jean-Joseph and Chapados Camille, (2003) Infrared spectroscopy of acetone–water liquid mixtures. I. Factor analysis J. Chem. Phys. 119, 5632 (2003).

Mazzanti Valentina, Malagutti Lorenzo and Mollica Francesco, 2019, FDM 3D Printing of Polymers Containing Natural Fillers: A Review of their Mechanical Properties, Polymers 2019, 11(7), 1094.

MDDT Q161252, Mddt Summary of Evidence and Basis Of Qualification Decision For: OsiriX CDE Software Module, August 01 2018

Melocchi Alice, Federico Parietti, Giulia Loreti, Alessandra Maroni, Andrea Gazzaniga, Lucia Zema, (2016), 3D printing by fused deposition modeling (FDM) of a swellable/erodible capsular device for oral pulsatile release of drugs, Journal of Drug Delivery Science and Technology 30 (2015) 360e367

Melocchi, A., Parietti, F., Maccagnan, S., Ortenzi, M.A., Antenucci, S., Briatico-Vangosa, F., Maroni, A., Gazzaniga, A., Zema, L., 2018. Industrial Development of a 3D-Printed Nutraceutical Delivery Platform in the Form of a Multicompartment HPC Capsule. AAPS PharmSciTech.

Melocchi, A.; Parietti, F.; Maroni, A.; Foppoli, A.; Gazzaniga, A.; Zema, L. Hot-melt extruded filaments based on pharmaceutical grade polymers for 3D printing by fused deposition modeling. Int. J. Pharm. 2016, 509, 255–263.

Merchant HA, Liu F, Orlu Gul M, Basit AW. Age-mediated changes in the gastrointestinal tract. Int J Pharm 2016;512(2):382–95.

Musazzi, U.M., Selmin, F., Ortenzi, M.A., Mohammed, G.K., Franze, S., Minghetti, P., Cilurzo, F., 2018. Personalized orodispersible films by hot melt ram extrusion 3D printing. Int. J. Pharm. 551, 52–59.

Muwaffak Zaid, Alvaro Goyanes, Vivienne Clark, Abdul W.Basit, Stephen T.Hilton, Simon Gaisford, Patient-specific 3D scanned and 3D printed antimicrobial polycaprolactone wound dressings, International Journal of Pharmaceutics, Volume 527, Issues 1–2, 15 July 2017, Pages 161-170.

Nagarkar Rigved and Patel Jatin, Polyvinyl Alcohol: A Comprehensive Study, Acta Scientific Pharmaceutical Sciences (ISSN: 2581-5423), Volume 3 Issue 4 April 2019

Nanev Christo N., Anita N. Penkova, (2002), Polyhedral (in-)stability of protein crystals, Journal of Crystal Growth Volumes 237–239, Part 1, April 2002, Pages 283-288

Palekar, S., Nukala, P.K., Mishra, S.M., Kipping, T., Patel, K., 2019. Application of 3D printing technology and quality by design approach for development of age-appropriate pediatric formulation of baclofen. Int. J. Pharm. 556, 106–116.

Patil Hemlata, Tiwari Roshan V., Repka Michael A., Hot-Melt Extrusion: from Theory to Application in Pharmaceutical Formulation, AAPS PharmSciTech. 2016 Feb;17(1):20-42.

Penny Matthew R. and Stephen T. Hilton, Design and development of 3D printed catalytically-active stirrers for chemical synthesis, (2020), Reaction Chemistry & Engineering, Issue 5, 2020, 5, 853-858.

Pereira Gabriela G., Sara Figueiredo, Ana Isabel Fernande,and João F. Pinto, Polymer Selection for Hot-Melt Extrusion Coupled to Fused Deposition Modelling in Pharmaceutics, Pharmaceutics 2020, 12, 795; doi:10.3390/pharmaceutics12090795

Pereira, B.C., Isreb, A., Forbes, R.T., Dores, F., Habashy, R., Petit, J.B., Alhnan, M.A., Oga, E.F., 2019. 'Temporary Plasticiser': A novel solution to fabricate 3D printed patient-centred cardiovascular 'Polypill' architectures. European journal of pharmaceutics and biopharmaceutics: V 135, 94-103

Pietrzak K, Isreb A, Alhnan MA. A flexible-dose dispenser for immediate and extended release 3D printed tablets. European journal of pharmaceutics and biopharmaceutics, eV. 2015; 96:380-7.

Pires Felipe Q., Ihatanderson Alves-Silva, Ludmila A.G.Pinho, Juliano A.Chaker, Livia L.Sa-Barreto, Guilherme M.Gelfuso, Tais Gratieri, Marcilio Cunha-Filho, Predictive models of FDM 3D printing using experimental design based on pharmaceutical requirements for tablet production, International Journal of Pharmaceutics Volume 588, 15 October 2020, 119728.

PMC (Personalized Medicine Coalition). Personalized Medicine at FDA. The Scope & Significance of Progress in 2019. February 21, 2020 Available from: http://www.personalizedmedicinecoalition.org/

Ponsar Hanna, Wiedey Raphael and Quodbach Julian, Hot-Melt Extrusion Process Fluctuations and Their Impact on Critical Quality Attributes of Filaments and 3D-Printed Dosage Forms, Pharmaceutics 2020, 12(6), 511.

Popov, V.V., Jr., Muller-Kamskii, G., Kovalevsky, A., Dzhenzhera, G., Strokin, E., Kolomiets, A., Ramon, J., 2018. Design and 3D-printing of titanium bone implants: brief review of approach and clinical cases. Biomedical engineering letters 8, 337-344.

Qijun Li, Haoyang Wen, Danyang Jia, Xiaoying Guan, Hao Pan, Yue Yang, Shihui Yu, Zhihong Zhu, Rongwu Xiang, Weisan Pan, Preparation and investigation of controlled-release glipizide novel oral device with three-dimensional printing, International Journal of Pharmaceutics, Volume 525, Issue 1, 2017, Pages 5-11.

Ozbolat Ibrahim T., Monika Hospodiuk, Current advances and future perspectives in extrusion-based bioprinting, Biomaterials, (76), 2016;321-343, ISSN 0142-9612

Rebong RE, Stewart KT, Utreja A, Ghoneima AA, (2018), Accuracy of three-dimensional dental resin models created by fused deposition modeling, stereolithography, and Polyjet prototype technologies: A comparative study, Angle Orthod. 2018 May;88(3):363-369.

Richey Roberta H., Clare Hughes, Jean V. Craig, Utpal U. Shahac, James L. Ford, Catrin E. Barker, Matthew Peak, Anthony J. Nunn, Mark A. Turner, A systematic review of the use of dosage form manipulation to obtain required doses to inform use of manipulation in paediatric practice, International Journal of Pharmaceutics Volume 518, Issues 1–2, 25 February 2017, Pages 155-166

Ritger, P. L., & Peppas, N. A. (1987). A simple equation for description of solute release I. Fickian and non-fickian release from non-swellable devices in the form of slabs, spheres, cylinders or discs. Journal of Controlled Release, 5(1), 23-36.

Röthel Christian, Michal Radziown, Roland Resel, Andreas Grois, Clemens Simbrunnerb and Oliver Werzer, (2017) Crystal alignment of caffeine deposited onto single crystal surfaces via hot-wall epitaxy, CrystEngComm, 2017

Ruiz-Caro Roberto, and María Dolores Veiga-Ochoa, 2009, Characterization and Dissolution Study of Chitosan Freeze-Dried Systems for Drug Controlled Release, Molecules. 2009 Nov; 14(11): 4370–4386.

Sadia, M., Arafat, B., Ahmed, W., Forbes, R.T., Alhnan, M.A., 2018. Channelled tablets: An innovative approach to accelerating drug release from 3D printed

tablets. Journal of controlled release : official journal of the Controlled Release Society 269, 355-363.

Sadia, M.; Sośnicka, A.; Arafat, B.; Isreb, A.; Ahmed, W.; Kelarakis, A.; Alhnan, M.A. Adaptation of pharmaceutical excipients to FDM 3D printing for the fabrication of patient-tailored immediate release tablets. Int. J. Pharm. 2016, 513, 659–668.

Salimbeygi Golestan, Komeil Nasouri, Komeil Nasouri, Ahmad Mousavi Shoushtari, Firoozmehr Mazaheri, 2013, Fabrication of polyvinyl alcohol/multi-walled carbon nanotubes composite electrospun nanofibres and their application as microwave absorbing material, Micro & Nano Letters 8(8):455-459, 2013

Sandler, N.; Preis, M. Printed drug-delivery systems for improved patient treatment. Trends Pharmacol. Sci. 2016, 37, 1070–1080

Schütz, P., Wahlberg, E., Karlberg, T., Hammarström, M., Collins, R., Flores, A., & Schüler, H. (2010). Crystal structure of human RNA helicase A (DHX9): structural basis for unselective nucleotide base binding in a DEAD-box variant protein. Journal of molecular biology, 400(4), 768-782.

Schwab, A., Levato, R., D'Este, M., Piluso, S., Eglin, D., & Malda, J. (2020). Printability and Shape Fidelity of Bioinks in 3D Bioprinting. Chemical Reviews.

Shaqour, B.; Samaro, A.; Verleije, B.; Beyers, K.; Vervaet, C.; Cos, P. Production of Drug Delivery Systems Using Fused Filament Fabrication: A Systematic Review. Pharmaceutics 2020, 12, 517.

Solaro Roberto, Corti Andrea & Chiellini Emo, "Biodegradation of poly (vinyl alcohol) with different molecular weights and degree of hydrolysis". Polymer 11 (2000): 873-878.

Su-Jin Park, Sang-Do Yeo, (2008), Recrystallization of caffeine using gas antisolvent process, The Journal of Supercritical Fluids, 47 (2008) 85–92.

Tagami, T., Nagata, N., Hayashi, N., Ogawa, E., Fukushige, K., Sakai, N., Ozeki, T., 2018. Defined drug release from 3D-printed composite tablets consisting

of drug-loaded polyvinylalcohol and a water-soluble or water-insoluble polymer filler. Int. J. Pharm. 543, 361–367.

Tagami, T.; Fukushige, K.; Ogawa, E.; Hayashi, N.; Ozeki, T. 3D printing factors important for the fabrication of polyvinylalcohol filament-based tablets. Biol. Pharm. Bull. 2017, 40, 357–364.

Takka, S. (2003). Propranolol hydrochloride–anionic polymer binding interaction. Il Farmaco, 58(10), 1051-1056.

Tan, D.K., Maniruzzaman, M., Nokhodchi, A., 2018. Advanced pharmaceutical applications of hot-melt extrusion coupled with fused deposition modelling (FDM) 3D printing for personalised drug. Delivery Pharm. 10.

Townsend, J. M., Beck, E. C., Gehrke, S. H., Berkland, C. J., & Detamore, M. S. (2019). Flow behavior prior to crosslinking: The need for precursor rheology for placement of hydrogels in medical applications and for 3D bioprinting. Progress in Polymer Science, 91, 126-140.

Trivedi, M., Jee, J., Silva, S., Blomgren, C., Pontinha, V. M., Dixon, D. L., Van Tassel, B., Bortner, M. J., Williams, C., Gilmer, E., Haring, A. P., Halper, J., Johnson, B: N., Kong, Z., Halquist, M: S., Rocheleau, P. F., Long, T. E., Roper, T., Wijesinghe, D. S. (2018). Additive manufacturing of pharmaceuticals for precision medicine applications: A review of the promises and perils in implementation. Additive Manufacturing, 23, 319-328.

U.S. Department of Health and Human Services Food and Drug Administration, Center for Devices and Radiological Health, Center for Biologics Evaluation and Research, Technical Considerations for Additive Manufactured Medical Devices - Guidance for Industry and Food and Drug Administration Staff December 5, 2017.

U.S. Department of Health and Human Services Food and Drug Administration Center for Drug Evaluation and Research (CDER), Quality Considerations for Continuous Manufacturing - Guidance for Industry, February 2019

U.S. Department Of Health And Human Services, U.S. Food And Drug Administration (FDA) Paving the Way for Personalized Medicine: FDA's Role in a New Era of Medical Product Development. 2013. Available from:

https://www.fdanews.com/ext/resources/files/10/10-28-13-Personalized-Medicine.pdf

United States Pharmacopeial Convention Inc. United States Pharmacopeia; USP43 NF38; United States Pharmacopeial Convention Inc.: Bethesda, MD, USA, 2019.

US Patent 5121329A, 1989, S. Scott Crump, Apparatus and method for creating three-dimensional objects

Verstraete, G.; Samaro, A.; Grymonpré, W.; Vanhoorne, V.; Snick, B.V.; Boone, M.N.; Hellemans, T.; Hoorebeke, L.V.; Remon, J.P.; Vervaet, C.; et al. 3D printing of high drug loaded dosage forms using thermoplastic polyurethanes. Int. J. Pharm. 2018, 536, 318–325.

Vitale A, Cabral JT. Frontal conversion and uniformity in 3D printing by photopolymerisation. Materials (Basel). 2016;9:760–72.

Vithani, K., Goyanes, A., Jannin, V., Basit, A. W., Gaisford, S., Boydl, B. J., (2019). An Overview of 3D Printing Technologies for Soft Materials and Potential Opportunities for Lipid-based Drug Delivery Systems. 36: 4.

Vo Anh Q., Jiaxiang Zhang, Dinesh Nyavanandi, Suresh Bandari, Michael A.Repka, 2020, Hot melt extrusion paired fused deposition modeling 3D printing to develop hydroxypropyl cellulose based floating tablets of cinnarizine, Carbohydrate Polymers, Volume 246, 15 October 2020, 116519

Vogel CL, Cobleigh MA, Tripathy D, et al. Efficacy and Safety of Trastuzumab as a Single Agent in First-line Treatment of HER 2-Overexpressing Metastatic Breast Cancer. J. Clin. Oncol. 2002;20:719–726

Wanjun Liu, Zhe Zhong, Ning Hu, Yixiao Zhou, Lucia Maggio, Amir K Miri, Alessio Fragasso, Xiangyu Jin, Ali Khademhosseini. and Yu Shrike Zhang, Coaxial extrusion bioprinting of 3D microfibrous constructs with cell-favorable gelatin methacryloyl microenvironments, Biofabrication, 2018 Jan 12;10(2):024102.

Waters Laura J., Susan Bedford, and Gareth M. B. Parkes, 2011, Controlled Microwave Processing Applied to the Pharmaceutical Formulation of Ibuprofen, AAPS PharmSciTech, Vol. 12, No. 4, December 2011.

Wei, C.; Solanki, N.G.; Vasoya, J.M.; Shah, A.V.; Serajuddin, A.T.M. Development of 3D printed tablets by fused deposition modeling using polyvinyl alcohol as a polymeric matrix for rapid drug release. J. Pharm. Sci. 2020, 109, 1558–1572

Wen, H., He, B., Wang, H., Chen, F., Li, P., Cui, M., Li, Q., Pan, W., & Yang, X. (2019). Structure-based gastro-retentive and controlled-release drug delivery with novel 3D printing. Aaps Pharmscitech, 20(2), 68.

Xiaoyan Xu, Alvaro Goyanes, Sarah J. Trenfield, Luis Diaz-Gomez, Carmen Alvarez-Lorenzo, Simon Gaisford, Abdul W. Basit; Stereolithography (SLA) 3D printing of a bladder device for intravesical drug delivery, Materials Science & Engineering C 120 (2021) 111773.

Yalkowsky SH, He Y, Jain P. Handbook of Aqueous Solubility Data. Second Edition ed. Boca Raton, FL: CRC Press; 2010

Yan Ting-Ting, Zhu-Fen Lv, Pan Tian, Min-Mei Lin, Wei Lin, Si-Yu Huang & Yan-Zhong Chen (2020) Semi-solid extrusion 3D printing ODFs: an individual drug delivery system for small scale pharmacy, Drug Development and Industrial Pharmacy, 46:4, 531-538.

Yiru Li, Aibo Zhang, Honglong Lu, Xin Zhang, Wen Zheng, and Miaomiao Li, 2018, Effect of Polar Polymers of PEG and PVA on the Enhanced Microwave-Absorbing Properties of MWNTs, J. Phys. Chem. C 2018, 122, 29, 16956–16963, 2018.

Zakeri Setareh, Minnamari Vippola, Erkki Levänen, A comprehensive review of the photopolymerization of ceramic resins used in stereolithography, Additive Manufacturing Volume 35, October 2020, 101177.

Zhang Y S et al 2016 Bioprinting 3D microfibrous scaffolds for engineering endothelialized myocardium and heart-on-a-chip Biomaterials 110 45–59

Zou, Y., Han, Q., Weng, X., Zou, Y., Yang, Y., Zhang, K., Yang, K., Xu, X., Wang, C., Qin, Y., & Wang, J. (2018). The precision and reliability evaluation of 3-dimensional printed damaged bone and prosthesis models by stereo lithography appearance. Medicine, 97(6), e9797.

List of publications and communications

Papers

Saviano M., Aquino R.P., Del Gaudio P., Sansone F., Russo P.*, Poly(vinyl alcohol) 3D printed tablets: The effect of polymer particle size on drug loading and process efficiency*, International Journal of Pharmaceutics, Volume 561, 20 April 2019, Pages 1-8

https://doi.org/10.1016/j.ijpharm.2019.02.025

Falcone G.[1], **Saviano M.**[1], Aquino R.P., Del Gaudio P. , Russo P., *Coaxial semi-solid extrusion and ionotropic alginate gelation: a successful duo for personalized floating formulations via 3D printing,* Carbohydrate Polymers, Volume 260, 15 May 2021, 117791

https://doi.org/10.1016/j.carbpol.2021.117791

Submitted manuscript

Saviano M., Penny M., Bowels B., Russo P., Hilton S.,

Development and analysis of a novel post-loading technique for FFF 3D printed systems: microwave-assisted impregnation of gastro-retentive PVA modular models, Submitted on 2021

Communications

Falcone G., **<u>Saviano M.</u>**, Aquino R.P., Russo P.

Development and characterization of gastroretentive drug delivery formulations produced via FDM 3D-printed coaxial semi-solid extrusion systems, NanoInnovation 2020 Conference & Exhibition V Edition, Rome, 15-18 September 2020

<u>Saviano M.</u>, Picardi E., Falcone G., Del Gaudio P., Aquino R.P., Russo P.

Poster *"3D printed tablets: the effect of polymer particle size on drug loading and process efficiency"*, 2019 ISM, 22nd International Symposium on Microencapsulation, Salvador, Brazil, 25-27 September 2019

<u>Saviano M.</u>, Picardi E., Falcone G., Aquino R.P., Russo P.

Poster *"Design and production of personalized devices via 3D-Printing based technologies"* 13° A.It.U.N. Meeting "New challenges in self assembling drug delivery systems" Castelraimondo (MC) 13-14 June 2019

Russo P., **<u>Saviano M.</u>**, Del Gaudio P., Aquino R.P.

Poster "*The New frontier of Pharmaceutical Compounding: 3D printing of personalized medicines*", 3rd European Conference on Pharmaceutics, Bologna, 25-26 March 2019

<u>Saviano M.</u>

Oral Presentation: *"Production of Hot Melt Extruded Poly(vinyl Alcohol)-Ciprofloxacin filaments for Fused Deposition Modeling-3D-Printing technology and personalized medicines",* 18th School for Doctorate in Pharmaceutical

Technology, Lake Como School of Advanced Studies, Innovation in local drug delivery, 25-28 September 2018

Saviano M., Filomena M. D., Falcone G., Aquino R.P., Russo P.

Poster *"Development of innovative FDM-3D-printing technologies for the production of patient-tailored medicines",* 12th A.It.U.N. Meeting "Medicines for older people: advances in drug delivery", University of Bologna, AAPS Italian University Network, 10-11 May 2018